Implanted Antennas and Intra-Body Propagation Channel for Wireless Body Area Network

ALI AHMED YOUNIS IBRAHEEM

Dissertation submitted to the faculty of the Virginia Polytechnic Institute and State University in partial fulfillment of the requirements for the degree of

Doctor of Philosophy
in
Electrical Engineering

Majid Manteghi
Sedki M. Riad
Ahmed Safaai-Jazi
Jeffrey H. Reed
Werner E. Kohler
Ahmed M. Attiya

NOVEMBER 19, 2014
BLACKSBURG, VIRGINIA

KEYWORDS: Electrically Small Antenna, Specific Absorption Rate, Electrically Coupled Loop Antenna, Path Loss, Wireless Power Transfer

Implanted Antennas and Intra-Body Propagation Channel for Wireless Body Area Network

ALI AHMED YOUNIS IBRAHEEM

ABSTRACT

Implanted Devices are important components of the Wireless Body Area Network (WBAN) as a promising technology in biotelemetry, e-health care and hyperthermia applications. The design of WBAN faces many challenges, such as frequency band selection, channel modeling, antenna design, physical layer (PHY) protocol design, medium access control (MAC) protocol design and power source. This research focuses on the design of implanted antennas, channel modeling between implanted devices and Wireless Power Transfer (WPT) for implanted devices. An implanted antenna needs to be small while it maintains Specific Absorption Rate (SAR) and is able to cope with the detuning effect due to the electrical properties of human body tissues. Most of the proposed antennas for implanted applications are electric field antennas, which have a high near-zone electric field and, therefore, a high SAR and are sensitive to the detuning effect. This work is devoted to designing a miniaturized magnetic field antenna to overcome the above limitations. The proposed Electrically Coupled Loop Antenna (ECLA) has a low electric field in the near-zone and, therefore, has a small SAR and is less sensitive to the detuning effect. The performance of ECLA, channel model between implanted devices using Path Loss (PL) and WPT for implanted devices are studied inside different human body models using simulation software and validated using experimental work. The study is done at different frequency bands: Medical Implanted Communication Services (MICS) band, Industrial Scientific and Medical (ISM) band and 3.5 GHz band using ECLA. It was found that the proposed ECLA has a better performance compared to the previous designs of implanted antennas. Based on our study, the MICS band has the best propagation channel inside the human body model among the allowed frequency bands. The maximum PL inside the human body between an implanted antenna and a base station on the surface is about 90 dB. WPT for implanted devices has been investigated as well, and it has been shown that for a device located at 2 cm inside the human body with an antenna radius of 1 cm an efficiency of 63% can be achieved using the proposed ECLA.

ACKNOWLEDGMENTS

I would like to express my deepest gratitude to my academic and research advisor Dr. Majid Manteghi for his guidance and help throughout my research and for gladly offering his knowledge and experience when needed. His trust and support was extremely encouraging and helpful.

I would like to express my special thanks and highest appreciation to Dr. Sedki M. Riad for his generous help during the last few years. I would also like to thank all other members of my PhD committee; Dr. Ahmed Safaai-Jazi, Dr. Jeffery H. Reed, Dr. Werner E. Kohler and Dr. Ahmed M. Attia for their support and help.

I would like to thank all members of Virginia Tech whom I interact with, especially my colleagues in the Virginia Tech Antenna Group for their cooperation and also helping me throughout my research and reviewing my writing.

Finally, I would like to express my thanks to my parents, brothers, sisters and all of my family. I especially thank my lovely wife and my daughters for helping and standing beside me through my research in the last few years.

TABLE OF CONTENTS

LIST OF FIGURES

LIST OF TABLES

LIST OF ABBREVIATIONS

ADC	Analog Digital Converter
BCC	Body Coupling Communications
BER	Bite Error Rate
DGF	Dyadic Green Function
ECLA	Electrically Coupled Loop Antenna
ECG	Electrocardiography
EEG	Electroencephalography
EIRP	Effective Isotropic Radiated Power
EM	Electromagnetic
EMG	Electromyography
ERC	European Radio Communication Commission
FCC	Federal Communication Commission
FDTD	Finite Difference Time Domain
HFSS	High Frequency Structure Simulator
HSCA	Horn Shaped Self-Complementary Antenna
IEEE	Institute of Electrical and Electronics Engineers
ISM	Industrial Scientific and Medical
LOS	Line-Of- Sight
MAC	Medium Access Control
MICS	Medical Implanted Communications Services
NLOS	Non line-Of-Sight
PEC	Perfect Electric Conductor
PHY	Physical
PIFA	Planner Inverted F Antenna
PL	Path Loss
PLL	Phase Locked Loop
PTMA	Printed Tapered Monopole Antenna
QoS	Quality of Services

RF	Radio Frequency
SAR	Specific Absorption Rate
UHF	Ultra-High Frequency
UMTS	Universal Mobile Telecommunication System
UTD	Uniform Theory of Diffraction
UWB	Ultra-Wide Band
VCO	Voltage Control Oscillator
WBAN	Wireless Body Area Network
WPT	Wireless Power Transfer
WSN	Wireless Sensor Network
XF7	X Stream Finite Difference Time Domain (XFDTD 7)

Chapter 1

Introduction

According to the World Health Organization, cardiovascular diseases cause around 30% of all deaths in the world; also, diabetes currently affects around 180 million people in the world [1]. So it is important to monitor all the physiological data of the human body and send these data immediately to the hospital or the clinic where these data will be analyzed and a feedback will be sent immediately to the users. Using the above technique will save the physicians and patients a lot of time, will reduce the cost associated with healthcare and will improve the quality of healthcare provided. Wireless technology plays an essential rule in most of the modern health monitoring systems. More specifically, implanted wireless devises are finding wider application within this new area of healthcare technology. These social and economic benefits highlight the needs for Wireless Body Area Network (WBAN) [2, 3].

1.1 Motivation & Essence of the Work

Currently, patients health information can be collected and retrieved remotely and efficiently using biotelemetry wireless networks such as WBAN [4]. WBANs are especially promising in biotelemetry, e-health care and hyperthermia applications. Also WBAN can be used in security services, defense, sports and fitness, entertainments & games and consumer electronics. Medical implanted and wearable devices are major components in WBAN [5-14]. Medical implanted devices are typically battery-operated, and once implanted should operate for several years on as little power as possible. The design of WBAN faces many challenges, such as frequency band selection, channel modeling, antenna design, physical layer (PHY) protocol design, medium access control (MAC) protocol design, power source and energy efficient hardware [6, 15, 16].

This research will focus on the design of implanted antennas, channel modeling between implanted devices and Wireless Power Transfer (WPT) for implanted devices. An implanted antenna should be heavily miniaturized to fit inside the human body and keep the Specific

Absorption Rate (SAR) inside the human body as small as possible for patients' safety. Also the implanted antenna should be less sensitive to the detuning effect due to the electrical properties of the human body tissues [17]. Most of the proposed antennas for implanted applications are electric field antennas, such as Planner Inverted F Antenna (PIFA) and micro-strip patch antenna, which have a high electric field and a small magnetic field in the near-zone regions [18] and, therefore, a high SAR value inside human body tissues for small antenna size [19]. In this work a miniaturized magnetic antenna will be designed as an implanted antenna to overcome the above limitation. The proposed Electrically Coupled Loop Antenna (ECLA) [20] has a high magnetic field intensity and a relatively low electric field intensity in the near-zone and, therefore, has a small SAR and is less sensitive to the detuning effect [21].

The propagation channel, which is measured and studied through physical experiments and simulations, is absolutely critical in successful transceiver design [22]. In the case of medical implants, physical experiments are extremely difficult if not impossible. Therefore, simulations are used in most studies. In Chapter 4, Path Loss (PL) between implanted antennas, as a measure of propagation characteristics, will be studied. PL between implanted devices will be investigated using our proposed ECLA antenna [20].

Most of the implanted devices are feed using batteries, but the amount of power and life time of batteries are challenges that need to be overcome. An alternative method is to use WPT for implanted devices can play an important role in the modern health monitoring system which will be considered [23]. WPT for implanted devices using our proposed ECLA will be described in this research.

1.2 Background

1.2.1 Wireless Body Area Network (WBAN)

WBAN as shown in Figure 1.1 consists mainly of wireless sensor nodes, wireless actuator nodes and wireless personal device. These nodes are placed in star or multi-hop topology. Wireless sensor nodes sense the physiological data of the human body and they consist of sensor hardware, a power unit, memory and transmitter or receiver. Wireless actuator nodes act as medicine delivery and they consist of actuator hardware, power unit and transceiver. The wireless personal device collects all information data from sensor and actuator nodes and communicates it to users; it consists of a power unit, large processor, large memory and transceiver [16, 24].

WBAN can be classified into two categories, on-body WBAN and in-body WBAN [25-27]. On-body WBAN refers to a network that has sensor nodes placed on or near the surface of the human body, while in-body WBAN refers to a network that has sensor nodes implanted inside human body tissues. Wireless transmission in both categories is characterized by extremely low peak power and low duty cycle to extend the life time of the batteries. For implants, low power and duty cycle also enable the body to safely dissipate the heat generated by the transmitters.

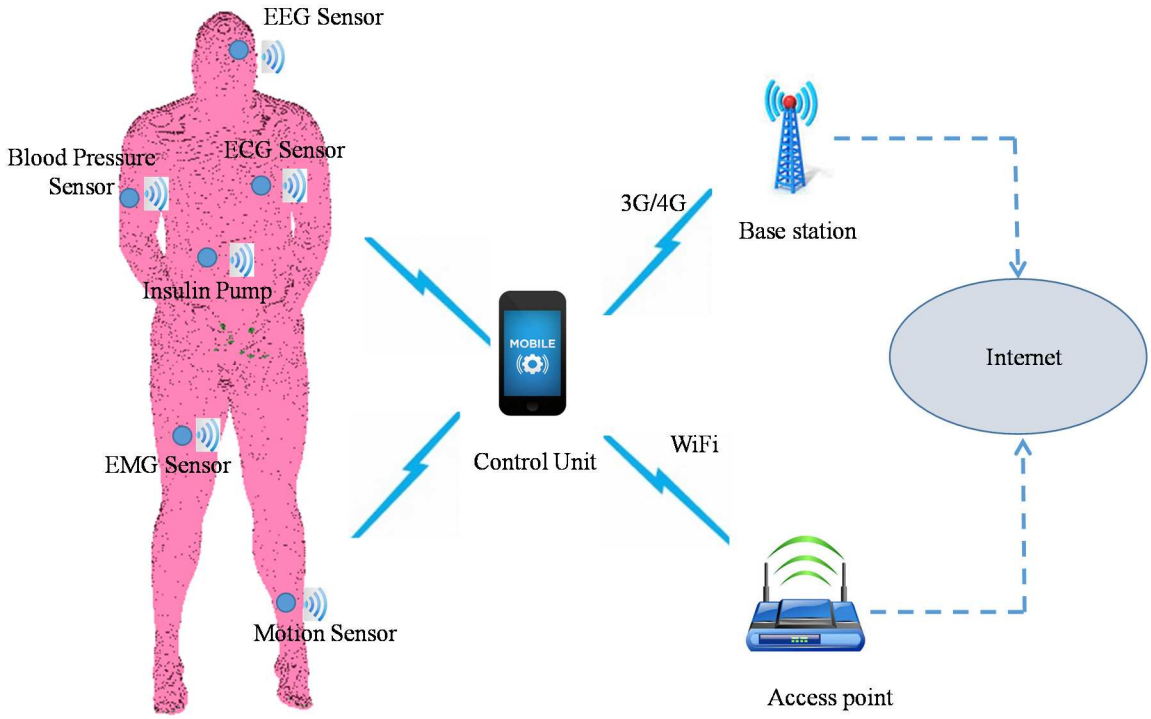

Figure 1.1: WBAN structure and components.

The design challenges of WBAN, such as frequency band selection, antenna design, channel model, and WPT will be explained in detail in Chapters 3, 4, and 5. The other design challenges will be briefly explained in this section. The characteristics of the physical layer are different for WBAN compared to Wireless Sensor Networks (WSN), or ad-hoc networks, due to the proximity of the human body, so in the design of physical (PHY) layer protocol, the human body has to be considered as a dynamic propagation channel [28].

The Radio Frequency (RF) communications in WBAN has two forms: propagation in the body and propagation along the body. For wave propagation inside the human body, the body acts as a communication channel where losses are mainly due to absorption of power in the human body

tissues. So the Electromagnetic (EM) waves are attenuated considerably before reaching the receiver. This attenuation inside the human body is very high compared to free space attenuation as will be studied later. Also the shape of different parts of the human body which host the implant and the location of the implant in that particular part can influence the radiation pattern and propagation loss dramatically [29].

The propagation channel along the body can be categorized into Line-Of-Sight (LOS) and Non Line-Of-Sight (NLOS) channels [30, 31]. In the LOS case the curvatures of the body are not taken into account where calculations and simulations are performed in a flat phantom [32]. In NLOS, there is no direct link between the transmitter and the receiver; the EM waves are refracted and scattered around the body rather than having a direct path through the body [33]. The PL in NLOS is higher compared to LOS due to diffraction around the body and absorption of a large amount of radiated power by the body. Besides the propagation of radio waves, several researches have investigated the possibility to transfer data by capacitive and galvanic coupling, and this is called Body Coupling Communications (BCC) [34, 35].

The MAC protocol design for WBAN is also a complicated, where the number of MAC protocols specifically developed for WBAN are limited. Due to similarities between WSN and WBAN, it is useful to consider the research in MAC protocols design for WSNs [15, 36-38]. The MAC protocols have two categories, contention-based and schedule-based [39]. The most commonly used technique for reducing energy consumption is contention-based MAC protocol [38]. Some implementations of WBAN use Bluetooth (IEEE 802.15.1), but this protocol does not support multi-hop communication, has complex protocol stack and high energy consumption compared to other protocols [40]. Most of the current implementation of WBANs use ZigBee (IEEE 802.15.4) as an enabling technology [41-43]. All the proposed MAC protocols for WBAN are shown in Table 1.1. IEEE 802.15.6 (Not shown in Table 1.1) is developing communication standards optimized for low power devices and operation on, in or around the human body to service a variety of applications including medical applications [44-48].

In the network layer, developing an efficient routing protocol in WBAN is also a complicated challenge due to the specific characteristics of wireless environment, such as the available bandwidth, is limited, and the nodes that form the network can be very heterogeneous in term of available energy or computing power. The proposed network protocols for WSNs are not suitable for WBAN because in many cases, the network is considered a static one but the WBAN has

heterogeneous mobile devices with stringent real time requirement due to the sensor actuator communication [49-51]. The proposed network layer protocols for WBAN are temperature routing protocols and cluster based routing protocols [52, 53].

In the design of WBAN, data rates are considered to be an important issue. Due to the strong heterogeneous nature of the applications, data rates will vary strongly, ranging from simple data at a few Kbits/s to video stream of several Mbits/s. Data can also be sent in bursts, which means that it is sent at a higher data rate during the bursts [54]. The reliability of the data transmission is provided in terms of necessary Bit Error Rate (BER), which is used as a measure for the number of lost packets and indication of channel quality [55]. For medical devices, the reliability depends on data rate; low data rate devices can cope with high BER and vice versa.

Table 1.1: Current standards for on-body and implanted WBANs

Standard	Frequency bands
MICS	402-405 MHz
IEEE 802.15.4	868 MHz Europe and 915MHz(US)/2.4 GHz
IEEE 802.15.4a	250-750 KHz and 3.1-5 GHz-6-10.6 GHz
UWB	3.1-10.6 GHz
WMTS	608-1395 MHz and 1400-1427 MHz
IEEE 802.11 a/b/g	2.4 GHz

Energy consumption is an important factor in the design of WBAN. Energy consumption can be divided into three domains: sensing, wireless communications and data processing. The wireless communication has the most power consumption. The power available at each node is often restricted by power generated by the attached batteries [56]. The life time of a node for a given battery capacity can be enhanced by saving energy during the operation of the system. If the scavenged energy is larger than the average consumed energy, such a system could run internally. A combination of lower energy consumption and energy scavenging is the optimal solution for achieving autonomous WBAN [57, 58].

Proper Quality of Service (QoS) handling is an important part in the frame work of risks associated with medical applications [59]. A critical issue is the reliability of transmission in order to guarantee that the monitored data is received correctly by the health care professionally. The reliability can be considered either end to end or per link. The reliability of the network directly

affects the quality of patient monitoring and in the worst case scenario it can be fatal in regards to detecting a life-threaten event.

Usability is also an important issue for WBAN. In most cases WBAN, will be set up in a hospital by medical staff and not by engineers. Consequently, the network should be capable of configuring and maintaining itself automatically.

Another important factor in the design of WBAN, is the security and privacy of the network. The communication of health related information between sensors in a WBAN and over the internet to servers is strictly private and confidential and should be encrypted to protect the patient's privacy [60, 61].

In conclusion, WBAN is carried globally by their users, hence, it's desirable that WBAN radio frequency must be worldwide. Experimental channel modeling for implanted or wearable device is difficult due to the involvement of the human body. Also, empirical validation of channel model is complicated due to the dynamic environment. Antenna design for WBAN is complicated due to restriction on antenna size, antenna material which must be "only non-corrosive and biocompatible", shape of the antenna, and hostile RF environment. PHY layer protocol design requires minimizing power consumption without compromising the fidelity. WBANs are intended to support life-saving medical applications, hence, safety, QoS, Security, and reliability are important for MAC protocol design.

1.2.2 Frequency Bands

In WBANs, the frequency bands have two groups, implanted (in-body) application group and on-body application group as shown in Table 1.2 [62]. According to Federal Communication Commissions (FCC) and European Radio- communication Commissions (ERC), the common frequency bands approved for implanted and wearable antennas can be classified into two categories, Ultra Wide Band (UWB) (3.1-10 GHz) applications and Narrow Band (NB) applications, such as Medical Implanted Communication Service (MICS) band (402-405 MHz) and Industrial Scientific and Medical (ISM) band (2.45-2.5 GHz). The receiver on NB systems requires power hungry devices as Voltage Controlled Oscillators (VCOs), Phase Locked Loops (PLL) and Analog to Digital Converter (ADCs). Also their power consumption does not scale down with data rates [63-66]. The UWB communications for implanted devices is a new topic and can be an interesting candidate for providing high data rate warranted in the future implantable

applications. Using UWB, the most complexity is in the receiver that allows the realization of an ultra-low power complex transmitter in the uplink (from implanted device to outside controller) [67-76]. The hardware simplicity of UWB transmitter offers the potential for low cost and highly integrated solutions. Due to high loss of the body tissues and the low transmitted power, the signal strength at the receiver becomes important to achieve high data rate transmission, thus the strategies to optimize the UWB communication link quality are important. The MICS band has relatively low power loss inside human body and is able to transmit its low data rate even though it needs a large antenna size [77]. On the other hand, the UWB systems are able to transmit high data rates with small antenna but have high propagation loss inside the human body. Although far-field communication using MICS band radio is increasing mobility and data rate. The stringent transmitted power regulation imposed by FCC is the main obstacle to the construction of the healthcare networks which need to cover at least a 10 m communication range around the patients. As the MICS band is shared with metrological and earth exploration satellites, the Effective Isotropic Radiated Power (EIRP) is limited to -16 dBm to generate non-interference with the primary users. The low emission power experiences huge propagation loss through the air channel and conductive human tissues.

Table 1.2: List of frequency bands for WBANs

WBANs	Frequency Bands
Implants	402-405 MHz(MICS)
On-body	13.5 MHz
On-body	5.5 MHz
On-body	400 MHz
On-body	600 MHz
On-body	900 MHz
On-body	2.4-2.5 GHz(ISM)
On-body	3.1-10.6 GHz(UWB)

1.2.3 Specific Absorption Rate (SAR)

Specific Absorption Rate (SAR) is a measure for Electromagnetic (EM) Energy absorbed by biological tissues mass when exposed to radiating devices. SAR can be expressed as [78]:

$$SAR = \frac{P}{\rho} = \frac{\sigma E^2}{2\rho} = \frac{J^2}{2\rho\sigma} \tag{1.1}$$

where, P is the power loss density (W/m^3), E is the electric field strength (V/m), J is the current density (A/m^2), ρ is the mass density (Kg/m^3) and σ is the conductivity (S/m). SAR can be defined in many terms as shown in Figure 1.2 [79].

- Point SAR: local SAR without mass or volume averaging.
- Total SAR: total power loss in the whole lossy structure divided by its total mass.
- Mass averaged SAR: for each point SAR, a cube with a defined mass (1 g or 10 g) is found, the power loss density is integrated over this cube and then the integrated power loss is divided by the cube mass.
- Volume averaged SAR: the same as mass averaged SAR but on fixed volume.

According to the FCC and ERC, the maximum limits for SAR averaged over 1 g and 10 g of tissue mass is 1.6 and 2 W/kg respectively [80, 81].

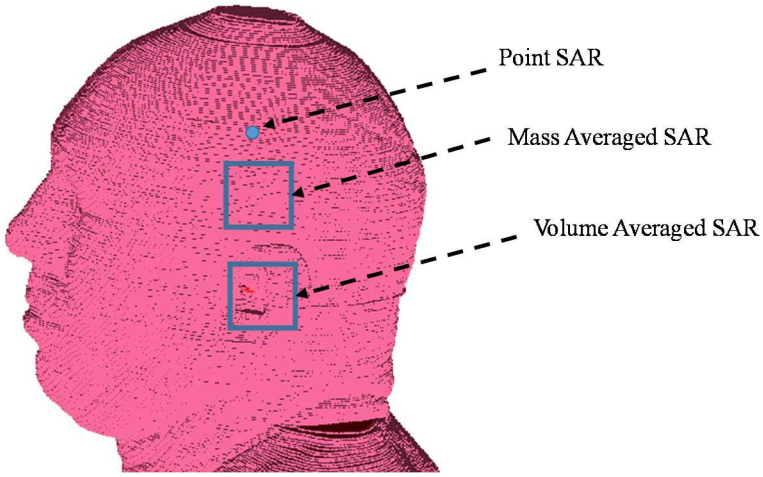

Figure 1.2: SAR types inside the human body.

1.2.4 Path Loss (PL)

An important factor in the development of WBAN is the estimation of PL in, on, or around the body. To estimate PL, this requires detailed characteristic of EM waves propagation in, on, or around the human body. We use the following definition for PL [82]-,

$$PL = \frac{P_{rec}}{P_{trans}} \tag{1.2}$$

where P_{rec} and P_{trans} are the receiving and transmitting power respectively. For WBAN, PL is often defined in term of scattering parameters (S_{21}) which includes the antenna loss as well, because it is easy to measure, so PL in dB can be expressed as [83, 84]:

$$PL(dB) = -|S_{21}|_{dB} \tag{1.3}$$

PL for WBAN depends mainly on the distance between transmitter and receiver, shadowing, which is a random variation in received power caused by obstruction, and multipath fading, which is a random variation in received power caused by sometimes constructive and sometimes destructive vector combination of electric field of reflected and refracted paths. In WBAN, the two types of random power fluctuation can not be easily distinguished because the wavelength is relatively long and the body parts that cause shadowing have size in order of wavelength.

Many theoretical and measurement based studies presented in literatures have shown that the average received signal decreases logarithmically with distance (d) and the average PL will be expressed as [85]

$$PL(dB) \propto \left(\frac{d}{d_0}\right)^n \qquad , d \geq d_0 \quad , \tag{1.4}$$

where n is the PL exponent and d_0 is the reference distance. The variations in PL exponent at different frequency bands are caused by the increase in absorption from human body tissues. The PL observed at any given point will deviate from this average value due to the variation in the environment. This variation has been shown to follow logarithmic normal distribution, therefore the average PL can be expressed as:

$$PL(dB) = PL(d_0) + 10nlog\frac{d}{d_0} + X_\delta \tag{1.5}$$

X_δ is the zero mean Gaussian distribution random variable with standard deviation δ. The PL inside the human body can be modeled using power function as [86, 87]:

$$PL(d) = ad^b + a_1 \tag{1.6}$$

where a , b, a_1 are constants [88]:

1.3 Antenna Design

The antennas used in WBAN are categorized as: implantable and wearable antennas. The design of the implanted antennas for WBAN face many different challenges [89-92], therefore a large amount of research has been performed for this task. The previous design for implanted antennas will be summarized as follows: In [89], a dipole antenna and a low profile patch antenna with resonant frequency in MICS band were analyzed inside the human body using Finite Difference Time Domain (FDTD) and Dyadic Green Function (DGF) for implanted applications. The radiation performance of the designed antenna was estimated in terms of radiation pattern, radiation efficiency and SAR. A micro-strip patch antenna was designed as an implantable antenna in MICS frequency band [92]. The antenna design was used as a guidance in the design of implantable micro-strip patch antenna. In [93], a compact stacked implantable antenna was designed for biomedical applications in MICS band. The antenna structure can improve the bandwidth and reduce the detuning effect due to electrical properties of human body tissues. A small size dual-band, MICS and ISM bands, implantable antenna was designed for continuous glucose monitoring [94]. The antenna performance was optimized for dual bands applications. In [95], a compact-shape with double L-strips PIFA was proposed for implantable applications in MICS band. The designed antenna has a broad bandwidth of 80 MHz at return loss of 10 dB. A first prototype of complete implantable device was proposed in MICS frequency band [18] . In [96], a 2.5x1.8 cm MICS band antenna combined with electrode was designed for body channel communication. An implanted H-shaped cavity slot antenna was proposed as an implantable antenna for short range communication in ISM band [97]. In [98], a helical folded dipole antenna was proposed as an implantable antenna in ISM band. The antenna design considers antenna size, power consumption and biocompatibility. A triple-band antenna was proposed for biotelemetry application in MICS band and ISM (433 MHz and 2.45 GHz) bands. The design procedure, realization and measurement of an implantable radiator for telemetry application in MICS and ISM bands were proposed [99]. The designed antenna can be used in rectifying antenna for wireless power transmissions. The antenna has a bandwidth of 113 MHz and 70 MHz at MICS band and ISM band respectively. In [100], a simple helical dipole antenna for implanted biocompatible

applications was proposed. The antenna has a gain for 10 m short range communication with 113 MHz bandwidth and SAR values less than the standard limitation. An overview of all patch antenna design challenges for implantable application was provided [19]. The design and radiation performance of novel miniaturized antennas for integration in head implanted medical device operating in MICS and ISM (433.1-434.8, 868-868.6, 902.8-928 MHz) bands were investigated [101]. The design process of the antenna can be applied to optimize antennas for several applications. In [102], an implantable UWB antenna in the UWB bands for purpose to be used in the human head was proposed. Antenna performance is studied using simulation software. A helical folded dipole antenna for implanted devices was proposed for patient monitoring systems in UHF band (924 MHz) [103]. The proposed antenna has adequate gain within 10 m transmission range with 225 MHz bandwidth. In [104], an implanted compact folded antenna was designed at UHF [950-956 MHz]. The proposed antenna has a maximum gain of -23 dBi which exceeds the link budget margin. Two kinds of design of implant antenna in UWB low band (3.4-4.8 GHz)were proposed for capsule endoscope [105]. The antenna performance was investigated using simulation and experiment. In [106], the deep investigation of the effect of body tissue thickness in the performance of UWB loop antenna was discussed. The antenna was designed for the examination which used in UWB WBAN applications. Most of the previous investigations on implanted antenna designs suffer from two main problems: a high value of SAR at a small antenna size and detuning effects due to the dielectric properties of the human body tissues. An Electrically Coupled Loop Antenna (ECLA) is proposed in this research to tackle the above issues [20].

Apart from the research on implanted antenna for WBAN, a large amount of research has been conducted in the design of wearable antenna for WBAN. This research will be summarized as follows. In [107], a horn shaped self-complementary antenna (HSCA) and planar inverted cone antenna were used to study the propagation channel in UWB for on-body communications. Results show that the hybrid use of different types of UWB antenna can efficiently improve channel behavior in body centric wireless network. A novel small size directional antenna based on a typical slot antenna with an added reflector was designed for WBAN in UWB band [108]. Antenna performance was improved in terms of radiation efficiency and SAR values. In [109], a textile antenna was designed as an UWB antenna for WBAN in UWB. Two designs of textile antenna have been realized: coplanar waveguide feed printed UWB disc monopole and UWB disc circular slot antenna. A novel compact micro-strip feed dual band coplanar antenna was designed for

WBAN in (2.4, 5.2, 5.8 GHz) bands [110]. The antenna generates two separate resonant modes to cover 2.5/5.2/5.8 GHZ bands. In [111], a single feed rectangular ring textile antenna was proposed for WBAN in ISM band. The robustness of the antenna characteristics with respect to bending was proven. A printed tapered monopole antenna (PTMA) was investigated for WBAN in UWB band for on-body applications [112]. The antenna is a good candidate for implanted applications. In [113], a PIFA with two shielding strips was designed for WBAN in ISM band. The proposed antenna can be placed very close to nearby conducting elements with small effect on the antenna performance. A cavity slot antenna was proposed for on-body communication for WBAN in ISM band [114]. In [115], an e-textile antenna was proposed for body centric applications. The antenna can be designed in two shapes: conventional micro-strip area and wide band multiple antenna systems. A wearable button antenna was designed in (2.5 and 5 GHz) with monopole type radiation pattern [116]. In [117], a miniaturized diversity antenna that had a combination of PIFA and top loaded antenna was proposed for WBAN. A new compact planar UWB antenna was designed for on-body communication in (3-11.2 GHz) range [118]. In [119], a flexible light weight and mechanically robust textile antenna was proposed for dual band satellite use. A zero order resonant antenna placed on wrist was proposed for WBAN applications [120]. In [121], a novel folded UWB antenna was proposed for WBAN application in (3.1-12 GHz) band. In [122], a triple-band monopole antenna was designed for WBAN in UWB band. The proposed antenna achieves a compact size with low profile and can be confined to the human body. A new easy-to-apply procedure was proposed for constructing wideband circular polarized bi-directional and unidirectional square slot antenna was proposed [123]. In [124], a new broadband textile based PIFA antenna structure was designed for WBAN in (1.8-3 GHz) range. The antenna radiation characteristics and bandwidth show satisfactory immunity against the detuning effect when operates on body. A novel low profile UWB antenna for WBAN application was proposed [125]. The antenna has a polarization perpendicular to the body- free space interface, which is interesting in order to minimize the coupling into the body. In [126], a textile micro-strip topology with UWB characteristics useful in WBAN was proposed. The antenna design reduces any on-body degradation, resulting in a very robust structure.

1.4 Channel Model

To provide a clear understanding of telemetry links between implanted or wearable devices and mobile or base station units located outside of the human body, in-depth analysis of wave attenuation in lossy human body tissues and propagation in the vicinity of the human body is essential. To ensure efficient performance of such a wireless telemetry system, propagation channel needs to be characterized and modeled to develop competent and reliable links including effect of surrounding environment and antenna. The wireless channel for WBANs can be classified as: around the body (around), within the body (in-in) and from inside to outside (in-out) channel models. PL inside the human body can't be easily measured in-vivo, so the measurement and simulation has to be done in a phantom model. Recently, a considerable effort has been devoted to investigate the propagation channel inside, on and around the human body. These research can be summarized as follows. In [127], the experimental measurement and electromagnetic modeling of propagation from 418 MHz and 916.5 MHz sources placed inside human vagina was described. A propagation loss model for homogenous tissues bodies was presented in the 900 MHz-3 GHz range [128]. In [30], a channel model for WBAN at 400 MHz, 900 MHz and 2.4 GHz bands was derived in the case of around the body channel model. An experimental investigation of UWB on-body propagation was presented [68]. In [29], a numerical and experimental investigation to study the radio channel characteristics of communication link inside and outside the body with transmitter placed in body organ at UHF, MICS and ISM bands were introduced. The radio wave propagation around the whole body was investigated by measuring electromagnetic waves near the torso and derived relevant statistics [129, 130]. In [82],a new empirical PL model for wireless communication at 2.4 GHz above a flat lossy medium was presented and this model is valid for dipole antenna. The UWB on-body radio channel modeling using a sub-band FDTD method and a model combining the Uniform geometrical Theory of Diffraction (UTD) and ray trajectory was presented [69]. In [70], radio wave propagation in the human head was investigated at UWB frequency using theoretical analysis and measurement. On-body propagation channel measurement using two micro-strip patch antennas for various links were presented and statistically analyzed [131]. In [35], galvanic coupling was presented as a promising approach for wireless intra-body communication between on-body sensor. The human body was characterized as a transmission medium for electrical current by means of numerical simulation and measurement. The implanted antenna and human body as a medium for wireless communication

were discussed over MICS band [132]. In [96], a numerical and experimental investigation of biotelemetry radio channel and wave attenuation in human subjects with ingested wireless implants was investigated at UHF, MICS and ISM bands. An analysis of radio channel characteristics for single and multiple antenna body worn system for use in body-to-body communication was presented at ISM band [133]. In [25], the theory of wave propagation near a surface was reviewed with an eye to gain insight into the mechanisms involved and to provide analytical based model for power efficient on body propagation. The radio wave propagation between two half wavelength dipole at ISM band, placed near the human body was discussed and presented as an application for cross layer design in order to optimize the energy consumption of different topologies [32]. In [134], the first analytical model of WBAN channel was presented using simulation and measurement with a PIFA antenna. The wave propagation in WBAN was analytically modeled as a polarized point source close to an elliptic lossy dielectric cylinder at 915 MHz and 2.4 GHz bands [22].In [27], the propagation channel for intra-body communications between implanted medical devices using simulation at MICS, ISM and UWB bands was investigated. A statistical channel model was presented for UWB propagation channel inside human chest in the 1.6 GHz range [135]. In [136], a new challenge in the area of wireless communication network, which is the need for statistical model describing the terminal behavior to operate under a variety of standards and in a close electromagnetic environment perturbed by a variety of disturbance was explored. A statistical model for UWB propagation channel inside the human chest was extended in the 1.6 GHz range by including the frequency dependent attenuation [137]. In [138, 139] an analytical model for estimating the link loss for the on-body wave propagation around the torso was presented. The on-body propagation performance measured totally wireless with monopole antenna was presented in the 867 MHz range [140]. In [141], a channel model for time variant multi-link WBAN was proposed. An evaluation on how Norton waves can be used to analytically model the on-body propagation channel for WBAN in the range 0.4 to 60 GHz [142]. In all the previous works, the propagation channel at all the allowed frequency bands were not investigated. Also in the case of WBAN, the implanted antenna plays an important role in the propagation channel. In this work, the intra and inter-body propagation channel inside the human body models will be investigated using ECLA at the allowed frequency bands.

1.5 Overview of the Dissertation

The Dissertation is organized into six chapters. The first chapter provides a brief background of WBAN and literature review of previous works on implanted antenna and channel model for WBAN. Since the present research is principally based on magnetic field antenna, Chapter 2 provides a comparison between the performance of ideal electric dipole (electric field antenna) and ideal magnetic dipole (magnetic field antenna) in a lossy medium. This comparison is based on power loss and power radiated inside the lossy medium using theoretical analysis and simulation. Chapter 3 describes our proposed ECLA as a magnetic field antenna. Also, it investigates the performance of ECLA inside different human body models at all the allowed frequency bands. Chapter 4 discusses the channel models between implanted antennas inside different human body models using our proposed ECLA. Also it provides the channel model between implanted and wearable antenna. The channel model is described using PL. Wireless Power Transfer (WPT) for implanted devices inside different human body models using square and circular ECLA will be described in Chapter 5. Chapter 6 summarizes and concludes the dissertation as well as suggesting future work.

Chapter 2

Electrically Small Antenna in a Lossy Medium

In this chapter, the near-field radiation characteristics of electric and magnetic antennas when surrounded by a lossy dielectric medium are described. This study is relevant for cases such as implanted antennas, submarine or underground communications where the antenna's near-field consists of lossy dielectric media such as human tissues, minerals or saline water. Theoretical results for both types of small antennas are presented and expressions to show the difference in stored energy and radiated power in the radian sphere around the antenna are formulated. These "ideal" results are then validated using simulation results from a center-feed small dipole and a small loop antenna as a dual of magnetic dipole. It is found that magnetic antennas give much better performance when surrounded by a lossy dielectric [143].

2.1 Introduction

The study of the near-field of antennas is of great significance in applications where the antenna is located next to or inside a lossy medium because the medium properties can greatly alter the performance of the antenna while themselves being subject to effects such as dielectric heating and magnetization. This is typically the case for antennas near the human body [89], soil [144], a submarine [145], or other lossy media. In order to reduce the time-to-market, an antenna designer may choose a simple design; however, this choice needs to take into consideration the nature of the surrounding medium. It will be shown that antenna performance in a lossy medium is directly linked to whether it has a dominant electric or magnetic field intensity in the near-zone. This chapter focuses on the specific case of how antennas in implanted medical devices are affected by the presence of the human body.

The demand for smart implanted medical devices has been growing exponentially during the last few decades [31, 146]. Most modern implanted devices are able to receive commands from the outside world or relay information from various sensors within the host body. Thus, it can be

seen that implanted antennas will play a significant role in the future of healthcare technology. However, there are many challenges involved in the design of implanted antennas, including but not limited to: antenna miniaturization, antenna loss due to miniaturization (structural loss), radiation loss that manifests itself in the immediate near-field (environmental or near-field loss), compatibility with the human tissues, detuning, etc. The goal of this chapter is to investigate losses that arise inside a conductive medium (such as the human body) due to the strong reactive and radiating near-field for two main classes of small antennas: electric antennas and magnetic antennas.

Previous research by Wheeler [147] , Chu [148], Harrington and others [149-151] has focused on the physical limitations of antennas with regard to size, gain, directivity, quality factor, and the interdependence of these quantities. References [152] and [153] have investigated antennas surrounded by a lossy or conducting medium, but with a focus on finding optimal values for antenna gain and radiation efficiency. To the best of the authors' knowledge, a study of the effect of the surrounding lossy media in the near-field based on the type of antenna has not been conducted before. This issue, with a focus on electrically small antennas [154], is addressed at length in this chapter by computing the power loss and radiated power for electric and magnetic antennas. Especially in the case of implanted devices, the power that is lost in the near-field goes into heating human tissues needs to comply with standards set by government agencies.

Through analytical expressions and simulations, the case for magnetic antennas will be made by comparing the power dissipated in the lossy medium and the radiated power for electric and magnetic antennas. In the next section, antenna gain, loss and efficiency particularly for small antennas in lossy media, will be described. In Section 2.3, some theoretical work to support our arguments is presented, followed by simulation results in Section 2.4. Chapter summary will be provided in Section 2.5.

2.2 Small Antenna Gain, Loss and Efficiency

The electric size of a small antenna is related to its quality factor based on the fundamental limits of the antenna [151],

$$Q_{lossless} = \frac{1}{(ka)^3} \tag{2.1}$$

where a is the radius of the smallest sphere enclosing the antenna (Figure 2.1) and k is the wave number. The quality factor of a lossy medium (loaded quality factor) is related to the lossless quality factor,$Q_{lossless}$, by the antenna efficiency η as:

$$Q_{loaded} = \frac{\eta}{(ka)^3} \Longrightarrow \eta = Q_{loaded} * (ka)^3 = \frac{Q_{loaded}}{Q_{lossless}} \tag{2.2}$$

Q_{loaded} has an equivalent circuit definition for narrow band antenna which can be easily measured as [155],

$$Q_{loaded} = \frac{1}{2}\frac{f_u + f_l}{f_u - f_l} \tag{2.3}$$

where, $f_u \ and \ f_l$ are the upper and lower 3dB crossing frequencies of the return loss of the antenna, respectively.

Small antennas converge to either a small electric dipole, magnetic dipole, or a combination of these two when the electric size of the antenna is much smaller than 1 radian ($ka < 1$); therefore, one can assume the directivity of any small antenna approximately equals 3/2, which is a directivity of a small dipole (the dominant far-field spherical modes are either $TE_{10} \ or \ TM_{01}$). Using the above equation, one can find an approximate value for Gain, G, and efficiency, η, of a small antenna by knowing its electric size and 3dB quality factor as,

$$D = \frac{3}{2}, \quad \eta = Q_{loaded} * (ka)^3 \Longrightarrow G = \frac{3}{2} Q_{loaded} * (ka)^3 \tag{2.4}$$

Realized Gain of antennas directly effects the total path loss in a communication link. In addition to polarization mismatch and impedance match, there are three different loss mechanisms that control the path loss of a communication link: structural loss, of the antenna, near-field loss and plane wave path loss.

2.2.1 Structural Loss

The structural loss of an antenna, which is converted to thermal energy, can be seen as the ohmic and dielectric losses of the antenna structure itself regardless of whether the antenna is surrounded

by free space [156], lossy media, or any other type of medium (see Figure 2.1). Reference [157] approaches this problem for optimizing maximum gain. Unlike electrically large antennas such as reflectors, structural loss is an important factor in the overall loss of electrically small antennas [147, 154]. These losses can be minimized during the antenna design stage. If the antenna is made of a Perfect Electric Conductor, PEC, and perfect dielectric material, the structural loss of an antenna can theoretically go to zero. The antenna still might have return loss which is not converted to further thermal energy. Structural and mismatch losses are not considered in this study.

2.2.2 Near-Field Loss

The reactive near-field of an antenna is strongly coupled to the current distribution on the antenna structure. Therefore, any disturbance in the reactive near-field will affect the current distribution and input impedance of the antenna. If the antenna is surrounded by a lossy material, the reactive near-field will contribute to the antenna overall loss. The loss associated with the reactive near-field of the antenna, which is converted to thermal energy in the surrounding material, is termed environmental or near-field loss in this chapter. There are some limits on the amount of thermal energy generated by an implanted transmitter which are set by regulatory bodies such as FCC and ERC which is usually characterized by SAR [158, 159]. The question is how does the antenna type affect the total radiated power for a given antenna size while still satisfying the FCC limits? Results of an investigation into this problem are studied in this chapter.

2.2.3 Path Loss

It is well known that the radiated fields of any antenna in the far-zone is a locally plane wave. For a plane wave, the ratio of electric field to the magnetic field is dictated by the material properties in the far-field and not the antenna type. However, the ratio of total electric field over the total magnetic field in the reactive near zone of a small antenna can vary from a very small number (0 for a magnetic point source at the origin) to a very large number (infinity for an electric point source at the origin). Thus, it is clear that the reactive near-field of a small antenna can vary dramatically from one antenna type to another based on the radiation mechanism. Since the reactive near-field of a small antenna is strongly coupled to the antenna structure, it is beneficial to define antenna loss in the reactive near zone as an antenna-dependent environmental loss which can be distinguished from the structural loss mentioned above. At the same time, one can

distinguish the near-field environmental loss from the path loss which usually deals with plane waves (far-field) and will be independent of the antenna type.

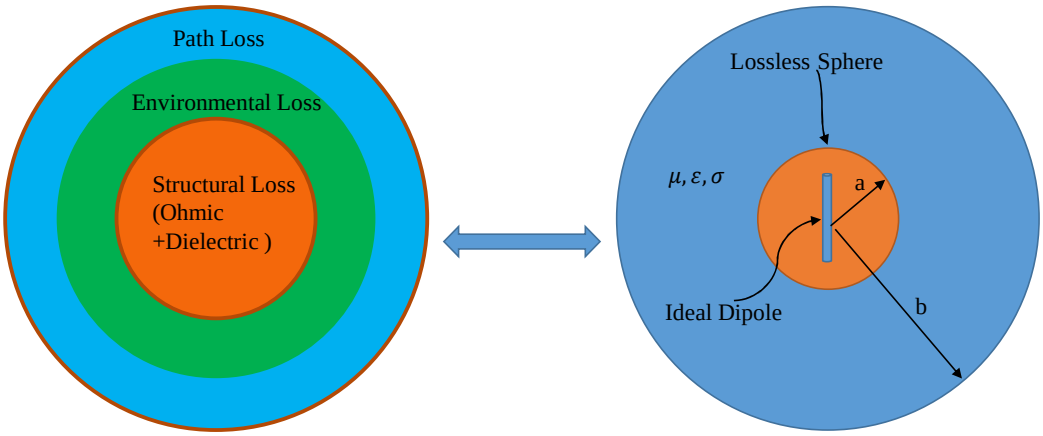

(a) (b)

Figure 2.1: Antenna in a lossy medium (a) antenna loss and (b) ideal dipole in a lossy medium.

2.3 Theoretical Analysis

For simplicity, two ideal dipoles (an electric dipole and a magnetic dipole) will be analyzed in a homogeneous lossy medium with a finite conductivity. The exact total field of these two antennas can be found analytically, and therefore, one will be able to compare their near-field stored energy, radiated power and dissipated power in the closed form. This analysis allows us to study the behavior of small antennas in a lossy medium without concerning ourselves with the antenna design, mismatch issues, and the antenna structural loss.

Consider a homogeneous medium with permittivity, permeability and conductivity of ε, μ, and σ respectively. An electric (magnetic) dipole of length Δz , carrying a uniform current I (M) in the z direction is located at the origin. One can find the electric and magnetic fields of these dipoles as:

$$\left\{ \begin{array}{l} \boldsymbol{E}_M = \frac{\Delta z M(1+\gamma r)e^{-\gamma r} sin\theta}{4\pi r^2}\left[0\hat{r}, 0\hat{\theta}, 1\hat{\varphi}\right] \\ \boldsymbol{H}_M = \frac{j\Delta z M e^{-\gamma r}}{4\pi\mu\omega r^3}\left[2(1+\gamma r)\cos\theta\,\hat{r}, (1+\gamma r+\gamma^2 r^2) sin\theta\,\hat{\theta}, 0\,\hat{\varphi}\right] \end{array} \right\} \quad (2.5)$$

$$\left.\begin{cases} \boldsymbol{E}_E = \frac{j\Delta z\mu\omega I e^{-\gamma r}}{4\pi r^3\gamma^2}[2(1+\gamma r)\cos\theta\,\hat{r}, (1+\gamma r+\gamma^2 r^2)sin\theta\,\hat{\theta}, 0\,\hat{\varphi}] \\ \boldsymbol{H}_E = \frac{\Delta z I(1+\gamma r)e^{-\gamma r}sin\theta}{4\pi r^2}\left[0\hat{r}, 0\hat{\theta}, 1\hat{\varphi}\right] \end{cases}\right\} \tag{2.6}$$

where,

$$\gamma = \alpha + j\beta = \sqrt{j\omega\mu(j\omega\varepsilon+\sigma)} \tag{2.7}$$

with,

$$\beta = \omega\sqrt{\frac{\mu\varepsilon}{2}}\sqrt{1+\sqrt{1+(\frac{\sigma}{\omega\varepsilon})^2}} \tag{2.8}$$

$$\alpha = \omega\sqrt{\frac{\mu\varepsilon}{2}}\sqrt{-1+\sqrt{1+(\frac{\sigma}{\omega\varepsilon})^2}} \tag{2.9}$$

The electric field intensity is proportional to the inverse of r^2 for the magnetic dipole in the near-zone while it is proportional to the inverse of r^3 for the electric dipole. It means that $\mathbf{E}\cdot\mathbf{E}^*$ in the near-zone is proportional to $1/r^4$ and $1/r^6$ for magnetic and electric dipoles, respectively. Therefore, the ohmic loss associated with conductance, σ, of the medium will be higher for an electric dipole in comparison to a magnetic dipole.

In order to proceed with these calculations, the input impedances of the antennas need to be found to be able to feed both antennas with the same amount of power. Since the surrounding lossy dielectric loads the antennas in different fashions, the antenna impedances will not be similar to its respective free space input impedance. At the same time, a finite thickness for both dipole antennas would need to be included to avoid field singularities, and consequently, numerical solutions are required to proceed. However, there is an alternative way to compare the performance of these two antennas in a lossy medium. To avoid impedance computation and field singularities, we assume that the antenna is located in an imaginary small sphere of radius a that just encloses the antenna and generates the same field distribution outside of that sphere as the ideal dipole in a homogeneous medium (see Figure 2.1). As mentioned in Section 2.2, we omit the stored energy

and any loss inside the small sphere of radius a as it represents the antenna's structural loss, similar to the assumptions made by Chu in [148].

The electromagnetic power lost in a homogeneous lossy dielectric spherical shell with an inner radius of a and an outer radius of b is computed as:

$$L^{a,b} = \int_0^{2\pi}\int_0^{\pi}\int_a^b \frac{1}{2}\sigma \boldsymbol{E}(r).\boldsymbol{E}^*(r) r^2 sin\theta d_r d_\theta d_\varphi \tag{2.10}$$

It is worth noticing that the electric energy can be computed in a fashion similar to this equation by replacing σ by $\varepsilon/2$. To show the significance of the near-zone antenna loss, we compute the antenna loss within the radian sphere $\beta b = 1$ for different a, and normalize it to the total power lost in the lossy material if it were to extend infinitely (it will be shown in the next section that the total loss is equal to the total energy passing through the sphere of radius a). The assumption is that the antenna size, $2a$, is smaller than the radian sphere which is a condition for small antennas. In the rest of this chapter, a will be used as the radius of a sphere enclosing the antenna structure.

The power lost for a magnetic dipole in a lossy medium from a to an arbitrary b is :

$$\begin{aligned} L_M^{a,b} &= \frac{\Delta z^2 M^2 \sigma}{24\pi\alpha}\left[e^{-2\alpha a}\frac{2\alpha+(\alpha^2+\beta^2)a}{a} - e^{-2\alpha b}\frac{2\alpha+(\alpha^2+\beta^2)b}{b}\right] \\ &\approx \frac{\Delta z^2 e^{-2\alpha a} M^2 \sigma[2\alpha+(\alpha^2+\beta^2)a]}{24\pi\alpha a}\Big|_{b\to\infty} \end{aligned} \tag{2.11}$$

The normalized power loss for magnetic dipole will be:

$$\frac{L_M^{a,b}}{L_M^{a,\infty}} = 1 - \frac{a e^{-2\alpha(b-a)}[2\alpha+(\alpha^2+\beta^2)b]}{b[2\alpha+(\alpha^2+\beta^2)a]} \tag{2.12}$$

The power lost for an electric dipole in a lossy medium from a to an arbitrary b is :

$$L_E^{a,b} = \frac{\Delta z^2 I^2 \mu^2 \sigma \omega^2 e^{-2\alpha(a+b)}}{24\pi\alpha a^3 b^3(\alpha^2+\beta^2)^2}[b^3 e^{2b\alpha} f(\alpha,\beta,a) - a^3 e^{2a\alpha} f(\alpha,\beta,b)]$$

$$\approx \frac{\Delta z^2 I^2 \sigma \omega^2 e^{-2\alpha a} f(\alpha,\beta,a)}{24\pi\alpha a^3(\alpha^2+\beta^2)^2}\Big|_{b\to\infty} \tag{2.13}$$

The normalized power loss for electric dipole will be:

$$\frac{L_E^{a,b}}{L_E^{a,\infty}} = 1 - \frac{a^3 e^{-2\alpha(b-a)} f(\alpha,\beta,b)}{b^3 f(\alpha,\beta,a)} \tag{2.14}$$

where,

$$f(\alpha,\beta,r) = 2\alpha + 4\alpha^2 r + 2\alpha(\alpha^2+\beta^2)r^2 + (\alpha^2+\beta^2)^2 r^3 \tag{2.15}$$

These ratios (2.12) and (2.14) are plotted in Figure 2.2. for a typical muscle tissue at 403 MHz, 2.4 GHz and 3.5 GHz (for material properties see [160]) as a function of a for an electric dipole and a magnetic dipole in a radian sphere ($\beta b = 1$) for each frequency. As Figure 2.2(a) shows, almost 91% of the power is dissipated in the radian sphere (b = 14.5 mm) for the electric dipole with $a = 5\,mm$ (antenna size 10 mm). This ratio is 60% for a magnetic antenna. It will be shown that outside of two radian spheres ($b = 2/\beta$), the wave impedance approaches intrinsic impedance of the medium and the antenna type does not affect the loss dramatically in this region.

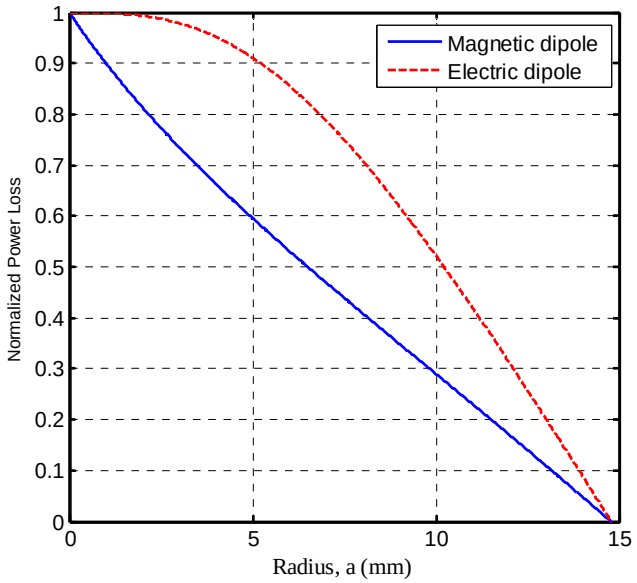

(a)

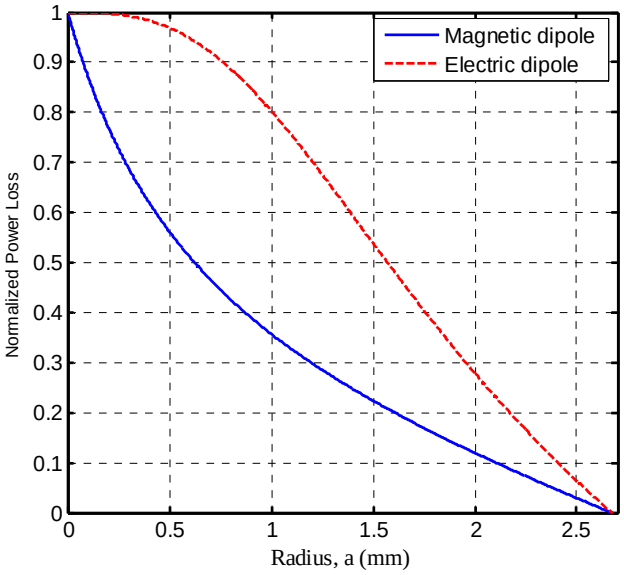

(b)

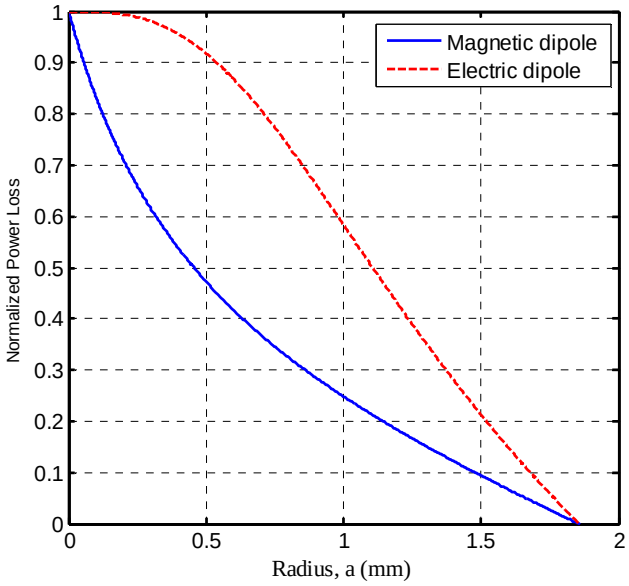

(c)

Figure 2.2: Normalized power loss for muscle tissue inside radian sphere (a) with radius 14.5 mm at 403 MHz (b) radius 2.7 mm at 2.4 GHz and (c) radius 1.9 mm at 3.5 GHz.

In addition to the electromagnetic loss due to σ, the Poynting vector variations can also be computed. One can find the real part of the radiated power passing through a sphere of radius r as:

$$P^{rad}(r) = \int_0^{2\pi} \int_0^{\pi} \frac{1}{2} R_e[\boldsymbol{E} \times \boldsymbol{H}^*] \cdot \hat{r} r^2 sin\theta d_\theta d_\varphi \tag{2.16}$$

The total radiated power of these antennas would be equal for a lossless medium (σ = 0) if

$$M = z_0 I \tag{2.17}$$

where z_0 is the intrinsic impedance of the lossy material in which the antenna is placed. To compare the radiation performance of ideal magnetic and electric dipoles in a lossy material, one can compute the real part of the radiated power passing through a sphere of radius r as:

$$P_M^{rad}(r) = \frac{\Delta z^2 e^{-2\alpha r} M^2 \beta [2\alpha + (\alpha^2+\beta^2) r]}{12\pi\mu\omega r} \approx \frac{\Delta z^2 e^{-2\alpha r} M^2 (\alpha^2+\beta^2)\beta)}{12\pi\mu\omega}\Big|_{r\to\infty} \tag{2.18}$$

$$P_E^{rad}(r) = \frac{\Delta z^2 e^{-2\alpha r} I^2 \beta\mu\omega}{12\pi r^3 (\alpha^2+\beta^2)^2} f(\alpha,\beta,r) \approx \frac{\Delta z^2 e^{-2\alpha r} I^2 \beta\mu\omega}{12\pi}\Big|_{r\to\infty} \tag{2.19}$$

To make a fair comparison between these two antennas, the radiated power needs to be normalized to the input power. As we ignore the effects of structural and mismatch losses in this study, we will define input power as the total real power that passes through a sphere of radius a. As the medium in which the antenna resides is lossy, the entire input power will be absorbed when $b \to \infty$ (or in the far-field).

$$\frac{P_M^{rad}(r)}{L_M^{\infty}(a)} = \frac{e^{-2\alpha(r-a)} a [2\alpha + (\alpha^2+\beta^2) r]}{r [2\alpha + (\alpha^2+\beta^2) a]} \tag{2.20}$$

$$\frac{P_E^{rad}(r)}{L_E^{\infty}(a)} = \frac{e^{-2\alpha(r-a)} a^3 f(\alpha,\beta,r)}{r^3 f(\alpha,\beta,a)} \tag{2.21}$$

Equations (2.20) and (2.21) provide the total radiated power passing through a sphere of radius r normalized to the input power for magnetic and electric ideal dipoles, respectively. The normalized power is plotted versus antenna size ($2a$) and distance r, inside a lossy dielectric, which has the properties of the muscle tissue at 403 MHz (Figure 2.3.). Figure 2.3 demonstrates the superior performance of a magnetic antenna in comparison with electric antenna with the same

size and the same accepted power. The difference between the two antennas increases at small antenna size.

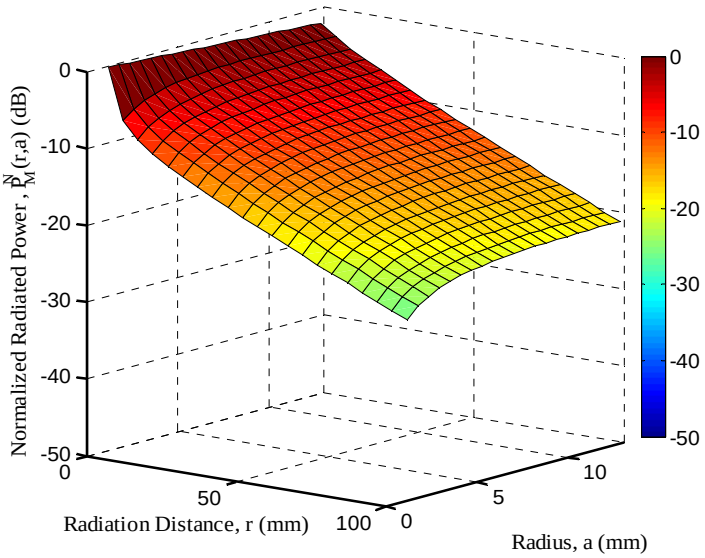

(a)

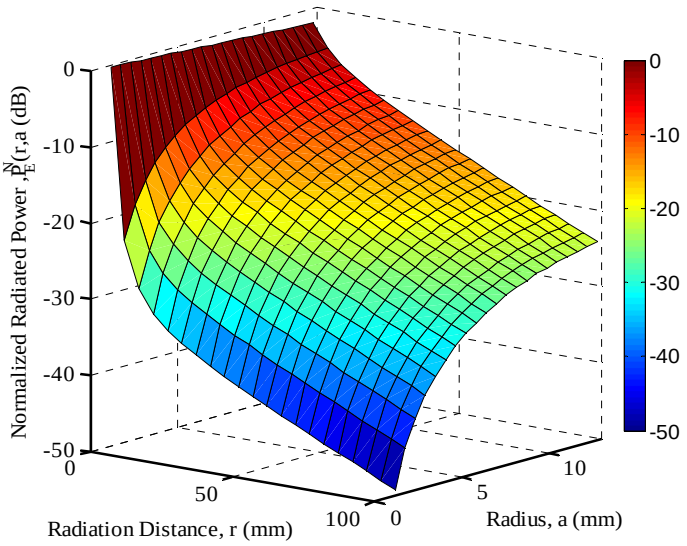

(b)

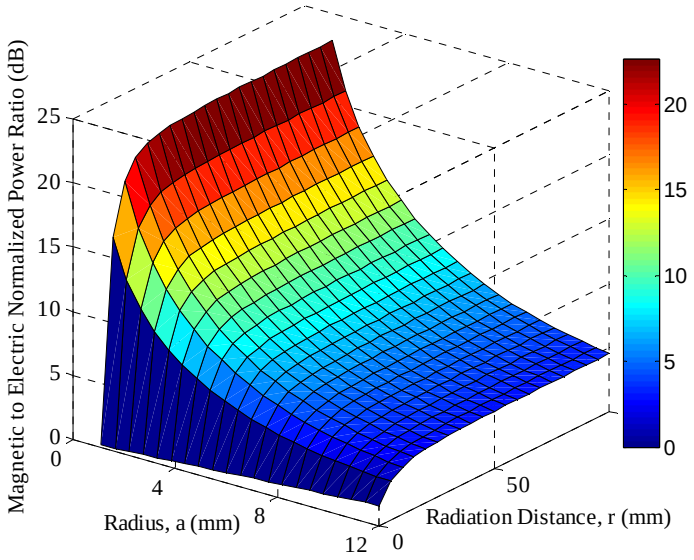

(c)

Figure 2.3: Normalized radiated power inside muscle tissue at 403 MHz for (a) magnetic dipole, (b) electric dipole and (c) differences.

The ratio of the normalized radiated power of both antennas for different value of a can be expressed as:

$$\frac{\frac{P_M^{rad}(r)}{L_M^{\infty}(a)}}{\frac{P_E^{rad}(r)}{L_E^{\infty}(a)}} = \frac{r^2 f(\alpha,\beta,a)[2\alpha+(\alpha^2+\beta^2)r]}{a^2 f(\alpha,\beta,r)[2\alpha+(\alpha^2+\beta^2)a]} \approx 1 + \frac{2\alpha(1+2\alpha a)}{a^2(\alpha^2+\beta^2)[2\alpha+(\alpha^2+\beta^2)a]}\Big|_{r\to\infty} \tag{2.22}$$

This ratio at fixed value of $r = 100\,mm$ and variable antenna size for 3 different human body tissues at the allowed frequency bands are shown in Figure 2.4. This figure shows that the radiated power from an ideal magnetic dipole is always more than that of an electric antenna with the same size and the same accepted power and this ratio increases at small antenna size.

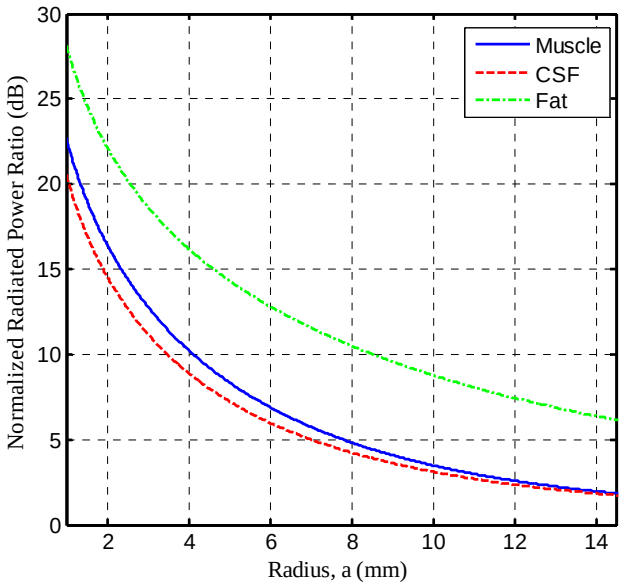
Muscle
CSF
Fat
Normalized Radiated Power Ratio (dB)
Radius, a (mm)
0
5
10
15
20
25
30
2
4
6
8
10
12
14

(a)

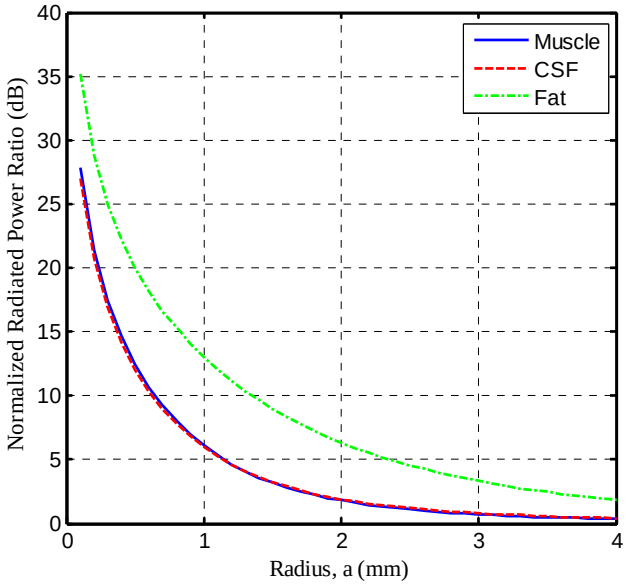
Muscle
CSF
Fat
Normalized Radiated Power Ratio (dB)
Radius, a (mm)
0
5
10
15
20
25
30
35
40
0
1
2
3
4

(b)

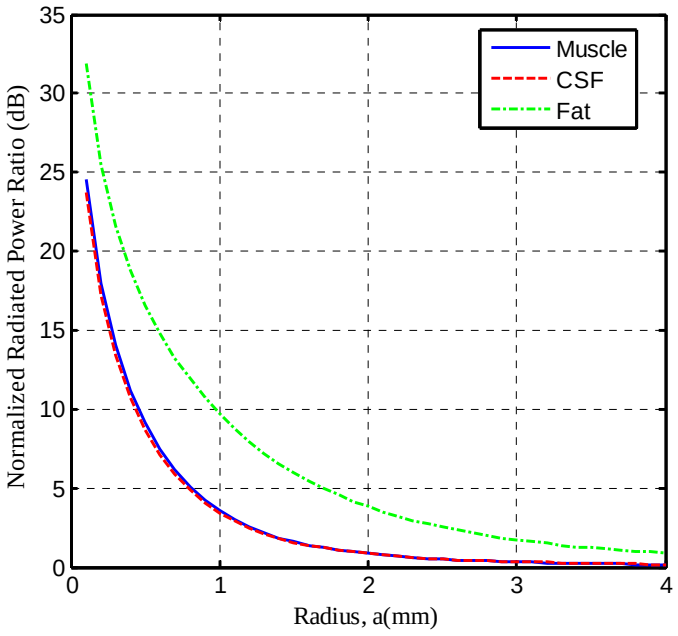

(c)

Figure 2.4: Normalized radiated power ratio for various tissues vs. antenna size at (a) 403 MHz (b) 2.4 GHz and (c) 3.5 GHz.

2.4 Simulation Results

In order to validate the theoretical results using full-wave simulations, a dipole antenna (electric field antenna) with a length of 0.5 mm and a rectangular loop antenna (magnetic field antenna) with the length of its diagonal as 0.5 mm were simulated using FEKO as shown in Figure 2.5. These sizes are chosen in order to ensure an electrically small antenna. These antennas are surrounded by a homogeneous medium that has properties of a lossy dielectric mimicking human muscle tissue at 403 MHz (for tissue properties see [160]). Here, a is the radius of the sphere enclosing the antenna as discussed previously in Sections 2.3 and 2.4 and this sphere can be assumed to be the antenna size. To remove the effects of any structural or mismatch loss from these computations, the total radiated power passing through an imaginary sphere of radius a is considered to be the total input power to the antenna (similar to the input power computation for the theoretical formulation) while keeping the size of the physical antennas the same (so as to ensure that the electrically small criterion is met as well as to prevent excitation of higher order modes in a larger antenna). The sphere radius a was varied from 1 mm to 14 mm in order to facilitate a comparison with the theoretical results. The total radiated power at various distances from $r = a$ to a maximum distance of $r = 100\,mm$ is computed for both antennas and it is

normalized to the input power (power at $r = a$). Then the ratio of the normalized radiated power for both antennas is computed for different radii of the imaginary sphere (which is considered to represent the antenna size). For various values of a and r, this ratio is plotted in Figure 2. 6. Clearly, from Figure 2.6., simulation results for normalized power agree well with the theoretical predictions in trend if not their absolute values. This can be compared to Figure 2.3., for muscle tissue for validation.

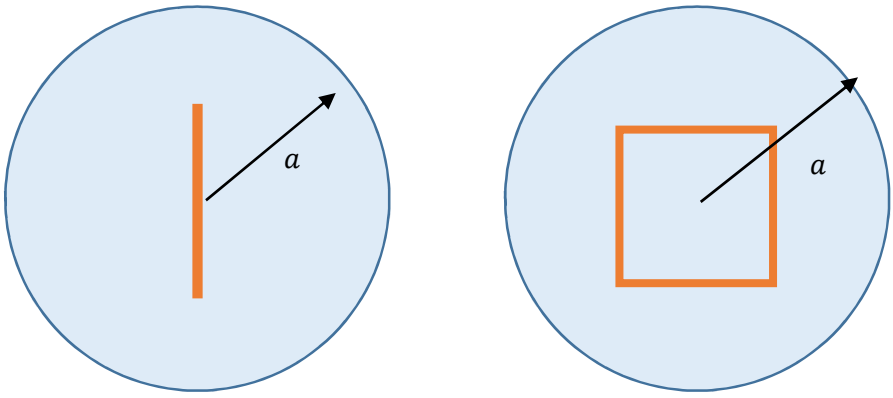

(a) (b)

Figure 2.5: Small antenna simulation (a) small dipole and (b) small loop antennas.

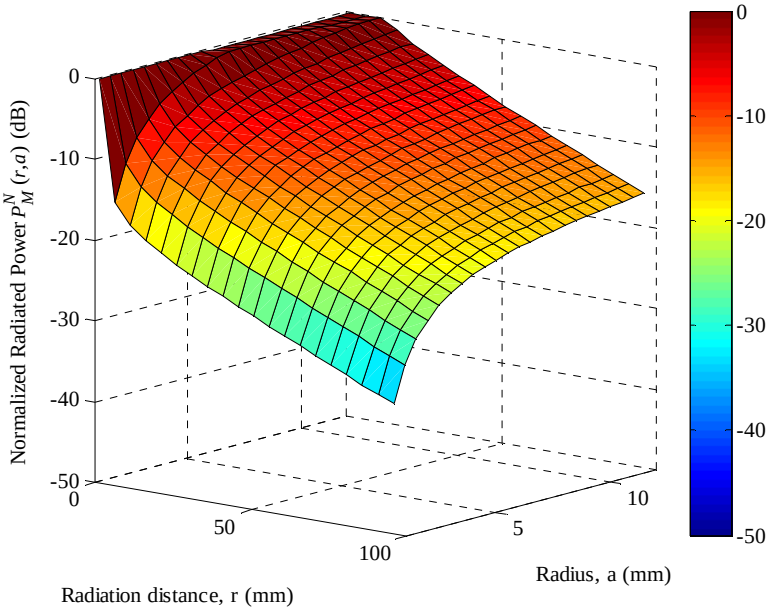

(a)

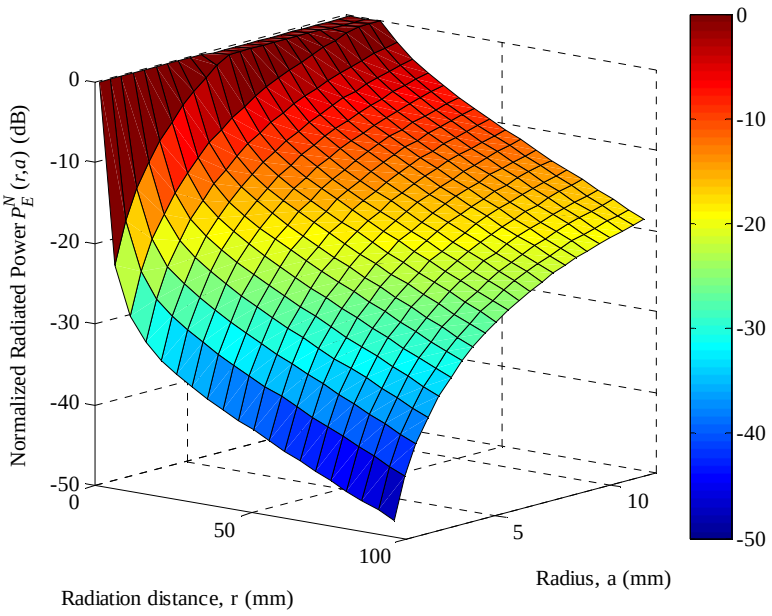

(b)

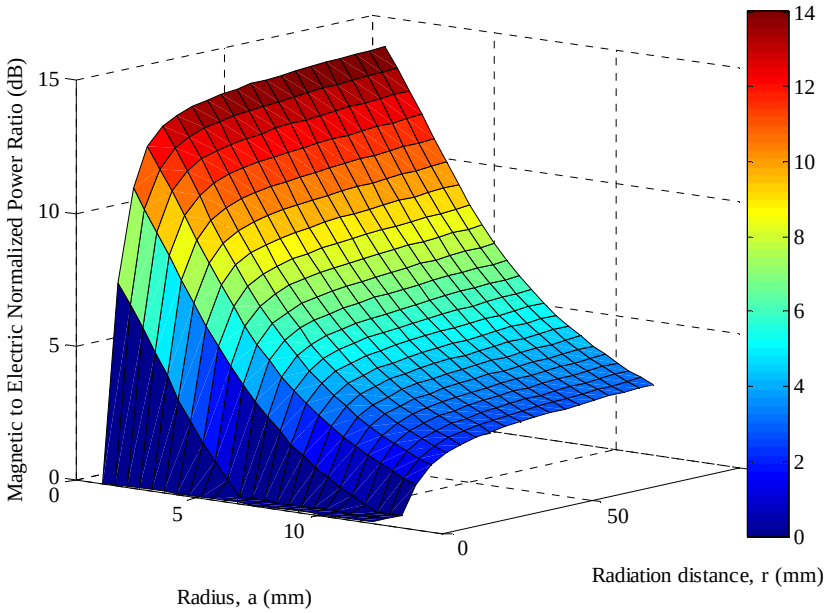

(c)

Figure 2. 6: Simulated results for normalized radiated power ratio, $P^{(N)}(r,a)$, inside muscle tissue at 403 MHz for (a) loop antenna and (b) electric dipole. (c) Ratio of values shown in (a) to (b).

In Figure 2.7, a comparative plot shows a side-by-side comparison between theory and simulation results. It can be seen that, as the antenna size becomes smaller, the difference between the two types of antennas becomes more significant which is in agreement with our theoretical results. However, a deviation from the theoretical results can also be noticed for smaller values of a. This is due to the fact that within close proximity to the loop antenna, it does not behave as a perfect magnetic dipole. Instead, we see a large contribution due to the voltage source that excites the structure. Thus, since the simulation results are not generated for the exact same antennas as the theoretical effort, the results follow the same behavior. A simulation with ideal dipoles in FEKO showed very close agreement to theoretical results for all values of a, as expected.

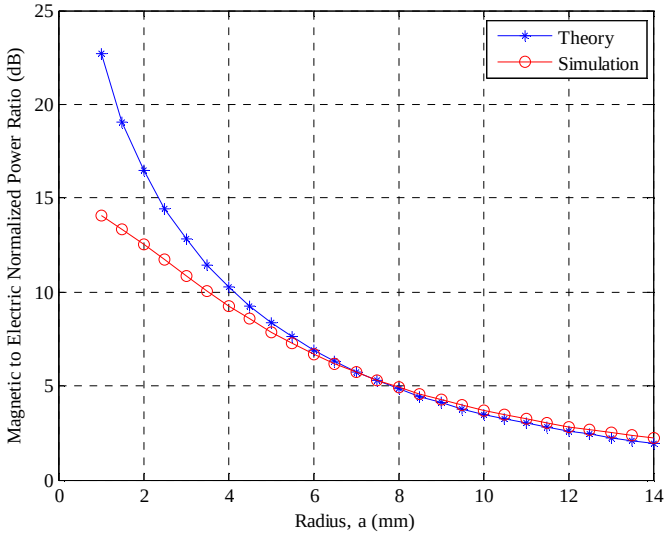

Figure 2.7: Comparison between theoretical and simulated results for normalized radiated power ratio, $P^{(N)}(r,a)$, inside muscle tissue at 403 MHz at r = 10 cm.

2.5 Chapter Summary

It can be seen that there is a fundamental difference in the near-field ohmic loss generated within a lossy medium surrounding electric and magnetic antennas. For electrically small antennas, this loss is more pronounced. Theoretical results were presented and later validated through simulation in a full wave simulator using small dipole and loop antennas. In conclusion, it is clear that magnetic antennas such as the loop antenna and/or its variants offer a significant advantage when compared to electric field antennas such as the dipole, PIFA, patch and others in terms of power

lost in dielectric media surrounding the antenna. Thus, for implanted applications where we have stringent regulations on SAR and where maximum efficiency is required (such as wireless power transfer to medical devices), it makes more sense to use efficient magnetic antennas. Even for magnetic antennas, one must choose a design that minimizes structural losses. ECLA is a self-matched high-Q resonator that can be conveniently engineered to suit different applications.

Chapter 3

Electrically Coupled Loop Antenna

The implanted antenna needs to be extremely small while maintaining a permissible SAR and being able to cope with the detuning effects due to the dielectric properties of human body tissues. This chapter is devoted to design a miniaturized magnetic field antenna to achieve the above requirements. The proposed ECLA has a high magnetic field and a low electric field in the near-zone and therefore, has a small value of SAR and is less sensitive to detuning effects. ECLA is designed for the MICS, ISM and 3.5 GHz (3.55-3.65 GHz) bands with dimensions of (5×5×3 mm^3), (3x3x3 mm^3) and (2x2x2 mm^3). These antennas will then be simulated inside one-layer human body model, three-layer spherical human head model, human head and human body. Also, a wearable ECLA with dimensions (20x20x5 mm^3) is simulated inside one-layer model. A comparison between ferrite-loaded ECLA and regular ECLA with the same dimensions will be investigated. At the end of the chapter, the simulation results are validated using experimental work. From the simulation results, ECLA inside the human body has a 5 MHz -3 dB bandwidth, -14 dB gain, and radiation efficiency of 0.525%. The 1g average SAR inside the human body for 10 mW input power is about 1 W/kg which is 7 times lower than a patch antenna of the same size. Also, the ECLA with ferrite beads has better performance compared to ECLA without a ferrite load of the same dimensions [21, 161].

3.1 Introduction

Implanted antennas inside human or animal bodies are widely used in biomedical telemetry (biotelemetry) and therapy applications. In biotelemetry, the implanted antennas are used to transmit power into or out of the host body. However, in therapy applications, the implanted antennas are used to provide energy as cancer treatment using hyperthermia applications [90].

The common frequency bands for implanted antennas, approved by FCC and ERC are MICS, ISM and 3.5 GHz bands [162]. The choice of the frequency band decides the implanted antenna size and power loss inside the host body. The antennas operating at the MICS band have lower power loss and larger antenna size, while on the other hand, the ISM and 3.5 GHz bands devices use smaller antennas having higher loss [19].

The design of an implanted antenna involves many challenges including biocompatibility, miniaturization, detuning effects of human body tissues, and patient safety [18, 89]. The implanted antenna must be biocompatible to prevent a short circuit which can occur due to the high conductivity of the human body tissues and to prevent rejection of the implanted antenna by the host body. To achieve biocompatibility, the implanted antenna should be surrounded by a biocompatible insulation layer such as PEEK, MACRO or Ceramic alumina [163]. The electrical properties of the human body tissues can change the resonant frequency of the implanted antenna. Therefore, the implanted antenna should be as robust as possible versus detuning effects. The antenna size has to be extremely miniaturized to satisfy the implanted devices requirements at the MICS band where the wavelength is about 750 mm. For the patient's safety, the power loss inside the human body, which is measured by SAR, should be minimized. According to the FCC and ERC, the maximum limits for SAR averaged over 1 g and 10 g of tissue mass is 1.6 and 2 W/kg respectively as explained in Chapter 1.

The early generations of implanted devices which used inductive coupling for communications, were able to transmit data over a range of only 2 cm [164]. Most of the previous investigations on implanted antenna described in Chapter 1, suffer from two main problems: high value of SAR at small antenna size and detuning effects due to the electric properties of the human body tissues. An ECLA is proposed in this chapter to tackle all the above issues.

The chapter is organized as follows, the structure of ECLA will be described in Section 3.2 and the performance of ECLA in different human body models will be simulated in Section 3.3. In Sections 3.4 and 3.5, the effects of human model dimensions and the insulation layer on the value of the antenna's SAR will be investigated respectively. ECLA performance at the allowed frequency bands will be investigated in Section 3.6. Wearable ECLA and ferrite loaded ECLA will be explained in Section 3.7 & 3.8 respectively. An experimental work to validate the simulation results will be provided in Section 3.9 and chapter summary will be provided in Section 3.10.

3.2 ECLA Structure

ECLA has been introduced in [20] as a magnetic field antenna. It consists of a high impedance transmission line (inductor) terminated to a short circuit at one end and a distributed capacitor at the other end providing a distributed LC resonator. The feeding probe is electrically coupled to the antenna as well (Figure 3.1). The antenna can be tuned to a particular frequency using the antenna dimensions (L, W, and h) and the distributed capacitance between the loop and the ground plane (t_s, W_s and L_s). The dimensions of the feeding head (L_p, W_p and t_p) are responsible for scaling the input impedance of the antenna allowing us to match it to different impedances. ECLA can be extremely miniaturized by adding a lumped capacitor in parallel to the distributed capacitor of the resonant antenna. One can employ a variable capacitor to use the ECLA as a tunable antenna as well.

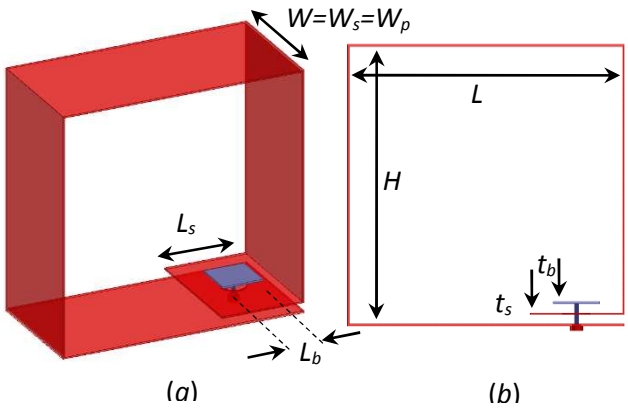

Figure 3.1: Electrically Coupled Loop Antenna, ECLA, (a) 3D view and (b) side view.

3.3 ECLA Performance inside the Human Body

The dimensions of ECLA (L, W, and h) used for the simulation in this section at MICS band are ($5\times5\times3$ mm^3), respectively. A shunt capacitor of 29 pF has been added in parallel with the distributed capacitor to reduce the resonant frequency of the antenna to 403.5 MHz. In the following subsections, the performance of the antenna will be studied inside different models of the human body.

3.3.1 ECLA inside One-Layer Rectangular Model

To study the performance and radiation characteristics of ECLA inside the human body, first a one-layer model is considered. The one-layer model reduces the size of the numerical model and allows us to optimize the antenna using HFSS (Figure 3.2) in a reasonable time. Different tissues have been used for the one-layer model (Table 3.1). The one-layer model is a ($100\times100\times100$ mm^3) cube and ECLA is located at the center of the model. To achieve compatibility between the ECLA and the human body tissues, ECLA is covered by a 1 mm-thick insulation layer (whose effects will be discussed in Section 3.5). The scattering parameter (S_{11}) of ECLA inside skin and muscle tissues are presented in Figure 3.3. Based on this figure, one can conclude that the input impedance of ECLA does not vary dramatically by changing the electrical properties of the surrounding materials. Table 3.2 shows the radiation characteristics (maximum gain, -3 dB bandwidth, efficiency and 1 g averaged SAR inside the model) of ECLA compared to the previous work of implanted antennas. This table shows that ECLA has the smallest size while still maintaining the lowest value of SAR.

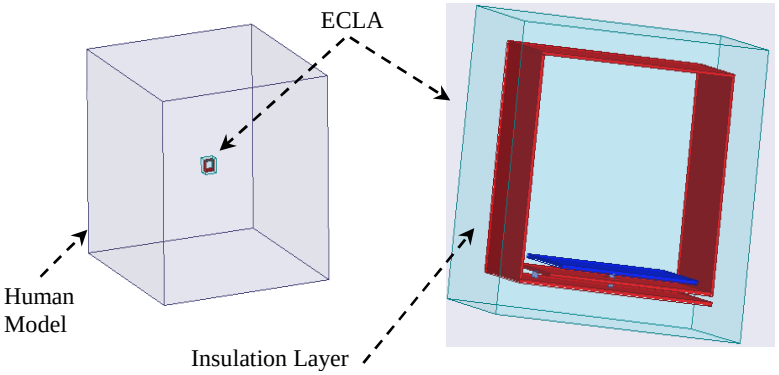

Figure 3.2: ECLA inside one-layer model of human body and magnified ECLA structure.

Table 3.1: Dielecric properties of human body tissues.

Tissue	Dielectric constant	Conductivity (S/m)	Density (kg/m^3)
Skin	47.6	0.68	1100
Muscle	53.8	1.18	1040
Fat	5.57	0.041	1000
Skull	17.8	0.16	1850
Brain	49.7	0.59	1030

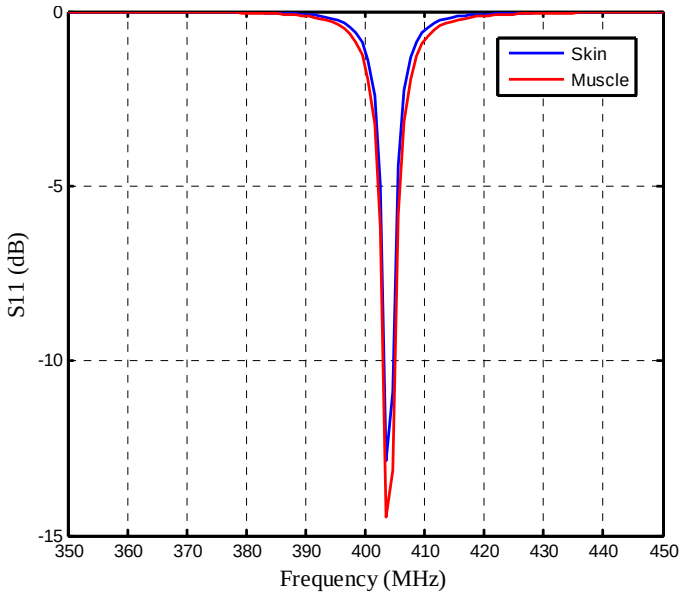

Figure 3.3: Scattering parameter (S_{11}) of ECLA inside one-layer model for skin and muscle tissues.

Table 3.2: Radiation characteristics of ECLA compared to other types of implanted antennas.

Antenna Dimensions (mm)	Gain (dB)	Bandwidth (MHz)	Efficiency (%)	SAR (W/kg)
PIFA (10×10×1.9)	-26	50	0.6	336
PIFA(8×8×1.9)	-25	122	0.55	903
PIFA(23×19×1.9)	-27	120	--	280
Micro strip (40×32×8)	--	50	0.16	180
PIFA (32×24×8)	--	70	0.25	209
Spiral PIFA (20×24×2.5)	--	--	0.34	310
Stacked PIFA(π×7.5×1.9)	-44	170	0.31	750
ECLA (5×5×3)	-14.7	5	0.4	152.8

3.3.2 ECLA inside Three- Layer Spherical Model

The next step would be simulating the optimized antenna in a three-layer model (Figure 3.4). A three-layer model is a more accurate model for the human head. The model consists of a brain layer with a radius of 85 mm and skull and skin layers with thickness of 10 and 5 mm respectively. ECLA is placed at the center of the three-layer model and simulated using HFSS. The scattering parameter (S_{11}) of ECLA inside the three-layer model is compared to those inside one-layer models of skin and muscle in Figure 3.5. This figure shows that the return loss of the antenna is the same for all three-models.

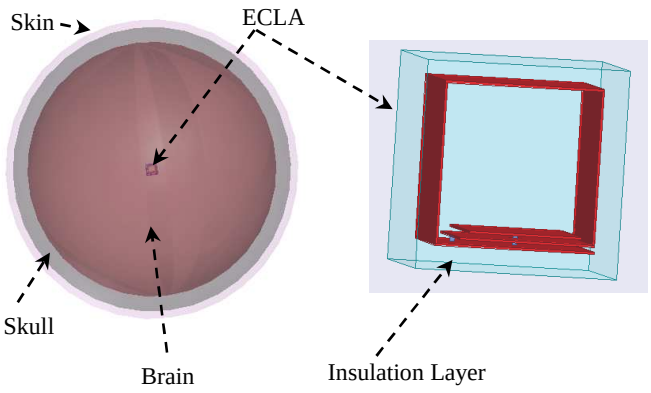

Figure 3.4: ECLA inside three-layer model of the human head and magnified ECLA antenna

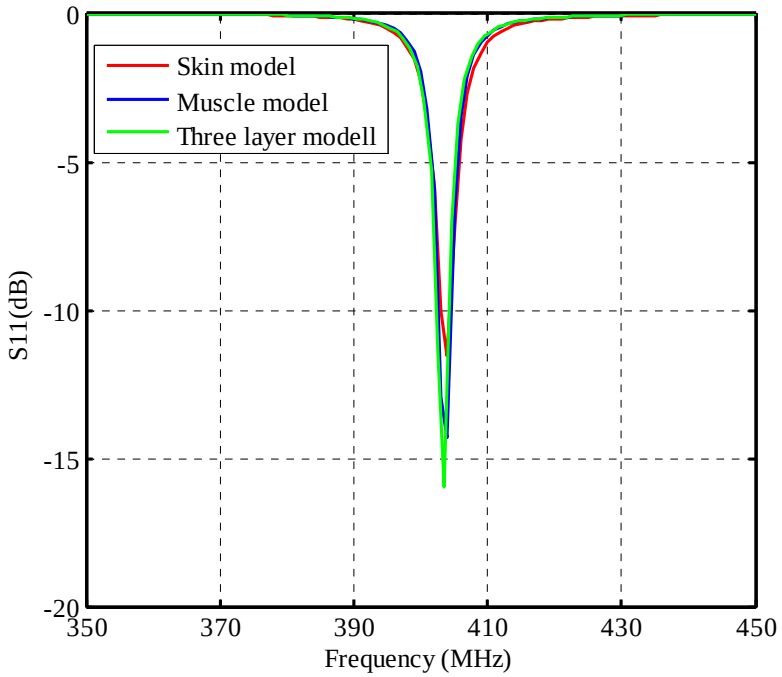

Figure 3.5: Scattering parameter (S_{11}) of ECLA inside one-layer and three-layer models.

TABLE 3.3: Radiation characteristics of ECLA inside three-layer spherical model and exact head.

Model	Gain (dB)	Bandwidth (MHz)	Efficiency (%)	SAR (W/kg)
Three-layer	-14.9	5	0.4	152
Head	-15	6	0.3	151

3.3.3 ECLA inside the Human Head

To study the performance of ECLA inside the human head, Remcom's XFDTD 7 (XF7) is employed with a model of the human head consisting of 39 human tissues. ECLA is placed at the skin tissue (2 mm from skin surface) of the model as shown in Figure 3.6. The scattering parameter (S_{11}) of ECLA inside the human head model is shown in Figure 3.7. The antenna with dimensions (5x5x3 mm^3) still has the same resonant frequency and a different value for the minimum return loss. The antenna can be matched by changing the dimensions of the feeding probe. Also, 1 g-averaged SAR values of ECLA inside the head model are shown in Figure 3.8. The radiation characteristics of ECLA inside the human head model are compared with the three-layer model in Table 3.3. From these results, one can conclude that the performance of ECLA inside the more accurate human head model is approximately the same as the three-layer model.

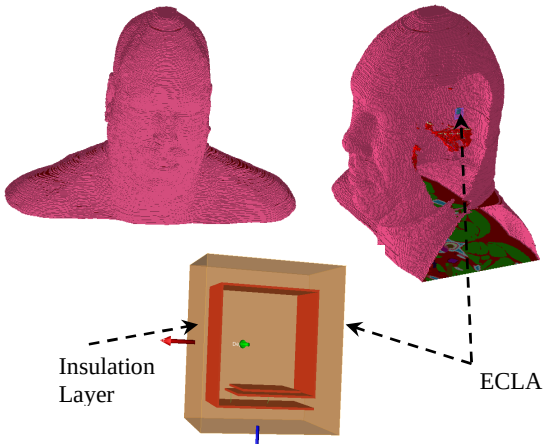

Figure 3.6: ECLA inside human head and cutting plane to show ECLA.

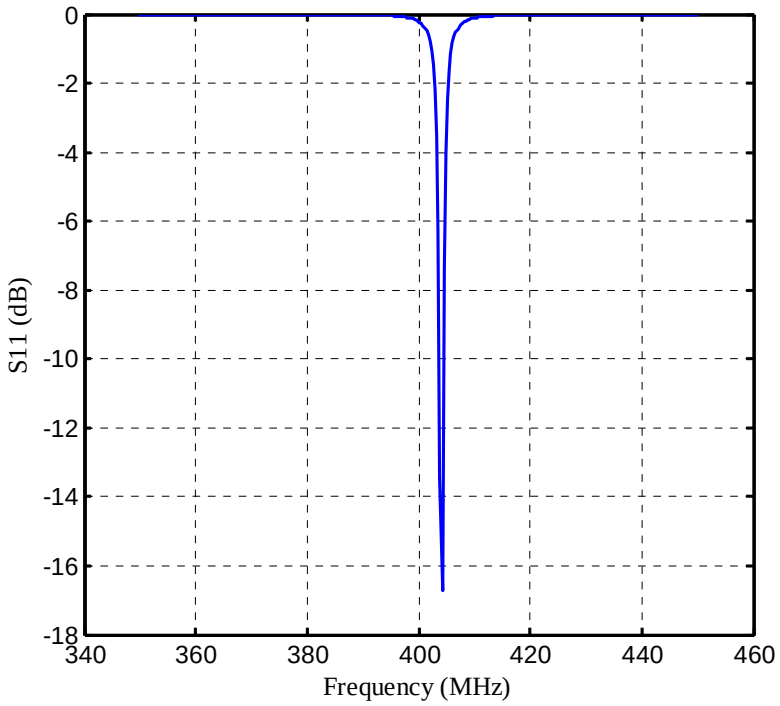

Figure 3.7: Scattering parameter (S_{11}) of ECLA inside human head model.

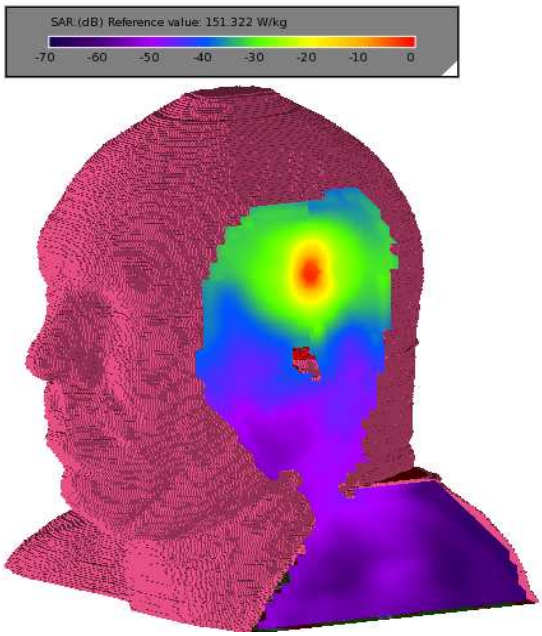

Figure 3.8: 1g-averaged SAR of ECLA inside human head.

3.3.4 ECLA inside the Human Body

The radiation characteristics of ECLA are investigated inside a human body using XF7 software. The model includes 39 human body tissues of an adult male. ECLA is placed at the chest of the human body model as shown in Figure 3.9. The simulation results for the scattering parameter (S_{11}) of ECLA inside the human body model are shown in Figure 3.10. This figure confirms that the impedance characteristics of ECLA do not change dramatically due to environmental effects.

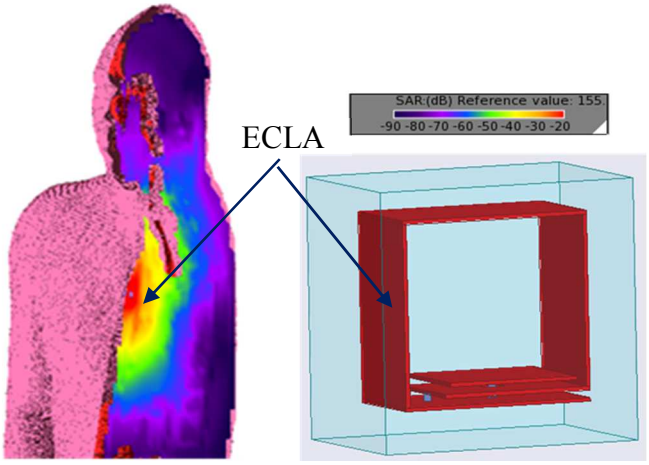

Figure 3.9: ECLA inside human body, cutting plane to show ECLA structure and its 1g-averaged SAR inside human body.

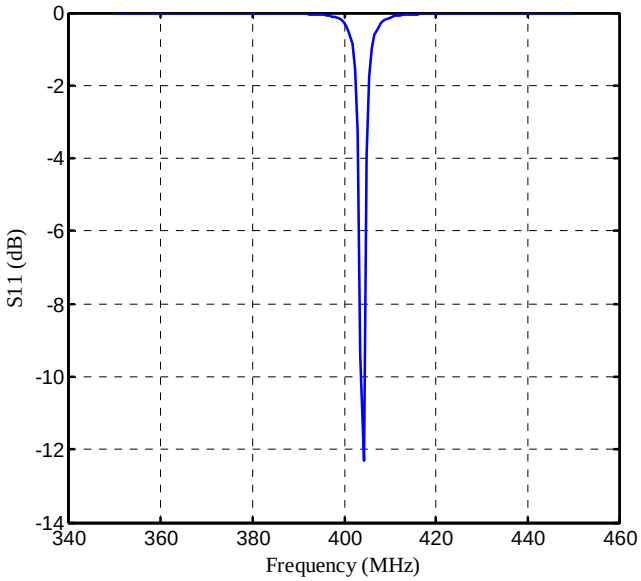

Figure 3.10: Scattering parameter (S_{11}) of ECLA inside human body.

3.4 Effect of ECLA Dimensions on SAR

The dimensions of ECLA have an important effect on its performance inside the human body. Specifically, the miniaturization factor plays an important role in deciding the SAR value. The total electric field intensity has been computed using HFSS for three different antenna dimensions at the same resonant frequency and the results are presented in Figure 3.11. Table 3.4 shows the effect of ECLA dimensions on its performance while maintaining the same resonant frequency by using different values of the lumped capacitor. The field intensity around the antenna increases by $1/a^p$ where a is the maximum dimension of the antenna and p is larger than 1 for an antenna size $a < \lambda/4$ (Figure 3.11) as explained in Chapter 2. This causes a significant jump in the SAR value for highly miniaturized electric field antennas. Due to the fact that ECLA is a magnetic antenna, the miniaturization factor does not increase the SAR dramatically. One can compare the electric field intensity for three different cases presented in Figure 3.11 and the associated SAR values presented in Table 3.4. These results show that the antenna miniaturization increases the electric field intensity and SAR value.

Table 3.4: Radiation characteristics of ECLA inside one-layer model with different ECLA dimensions.

ECLA dimensions (mm)	Quality factor(Q)	Bandwidth (MHz)	SAR1g (W/kg)	SAR10g (W/kg)
5×5×3	50	8	154	44
6×6×4	37	11	151	40
7×7×5	29	14	143	39
8×8×6	25	17	138	38
9×9×7	20	20	125	36
10×10×8	18	23	115	32

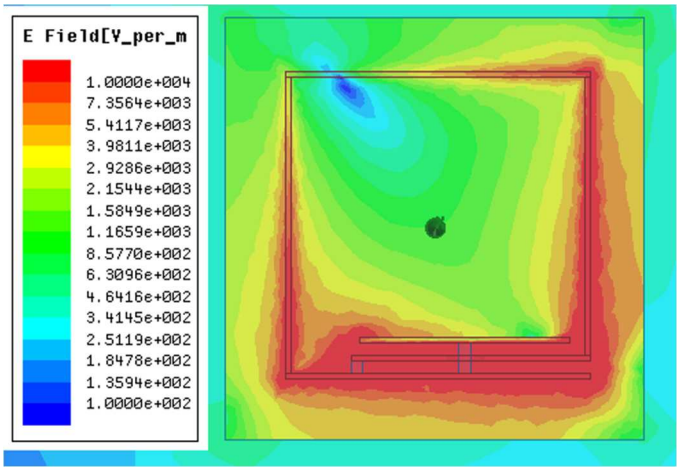

(a)

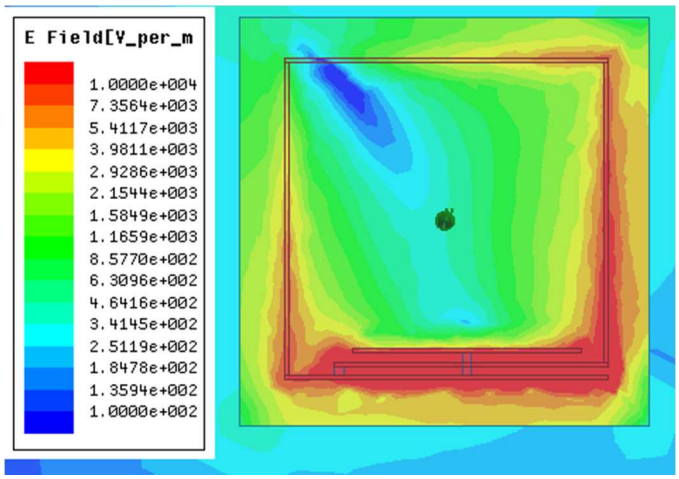

(b)

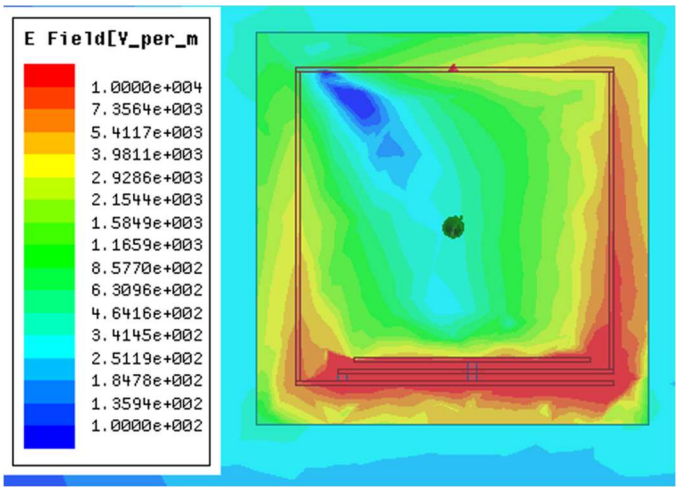

(c)

Figure 3. 11: Computed total electric field around the antenna for three different dimensions: a) $5\times5\times3mm^3$, b) $7\times7\times5mm^3$, and c) $8\times8\times6mm^3$.

3.5 Effect of Insulation Layer on SAR

To prevent the rejection of the implanted antenna by the human body tissues, ECLA with dimensions (5x5x3 mm^3) is surrounded by a biocompatible insulation layer. The insulation layer thickness and type play an important role on the SAR of ECLA inside the human body model. Tables 5 and 6 show the performance of ECLA surrounded by different types of insulations with different thicknesses inside the one-layer model of the human body. The radiation characteristics of ECLA are calculated using HFSS software.

Table 3.5: Radiation characteristics of ECLA inside one-layer human body model with different Teflon material insulation thickness.

Insulation thickness (mm)	Gain (dB)	Bandwidth (MHz)	Efficiency (%)	SAR1g (W/kg)
1	-15.5	8	0.35	154
2	-14.8	7.2	0.38	74.9
3	-14.5	6.9	0.42	41.2
4	-14.4	6.6	0.43	25.2
5	-14.2	6.4	0.45	15.7
6	-14.1	6.2	0.46	11

Table 3.6: Radiation characteristics of ECLA inside one-layer human body model with different insulation materials.

Insulation Types	Gain (dB)	Bandwidth (MHz)	Efficiency (%)	SAR1g (W/kg)
Teflon	-14.7	5	0.4	152.8
MACRO	-15.5	6	0.35	141.4
PEEK	-15.3	9	0.34	173.5
Ceramic Alumina	-16	11.2	0.28	201

It can be seen from the results presented in Tables 3.5 and 3.6 that the size and type of the insulating material can change the performance of the implanted ECLA. The capacitive part of the antenna (distributed capacitor) has the highest electric field intensity compared to the inductive parts as shown in Figure 3.11. Since the electric field intensity is responsible for increasing the SAR values, one needs to either make the distributed capacitor smaller or use thicker insulating material layer around it (Figure 3.12). The performance of ECLA has been computed using HFSS inside the one-layer human body model with different sizes of insulating material layer around the

feeding probe and the results are presented in Table 3.7. The inductive part of the antenna has the same size of insulating material while the thickness of the insulating layer increases at the capacitive part. The results presented in Table 3.7 when compared to the results obtained in Table 3.2 demonstrate the effectiveness of this method.

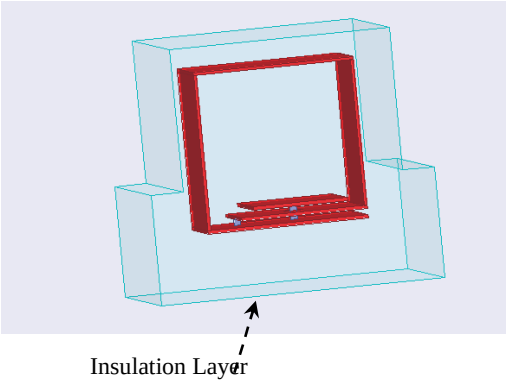

Figure 3.12: ECLA surrounded with insulation layer around the feeding head.

Table 3.7: The ECLA performance with different insulation thickness around feeding head and capacitance.

ECLA Volume (mm^3)	Gain (dB)	Bandwidth (MHz)	Efficiency (%)	SAR1g (W/kg)
337	-18.3	4.2	0.17	48
252.3	-18.5	4.1	0.17	71
168.2	-28.4	3.7	0.17	81.6
121	-18.7	3.9	0.16	113

3.6 ECLA Performance at the Allowed Frequency Bands

ECLA performance inside the one-layer rectangular human body model and the 3-layer spherical human head model will be investigated using HFSS. These simple models are used to reduce the problem complexity and simulation time. ECLA is designed at MICS, ISM and 3.5 GHz frequency bands with dimensions (5x5x3 mm^3), (3x3x3 mm^3) and (2x2x2 mm^3), respectively. To achieve biocompatibility, ECLA is covered by a 1 mm insulation layer, which has a relative dielectric constant 2.07 and zero conductivity. The one-layer model has dimensions (100x100x100 mm^3) and it has the properties of muscle and skin tissues at different frequency bands as shown in Table 3.8. The three-layer spherical model has the properties of brain with radius 85 mm, skull with thickness 10 mm and skin with thickness 5 mm (Figure 3.13.). The scattering parameter (S_{11}) of

ECLA inside the human body models at the three frequency bands is shown in Figure 3.14. From this figure, we see that ECLA is less-sensitive to the detuning effect of the human body tissue electrical properties.

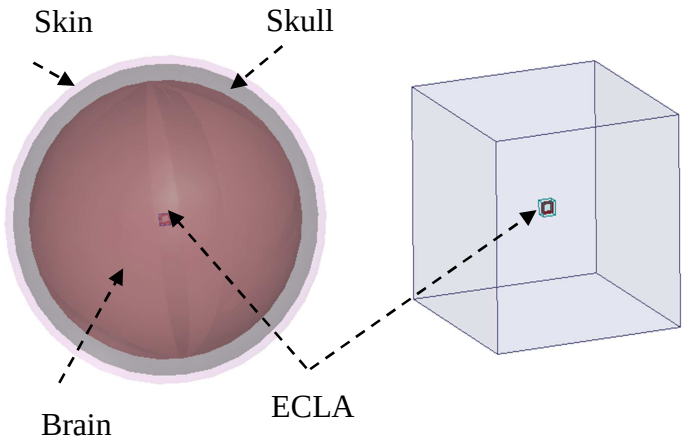

Figure 3.13: ECLA inside one-layer and three-layer models.

Table 3.8: Electrical properties of human body tissues at different frequency bands.

Band	Tissue	Dielectric constant	Conductivity (S/m)	Density (W/Kg)
MICS	Skin	49.85	0.67	1100
	Muscle	57.95	0.81	1040
	Brain	49.7	0.59	1030
	Skull	17.78	0.16	1850
ISM	Skin	42.85	1.59	1100
	Muscle	53.6	1.81	1040
	Brain	42.25	1.51	1030
	Skull	14.96	0.599	1850
3.5 GHz	Skin	41.41	2.35	1100
	Muscle	52.12	2.72	1040
	Brain	41.09	2.26	1030
	Skull	14.07	0.922	1850

The radiation characteristics of ECLA for 1W input power are shown in Table 3.9. From these results, as the frequency increases, ECLA dimensions decrease, -3 dB bandwidth increases, quality factor decreases and average SAR increases. Also, due to the SAR limitations, the maximum allowed input power (P_{in}) decreases as the frequency increases.

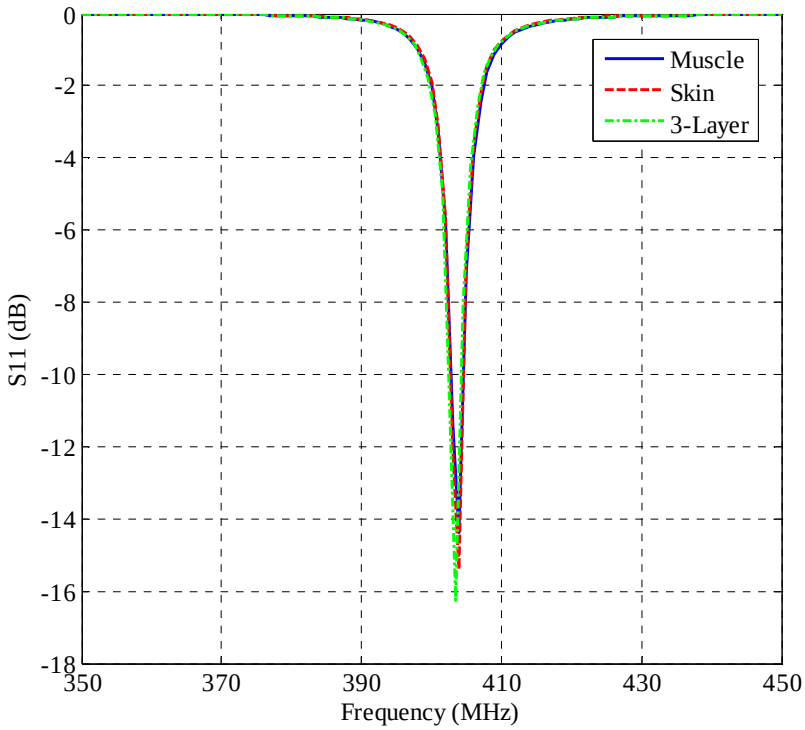
Muscle
Skin
3-Layer
S11 (dB)
Frequency (MHz)
0
-2
-4
-6
-8
-10
-12
-14
-16
-18
350
370
390
410
430
450

(a)

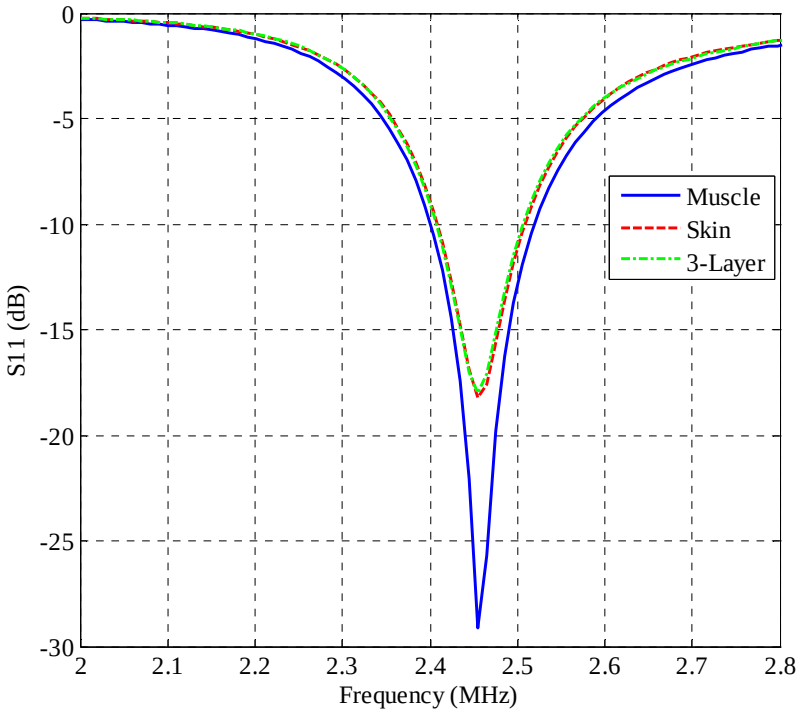
Muscle
Skin
3-Layer
S11 (dB)
Frequency (MHz)
0
-5
-10
-15
-20
-25
-30
2
2.1
2.2
2.3
2.4
2.5
2.6
2.7
2.8

(b)

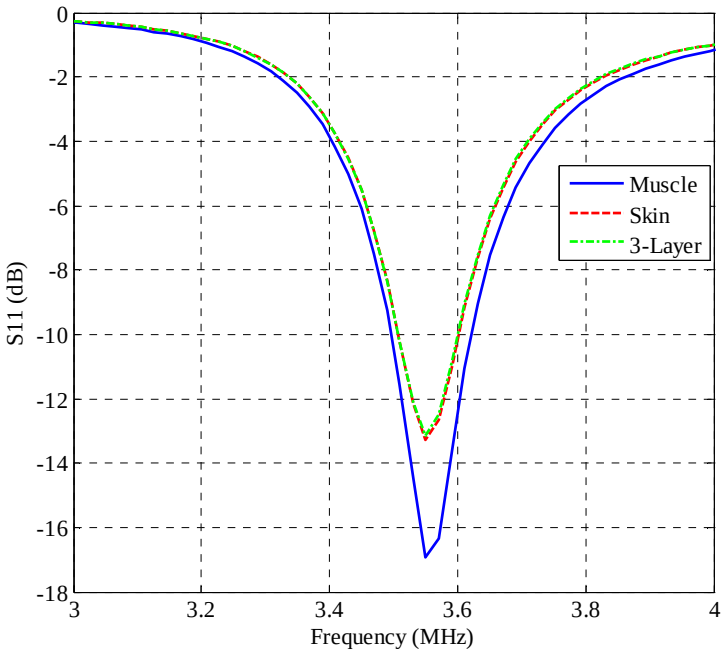

(c)

Figure 3.14: Scattering parameter (S_{11}) of ECLA inside muscle, skin and three-layer human models at (a) MICS band (b) ISM band (c) 3.5 GHz band.

Table 3.9: Radiation characteristics of ECLA inside human body model at different frequency bands.

Band	Model	Bandwidth (MHz)	SAR 1g (W/kg)	SAR10g (W/kg)	Max. P_{in} (mW)
MICS	Skin	5.53	161.7	36.5	9.9
	Muscle	5.83	180	40.2	8.9
	3-layers	5.73	141	31.9	11.3
ISM	Skin	330	264	60.8	6.1
	Muscle	363	269.4	62.3	5.9
	3-layers	330	267.1	60.3	6
3.5 GHz	Skin	380	385.1	71.3	4.2
	Muscle	413	406.8	74.9	3.9
	3-layers	369	384.1	70.9	4.2

3.7 Wearable ECLA

An antenna for WBAN may be implanted inside the human body or wearable on the skin surface of the body. The implanted antenna needs to be extremely small while maintaining SAR requirements inside the human body as designed in the previous sections. The wearable antenna

does not need to be heavily miniaturized but it needs to have high radiation efficiency and small SAR inside the human body. The wearable antenna is radiated in free space near the human body surface, which affects the radiation characteristics of the antenna. An ECLA with dimensions (20x20x5 mm^3) is designed as a wearable antenna as shown in Figure 3.15. Using HFSS, the scattering parameter (S_{11}) of ECLA in free space is shown in Figure 3.16. Using XF7, wearable ECLA with dimensions (20x20x5 mm^3) is placed 2 mm from the chest of the human body surface as shown in Figure 3.17. The scattering parameter of wearable ECLA near the human body is shown in Figure 3.18. The insulation layer thickness has a significant effect on the radiation characteristics of wearable ECLA as the implanted ECLA. The radiation characteristics of wearable ECLA using an insulation layer with relative dielectric constant 2.07 and zero conductivity with different thickness are shown in Table 3.10. Based on these results, the resonant frequency of the wearable ECLA near the human body changes slightly from that in free space due to the effect of the human body on antenna scattering parameters. Also, the insulation layer thickness has a significant effect on ECLA performance radiated near the human body, whereas the insulation thickness increases, the SAR inside the human body decreases so the maximum allowed input power to the antenna will increase.

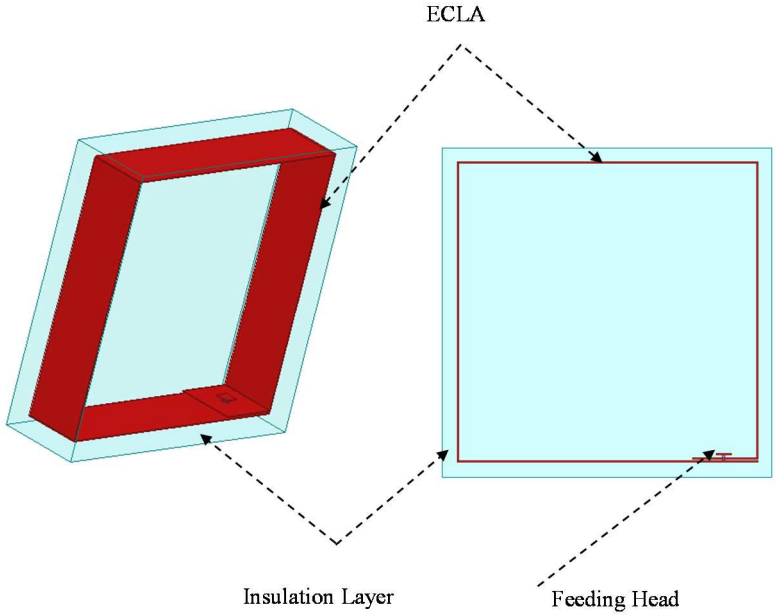

Figure 3.15: Wearable ECLA inside free space medium, angled and front views.

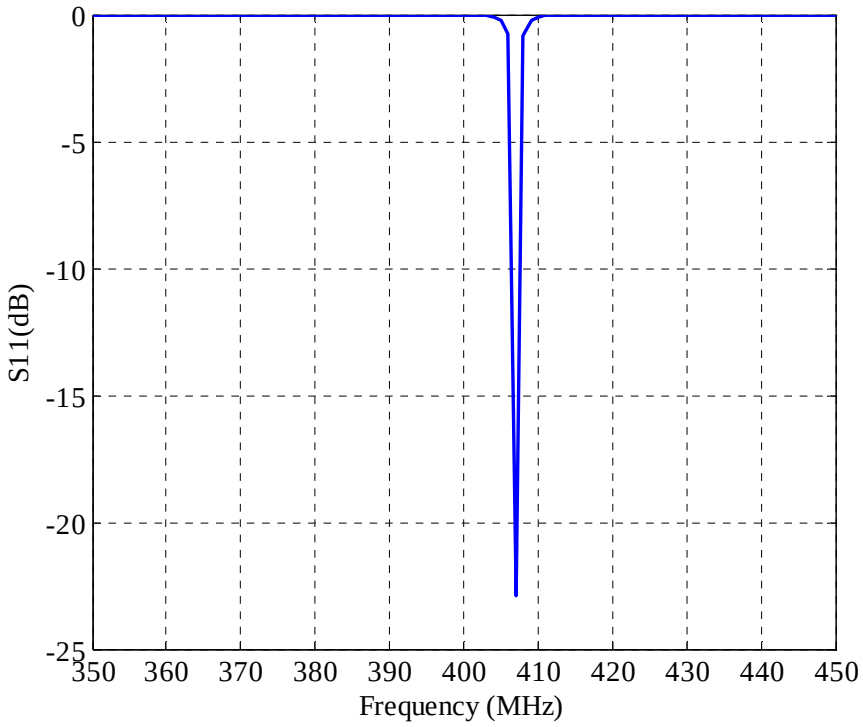

Figure 3.16: Scattering parameter (S_{11}) of wearable ECLA in free space medium.

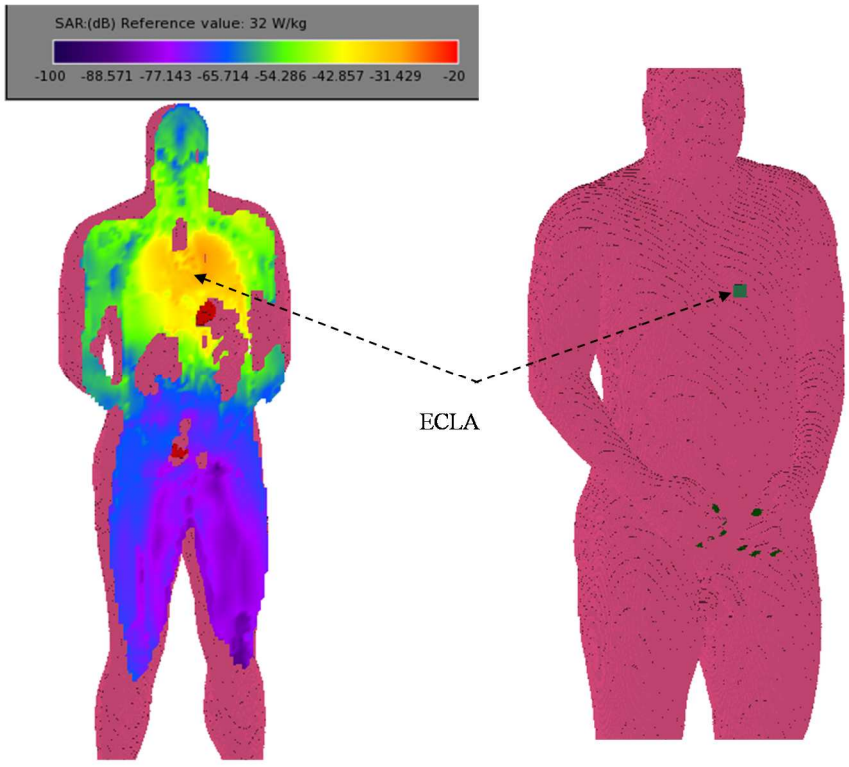

Figure 3.17: Wearable ECLA near human body chest and its 1g averaged SAR.

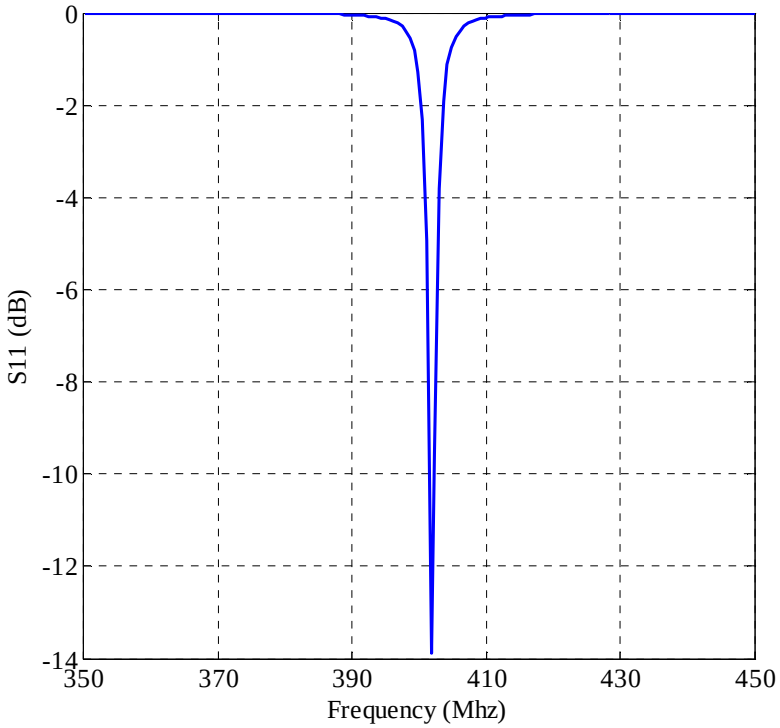

Figure 3.18: Scattering parameter (S_{11}) of Wearable ECLA near the human body chest.

Table 3.10: Radiation characteristics of wearable ECLA with different insulation thickness near human body model.

Thickness /Parameter	1 mm	2 mm	4 mm
Available power (W)	1	1	1
Input Power (W)	0.97	0.74	0.8
Input impedance (**Ω**)	49.8-j16.6	74+j72	82-j58
Efficiency (%)	0.99	0.8	0.72
S_{11} (dB)	-16	-6	-7
SAR1g (W/Kg)	32.16	19	12.3
SAR10 (W/Kg)	9.22	5.4	3.8
Max input power	50	84	130

3.8 Ferrite-Loaded ECLA

To reduce the size of ECLA at the MICS frequency band, the antenna will be loaded with a magnetic material such as ferrite as shown in Figure 3.19. ECLA is a magnetic field antenna so,

when ECLA is loaded with a ferrite material, the resonant frequency of the antenna will reduce so the antenna size can be miniaturized to an arbitrary small size. The ferrite material is a chemical compound of ceramic material with iron oxide as its main component. The ferrite material has the electrical properties of $\varepsilon_r = 12$, $\mu_r = 1000$ and $\sigma = 0.01\ S/m$. In this section the performance of ferrite- loaded ECLA inside the human body model will be studied and compared with the performance of non- ferrite-loaded ECLA. ECLA with dimensions (5x5x3 mm^3) , (3x3x3 mm^3) ,(2x2x2 mm^3) and (1x1x1 mm^3) are designed and its performance will be studied inside the one-layer human body model with dimensions (100x100x100 mm^3). The model has the electrical properties of skin tissue as shown in Figure 3.20. The scattering parameters (S_{11}) of ECLA with and without ferrite material for different ECLA dimensions are shown in Figures 3.21 3.22, 3.23 and 3.24. From these figures, the -3 dB bandwidth of ferrite-loaded ECLA is larger than that of non-ferrite-loaded ECLA with the same dimensions due to the conductivity of the ferrite material. Radiation characteristics of ECLA with and without ferrite-loaded are shown in Table 3.10. Based on this table, ferrite-loaded ECLA has the lowest SAR values inside the one-layer model compared to non-ferrite-loaded ECLA. The SAR value depends on the power lost due to the size reduction of the implanted antenna. Also, as the size of ECLA reduces, the bandwidth of the ECLA without ferrite increases but the bandwidth decreases for ferrite-loaded ECLA. The gain for both ECLAs will decrease as the size decreases.

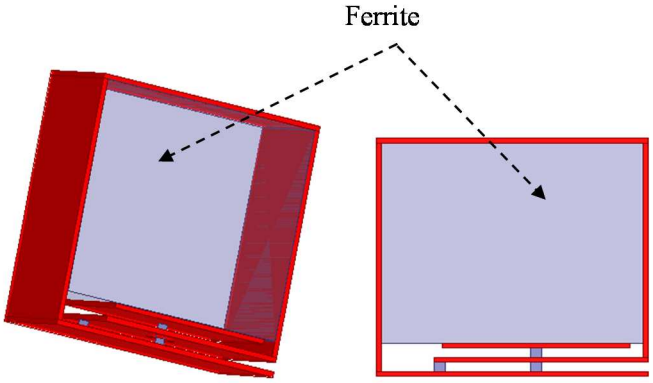

Figure 3.19: Ferrite-loaded ECLA, angled view and front view.

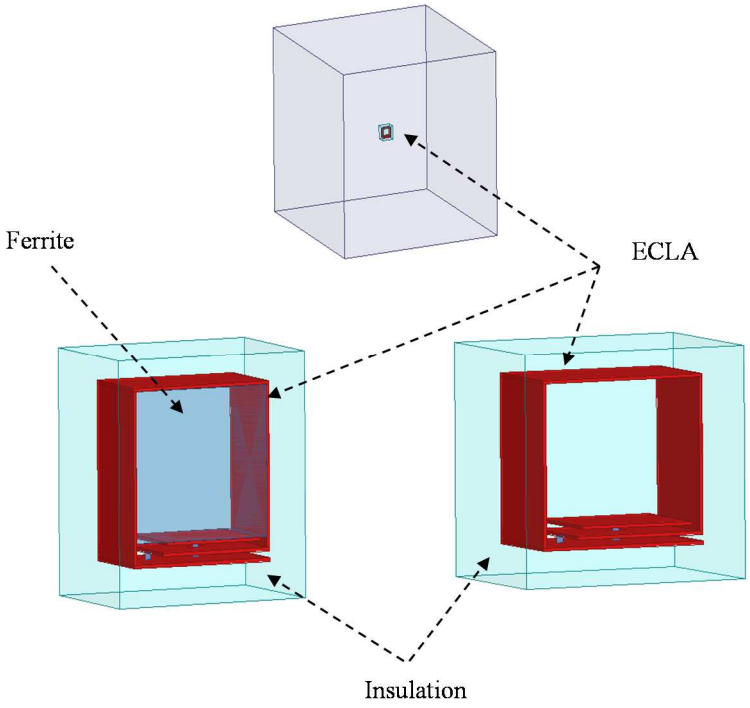

Figure 3.20: ECLA with and without ferrite-loaded inside one-layer human body model.

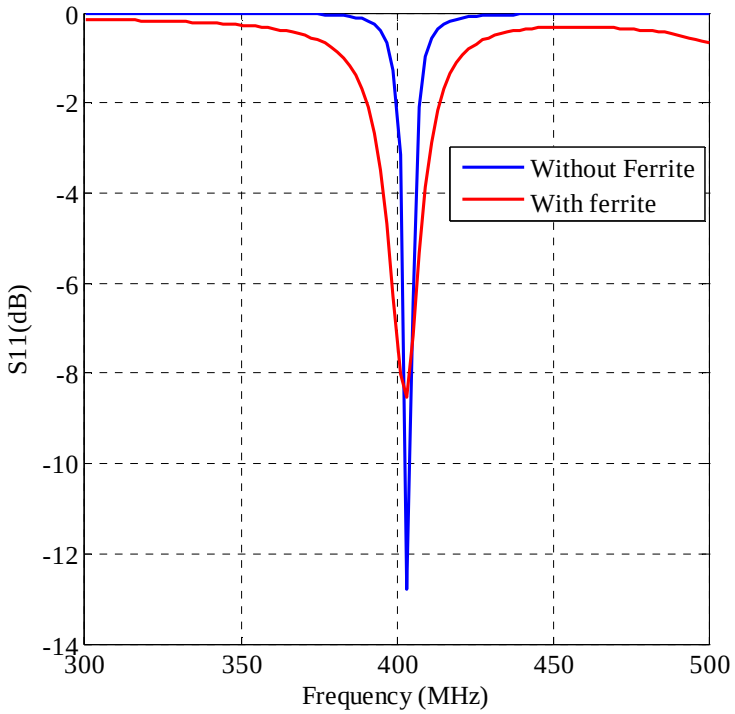

Figure 3.21: Scattering parameter (S_{11}) of ECLA has dimensions (5x5x3 mm^3) without ferrite and with ferrite.

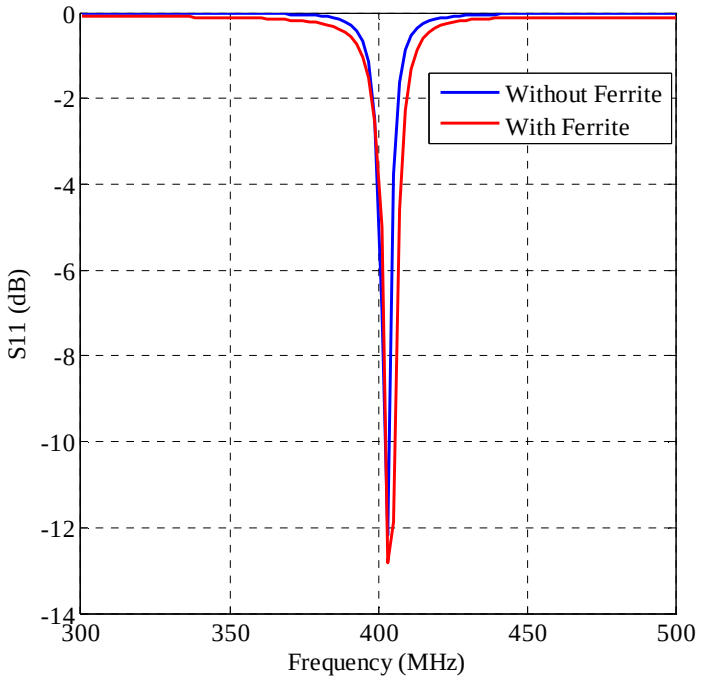

Figure 3.22: Scattering parameter (S_{11}) of ECLA has dimensions (3x3x3 mm^3) without ferrite and with ferrite.

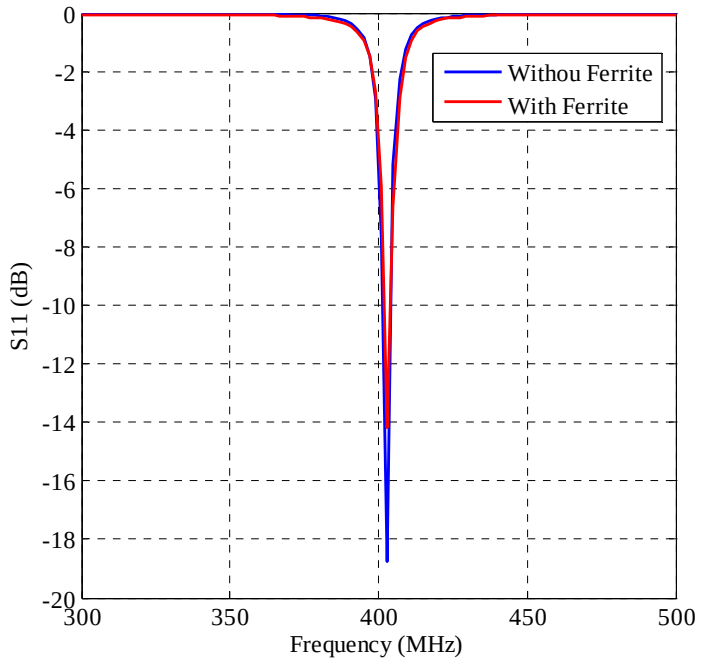

Figure 3.23: Scattering parameter (S_{11}) of ECLA has dimensions (2x2x2 mm^3) without ferrite and with ferrite.

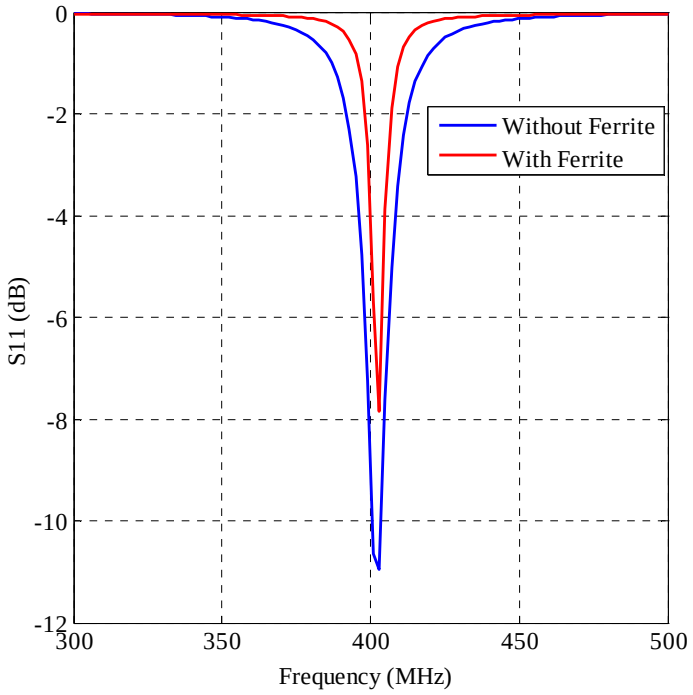

Figure 3.24: Scattering parameter (S_{11}) of ECLA has dimensions (1x1x1 mm^3) without ferrite and with ferrite.

Table 3.11: Radiation Characteristics of ECLA with and without Ferrite-loading

ECLA (mm)	Ferrite Loaded	f_r (MHz)	S_{11} (dB)	Bandwidth (MHz)	Gain (dB)	SAR1g (W/kg)
5x5x3	No	403	-13	5.8	-14.3	158
	Yes	403	-8.6	17.1	-14.4	148.5
3x3x3	No	403	-12.2	6.5	-18.8	95
	Yes	403	-12.8	9	-16.7	167.3
2x2x2	No	403	-18.8	7.5	-25.6	33.7
	Yes	403	-14.2	7.8	-20.8	103
1x1x1	No	403	-11	15	-37.6	3.2
	Yes	403	-8	7	-32	9.8

3.9 Experimental Work

Two ECLAs, one with dimensions (5x5x3 mm^3) as an implanted antenna and other with dimensions (20x20x5 mm^3) as a wearable antenna, are designed. A box with dimensions (30x20x10 cm^3) filled with the ground pork, which has electrical properties near the electrical properties of the human body, is designed as a one-layer model. Implanted ECLA is placed 7 cm inside the ground pork and the wearable ECLA is placed 2 mm from the ground pork (Figure 3.21). The scattering parameters (S_{11}) of the two ECLAs are shown in Figure 3.22. The shift in the resonant frequency is due to the lumped capacitor values (29 pF in simulation and 20 pF in experiment). Also, the wearable ECLA has a large bandwidth compared to implant ECLA due to the large dimension of the wearable ECLA as the antenna bandwidth increases when the antenna dimensions increase.

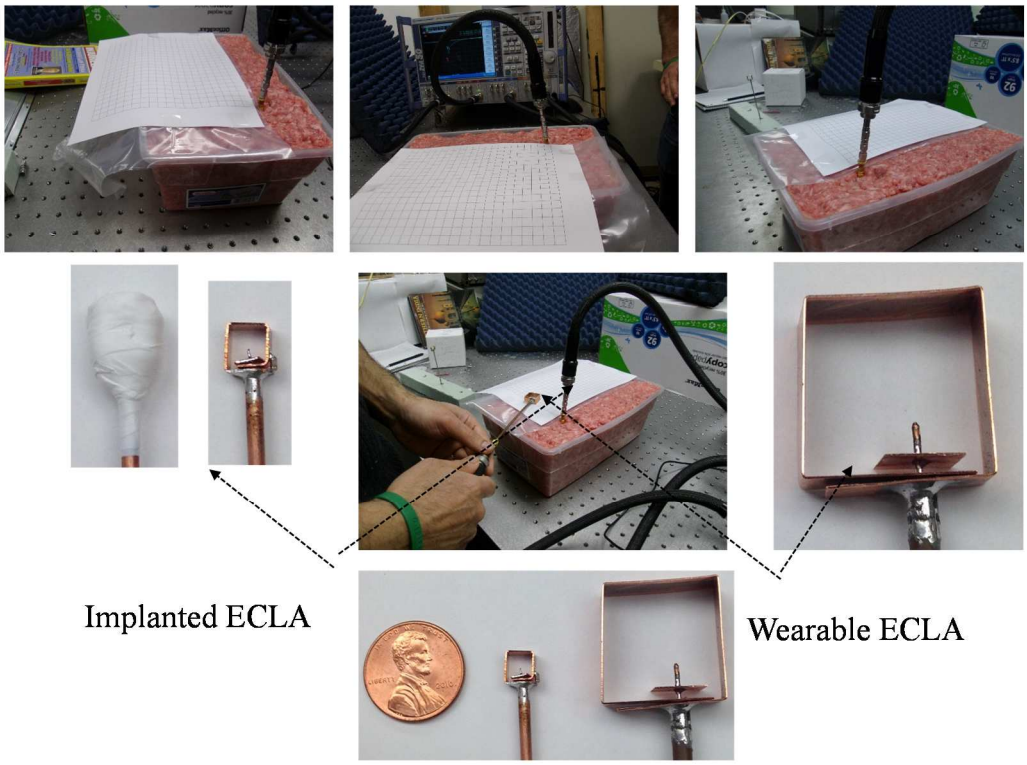

Figure 3.25: Experimental setup for ECLA with ground pork.

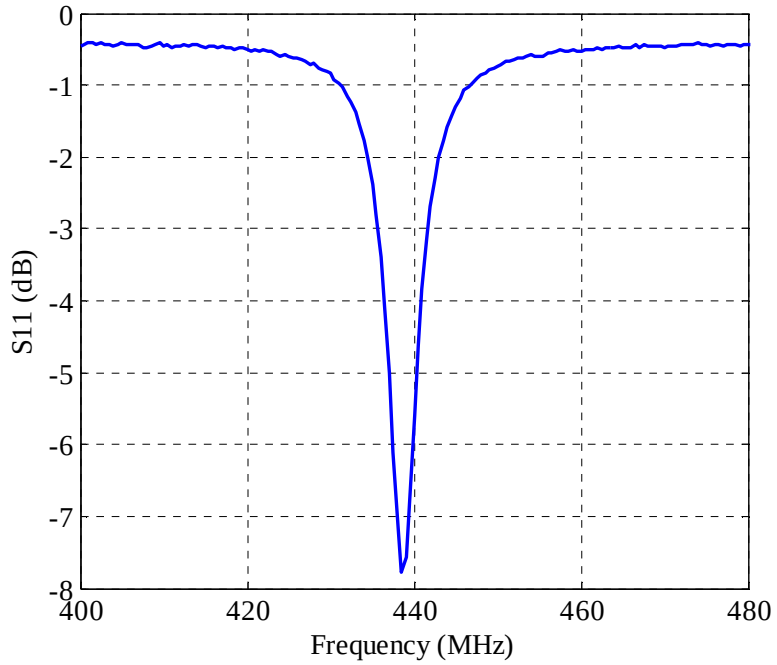

(a)

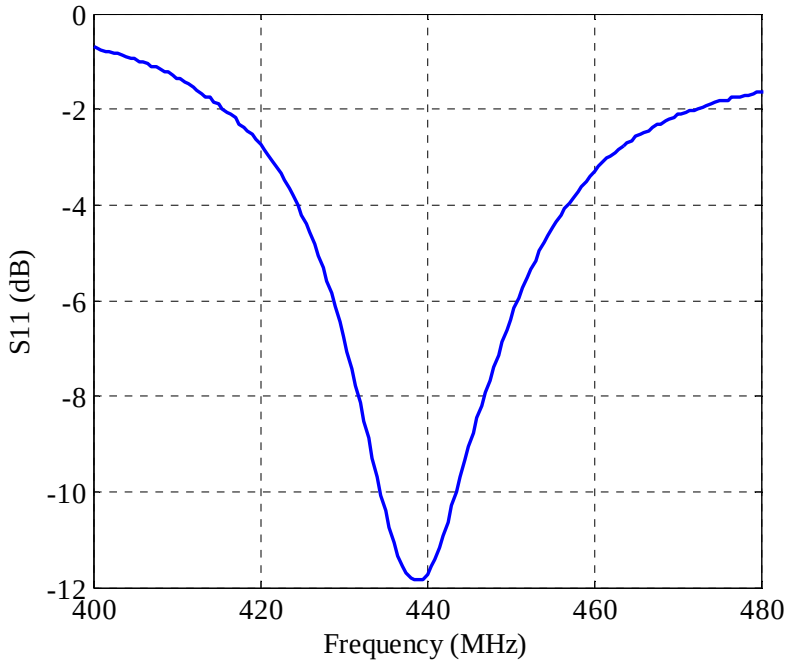

(b)

Figure 3.26: Scattering parameter (S_{11}) of (a) implanted and (b) wearable ECLA with ground pork.

3.10 Chapter Summary

The ECLA was proposed as a suitable candidate for an implanted and wearable antennas applications. ECLA has different dimensions at different frequency bands. Different parameters of the antenna were studied for various cases to demonstrate the effectiveness of ECLA for implanted devices. To heavily miniaturize the ECLA antenna, the ferrite-loaded ECLA was proposed and its performance inside the human body model was studied. Also, the simulation results were validated using experimental work. From the simulation results it was shown that, while ECLA has the smallest size among the published results in the literature, it maintains the smallest value of averaged SAR inside different types of human body models. Also, ECLA was shown to be less-sensitive to the detuning effect due to dielectric properties of human body tissues. The antenna dimensions have a large effect on ECLA performance, because as the ECLA dimensions decrease, the SAR value inside the human body increases. The effect of insulating material around ECLA was studied as well. It was shown that a thicker layer of insulation around the distributed capacitor can reduce the SAR values. The performance of ferrite-loaded ECLA inside the one-layer model was studied as well. From these results, it was found that ferrite-loaded ECLA antenna has better performance as an implanted antenna compared to ECLA without ferrite-loaded material with the same dimensions.

Chapter 4

Inter and Intra-Body Propagation Channel

Knowledge of propagation media, which typically gathered by physical experiments and simulations, is a key step toward a successful transceiver design. In case of medical implants physical experiment is extremely difficult if not impossible, therefore we rely on simulations in most studies. In this chapter, PL between implanted antennas, as a measure of propagation channel characteristics, is investigated using HFSS and XF7. An ECLA is designed to study PL inside the human body models at MICS, ISM and 3.5 GHz bands. ECLA has dimensions ($5\times5\times3mm^3$), ($3x3x3\ mm^3$) and ($2x2x2\ mm^3$) at MICS, ISM and 3.5 GHz respectively. The effect of frequency bands, antenna polarization, human model electrical properties, human model shape, human model dimensions and distance between implants on PL are considered. PL between two ferrite-loaded ECLA will be studied as well and will be compared to PL between non-ferrite- loaded ECLA. Also our simulation results are validate using experimental work. It was found that, MICS band has the best propagation channel inside the human body model and the maximum PL is 90 dB [165].

4.1 Introduction

Now days, patients' health information can be collected and retrieved remotely and efficiently using biotelemetry wireless networks such as WBAN. Implanted devices are important components of WBAN which is a promising technology in biotelemetry, e-health care and hyperthermia applications [3]. An important step in the development of WBAN is to understand the propagation channel characteristics as an essential requirement for efficient design of wireless communication systems.

The inductive coupling technique widely adopted in primitive design of implantable devices is not appropriate to recent biomedical systems due to its low data rate and short communication range [166]. Recently a considerable effort has been devoted to investigate the propagation channel

inside the human body as explained in Chapter 1. In all previous works, propagation channel at all the allowed frequency bands were not investigated, also in the case of WBAN, near-field characteristics of the implanted antenna play an important role in the propagation channel. In this chapter, inter and intra-body propagation channel will be investigated for the human body models using ECLA at the allowed frequency bands.

The chapter will be organized as follows: PL inside one-layer model at the allowed frequency bands will be investigated in Section 4.2. Effect of ECLA polarization and human body model on PL will be explained in Sections 4.3 and 4.4 respectively. PL inside one-layer model for the upper part of the human body will be investigated in Section 4.5. In Section 4.6, PL inside simple model of the human body will be investigated and PL inside exact human body model will be explained in section 4.7. PL using ferrite-loaded ECLA and PL models will be investigated in Section 4.8 and 4.9 respectively. In Section 4.10, Experimental work will be described and chapter summary will be provided in Section 4.11.

4.2 Effect of Frequency Bands on PL

Electrical properties of the human body tissues are function of frequency, time, emotional mode and diet. This fact makes the propagation phenomena more sophisticated for implanted antenna. PL inside the human body model is investigated using HFSS at the allowed frequency bands. The transmitting and receiving antennas are ECLAs with dimensions (5x5x3 mm^3), (3x3x3 mm^3) and (2x2x2 mm^3) at MICS, ISM and 3.5 GHz frequency bands, respectively. Also ECLA is surrounded by a biocompatible insulation layer of 1mm thickness with a relative dielectric constant of 2.07 and zero conductivity. ECLAs are located at the center of the human body model. Simple models for the human body as one-layer and three-layer models are used to reduce the simulation time and problem complexity. After optimizing the antenna for each frequency range and computing primitive values for PL at different frequency range, the antenna will be simulated in a full human body model to compute the values for PL more accurately. The one-layer model has dimensions (200x50x50 mm^3) which can represent human arm or leg and it has the electrical properties of muscle tissue at the allowed frequency bands as shown in Table 4.1. The three-layer model consists of muscle with thickness of 35 mm, fat with thickens of 5 mm and skin with thickness of 2.5 mm as shown in Figure 4.1.

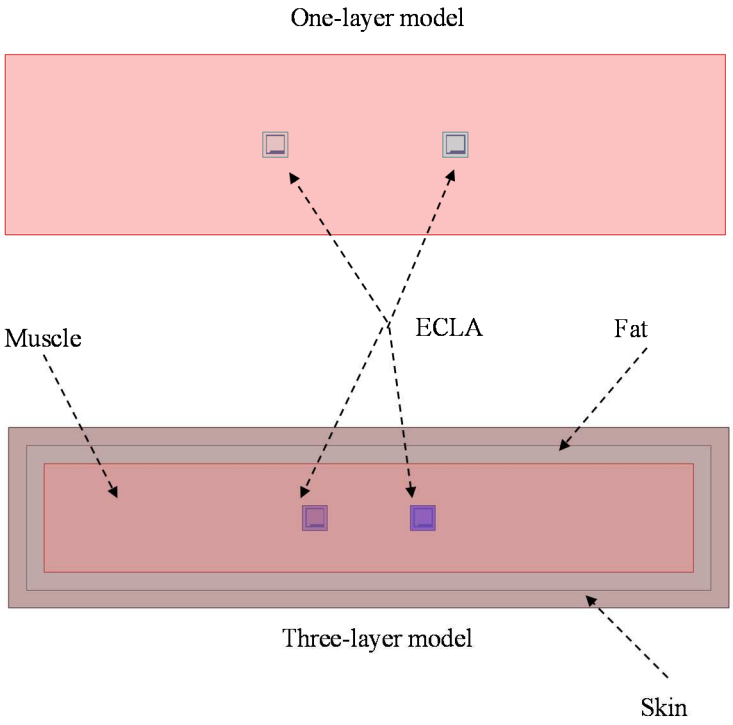

Figure 4.1: Two ECLAs inside one-layer and three-layer human body models.

Table 4.1: Electric properties of human body tissues at MICS, ISM and 3.5 GHz frequency bands.

Band	Tissue	Dielectric constant	Conductivity (S/m)	Density (W/Kg)
MICS	Skin	49.85	0.67	1100
	Muscle	57.95	0.81	1040
	Fat	11.62	0.081	1850
ISM	Skin	42.85	1.59	1100
	Muscle	53.6	1.81	1040
	Fat	10.82	0.27	1850
3.5 GHZ	Skin	41.41	2.35	1100
	Muscle	52.12	2.72	1040
	Fat	10.5	0.42	1850

PL inside one-layer and three-layer models at the allowed frequency bands are computed versus distance of two ECLAs and the results are shown in Figure 4.2. It is worth mentioning that these path losses include the antenna loss and mismatch loss as well. Also the magnitude of electric field intensity and real part of Poynting vector inside one-layer model at the allowed frequency bands at distance 100 mm between ECLAs are shown in Figures 4.3 and 4.4, respectively. Based

on these figures the electric field intensity and real part of the Poynting vector decay exponentially due to the lossy medium in addition to the spherical decaying factors. Away from the transmitting antenna an interesting phenomenon arises; our computation shows that energy reenters the body from different directions, especially at MICS band, which may be the dominant communication link at larger distances. Basically the LOS link might not be the dominant propagation channel far away from the antenna. The energy exits the body, travels as a creeping wave around the body and gradually enters the body from the surface (Figure 4.4). This effect is more prominent at the MICS frequency band. This makes the MICS band a suitable frequency band for inter and intra-body communication applications. Therefore, in the remaining parts of this chapter PL will be explained in details inside the human body at MICS band.

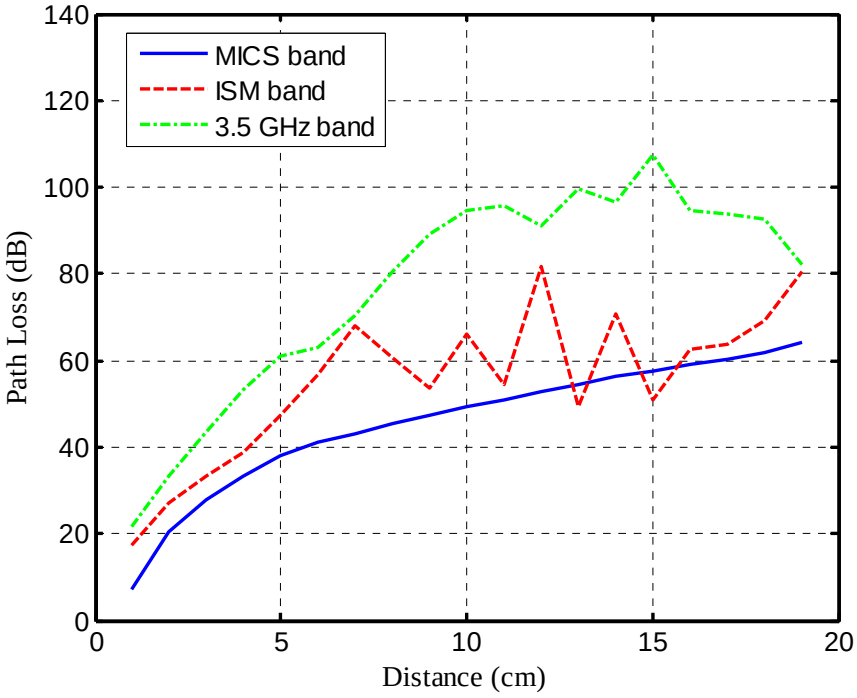

(a)

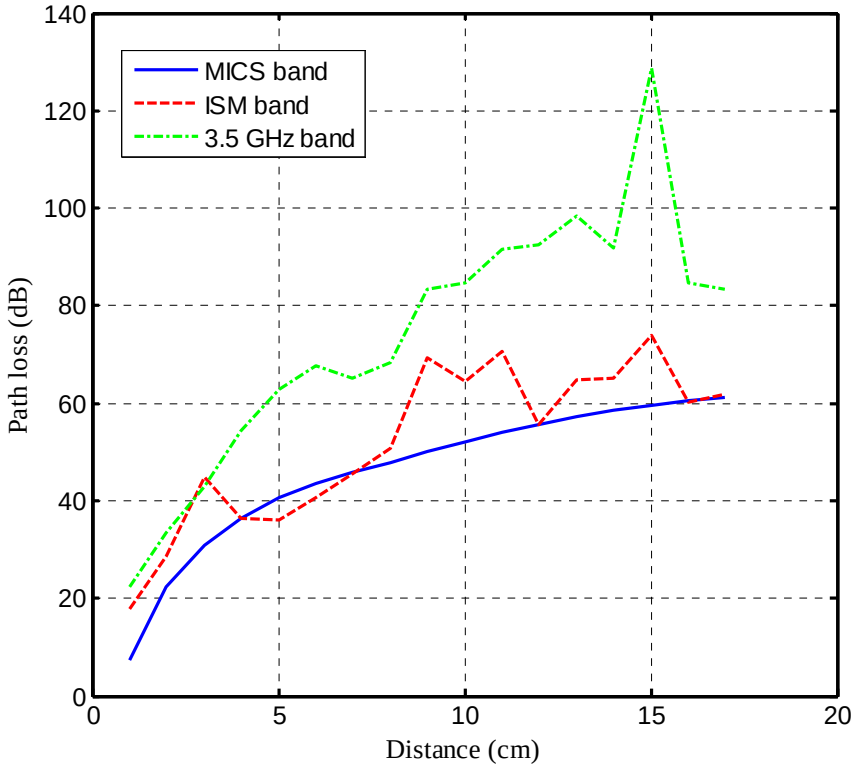

(b)

Figure 4.2: PL inside human body models (a) one-layer model and (b) three-layer model.

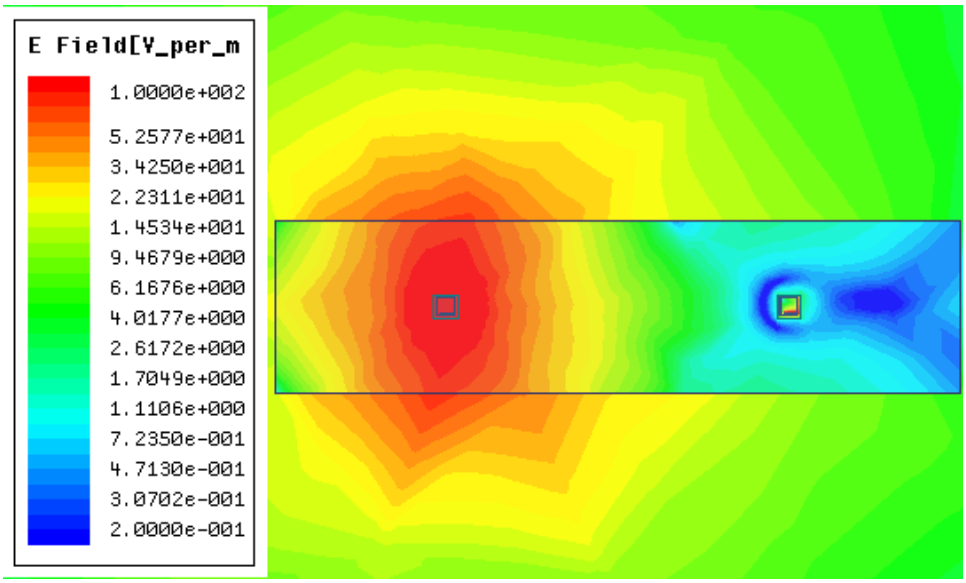

(a)

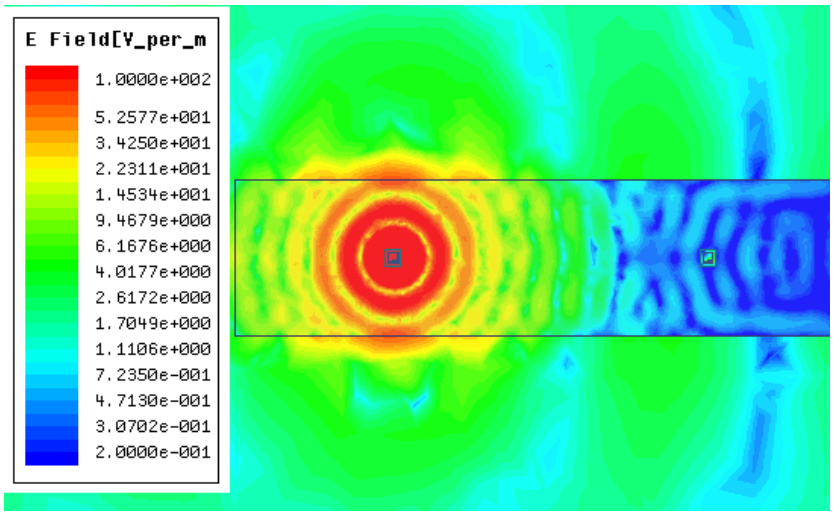

(b)

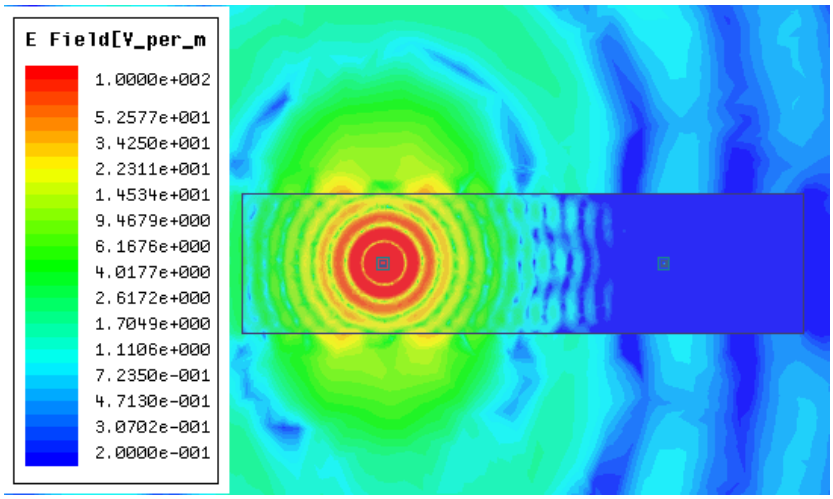

(c)

Figure 4.3: Magnitude of electric field inside muscle model (a) MICS band, (b) ISM band and (c) 3.5 GHz band.

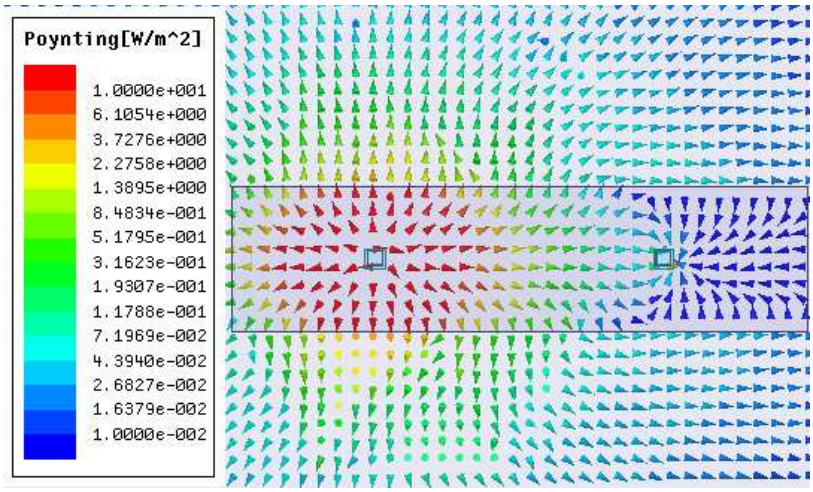

(a)

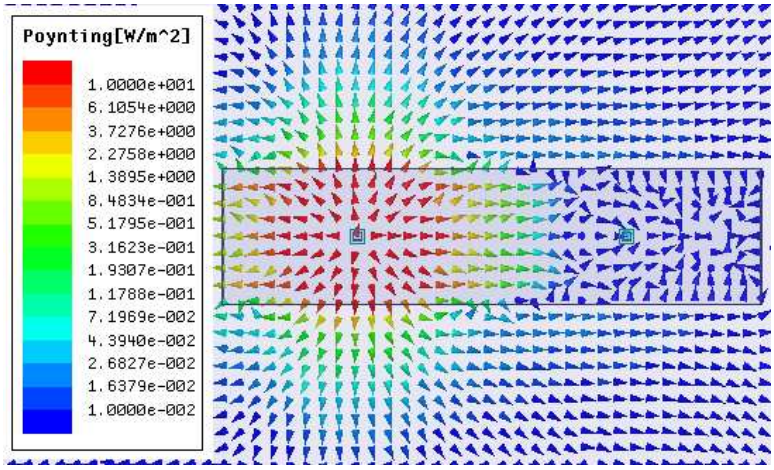

(b)

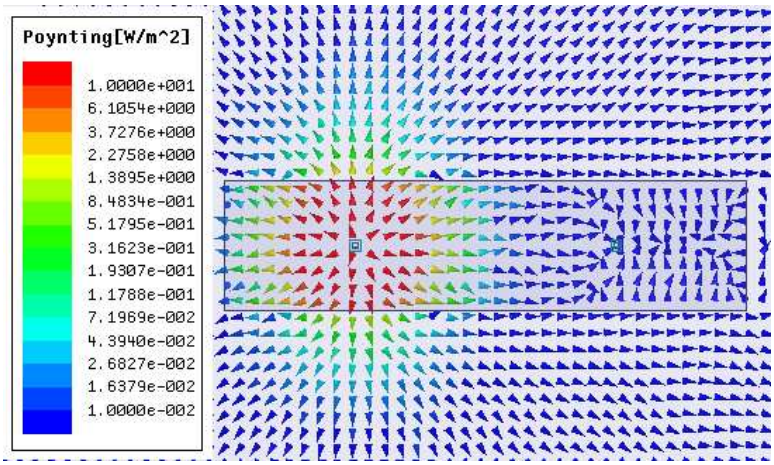

(c)

Figure 4.4: Real part of the Poynting vector inside muscle model (a) MICS band, (b) ISM band and (c) 3.5 GHz band.

4.3 Effect of ECLA Polarization on PL

ECLA inside the human body can have parallel or perpendicular polarization, where ECLA plane is oriented parallel or perpendicular to the human body model respectively as shown in Figure 4.5. PL versus distance between ECLAs inside one-layer muscle equivalent model with dimensions (200x50x50 mm^3) at MICS band in the two cases of polarization is shown in Figure 4.6. Based on this figure ECLAs with parallel polarization have around 10 dB gain in PL compared to ECLAs with perpendicular polarization.

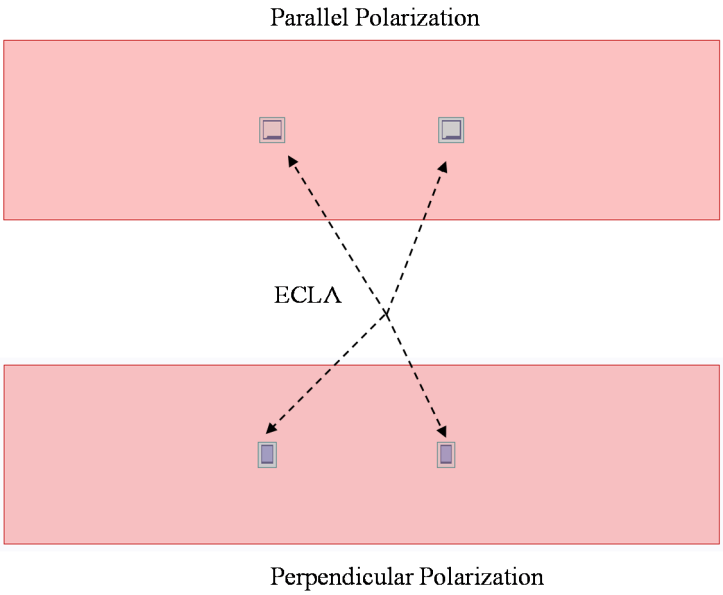

Figure 4.5: Two ECLAs with parallel and perpendicular polarizations inside one-layer muscle equivalent human body model.

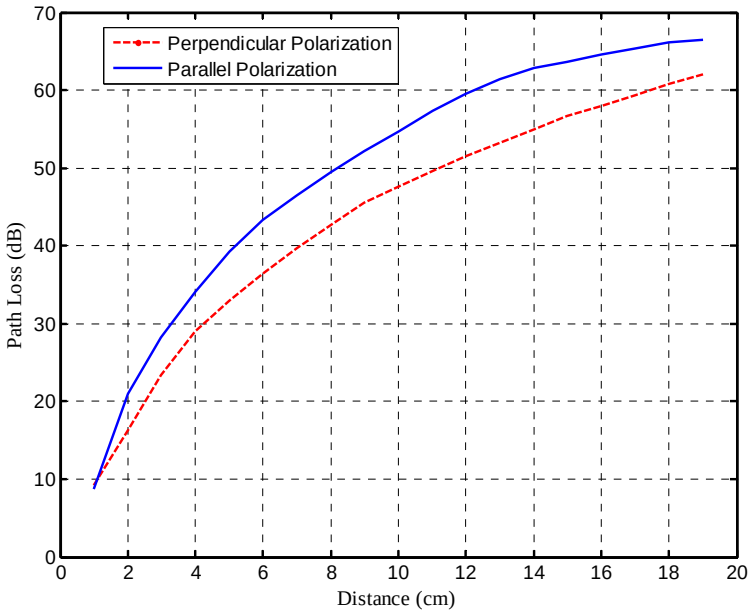

Figure 4.6: PL inside muscle human body model in the case of parallel and perpendicular polarization.

4.4 Effect of Human Body Model on PL

To study the effect of human body model on PL, PL inside one-layer human body model with different electrical properties, antenna location and model shape and dimensions at MICS frequency band will be investigated using HFSS.

4.4.1 Effect of Model Electrical Properties on PL

A block of dimensions (200x50x50 mm^3) with different electrical properties is used to study the variation of PL due to tissues properties inside the human arm at MICS frequency band will be investigated at different values of ε_r and σ. PL inside the human body model at $\varepsilon_r = 53.8$ and different values of σ is shown in Figure 4.7 (a). Also PL inside the model at $\sigma = 1.18$ and different values of ε_r is shown in Figure 4.7 (b). From these results, σ has large effect on PL values and ε_r has small effect on PL values. Also our simulation results agree with the theoretical results for wave propagation inside a lossy medium. For wave propagation inside lossy medium, PL in dB is linearly proportional with the attenuation constant α,

$$PL(dB) \propto \alpha \tag{4.1}$$

And for a uniform plane wave in a lossy medium α can be expressed as-

$$\alpha = \omega\sqrt{\frac{\mu\varepsilon}{2}}\sqrt{-1+\sqrt{1+(\frac{\sigma}{\omega\varepsilon})^2}} \tag{4.2}$$

where $\mu = \mu_0\mu_r$ and $\varepsilon = \varepsilon_0\varepsilon_r$ are the permeability and permittivity of the medium respectively. $\omega = 2\pi f$, is the angular frequency and f is the frequency. For human body tissues medium in MICS band, α can be expressed as-

$$\alpha = 5.96\sqrt{\sqrt{\varepsilon_r^2 + (44.7\sigma)^2} - \varepsilon_r} \tag{4.3}$$

Based on equation (4.3), σ has large effect on PL values and ε_r has small effect on PL values.

4.4.2 Effect of Model Shape and Dimensions on PL

The effect of model dimensions and shape on PL will be investigated using HFSS. PL inside a rectangular model with dimensions (200x50x50 mm^3), which represents a human arm, and with dimensions (300x100x100 mm^3), which represents human body leg, is shown in Figure 4.8.

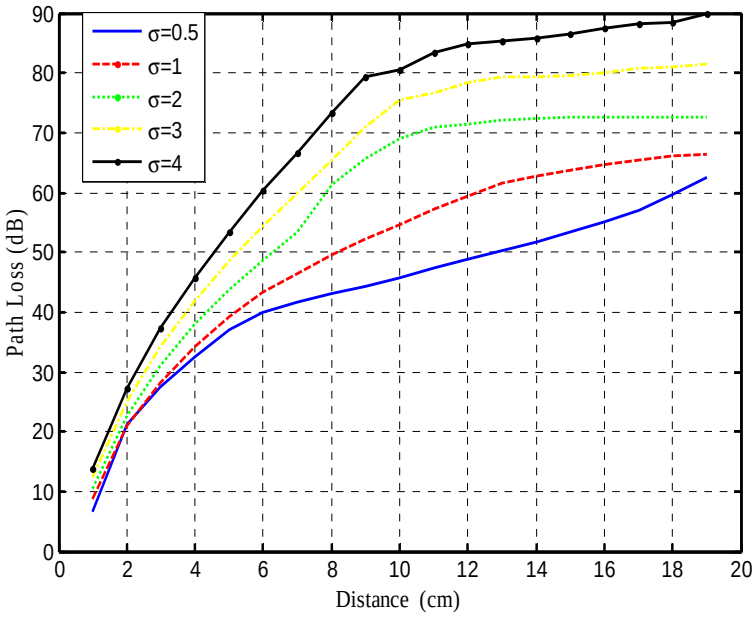

(a)

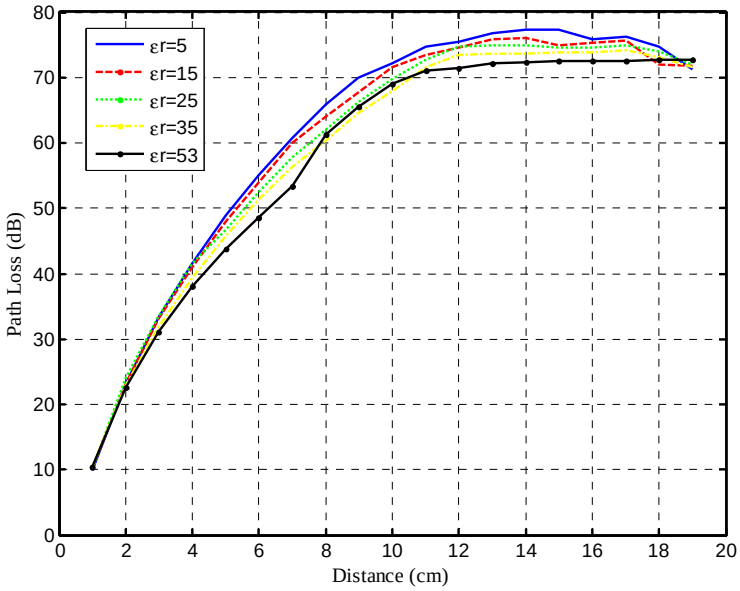

(b)

Figure 4.7: PL inside human body model for (a) different values of σ and constant ε_r and (b) different values ε_r and constant σ.

Based on this figure, at small distance between ECLAs, the model dimensions has a negligible effect on PL. At large distance between implants the peaks in PL are due to the standing wave pattern described in Section 4.2. PL inside a rectangular model with dimensions (300x100x100 mm^3), cylindrical model with radius 50 mm and length 300 mm, which represents a human leg, and spherical model with radius 150 mm, which represents a human head (Figure 4. 9) is shown

in Figure 4.10. All these models have the electrical properties of muscle equivalent model at the MICS frequency band. From this figure, the model dimensions and shape have a small effect on PL. The peaks on PL at large distance between ECLAs are due to standing wave pattern explained in Section 4.2.

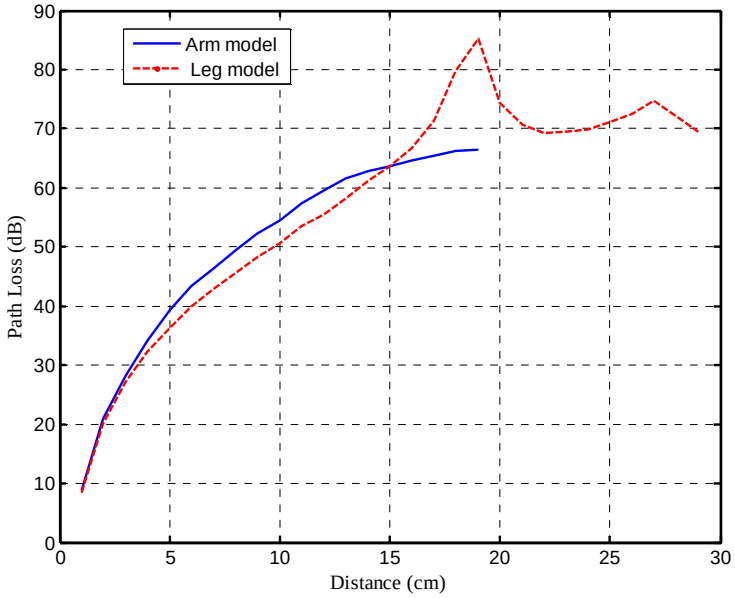

Figure 4.8: PL inside one-layer muscle equivalent arm model and leg model.

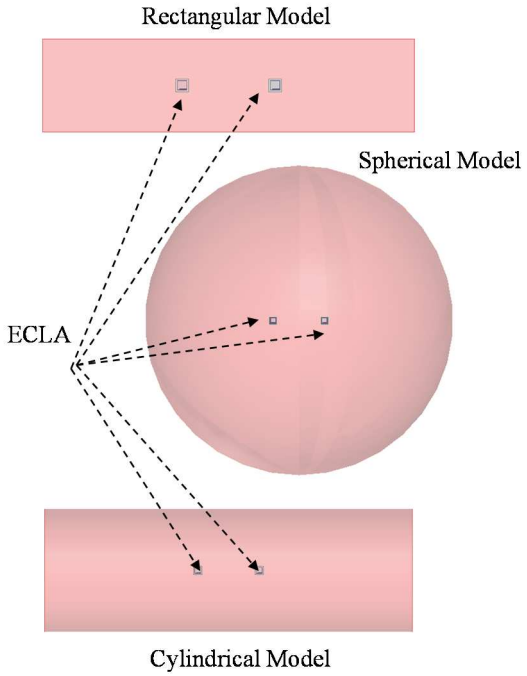

Figure 4.9: Two ECLAs inside one-layer muscle equivalent human body model with rectangular, cylindrical and spherical shapes.

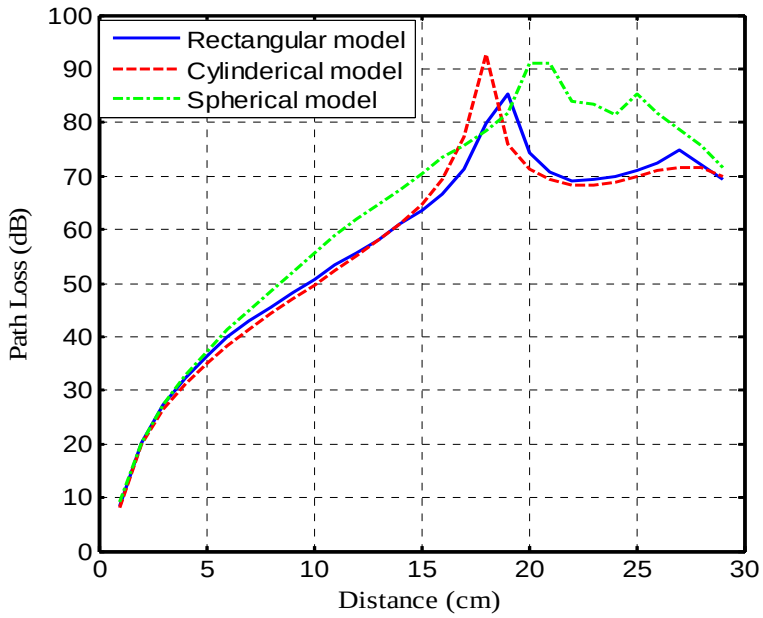

Figure 4.10: PL inside one-layer muscle equivalent human body model with rectangular, cylindrical and spherical shapes.

4.4.3 Effect of ECLA Height on PL

The propagation mechanism inside the human body is a function of the position of implant in the body and its distance from the surface. In this part, effect of antenna height inside the human body on PL will be investigated using HFSS as shown in Figure 4.11. A muscle equivalent model with dimensions (300x100x100 mm^3) is used and ECLA location with respect to the human body model center (s) will change from s=0 mm (ECLAs are located at the center of the model) to s=65 mm (ECLAs are located 15 mm above the human body model in free space). The ECLA is forced to resonate at MICS band using the feeding head and distributed capacitor dimensions. PL inside the human body model at MICS band at different antenna locations is shown in Figure 4.12. Based on these results, at s=55 mm and s=65 mm ECLAs are located in free space, PL is nearly the same and the human body has a small effect on PL. At s=45 mm, where ECLAs are located 5 mm below the surface of the model, PL increases around 10 dB above that that in free space. As ECLAs location moves deeper inside the human body, PL increases and shows some peaks due to the multipath fading. The waves exiting the body traveling as creeping waves around the body and entering the body from other directions which form a standing wave pattern inside the human body model.

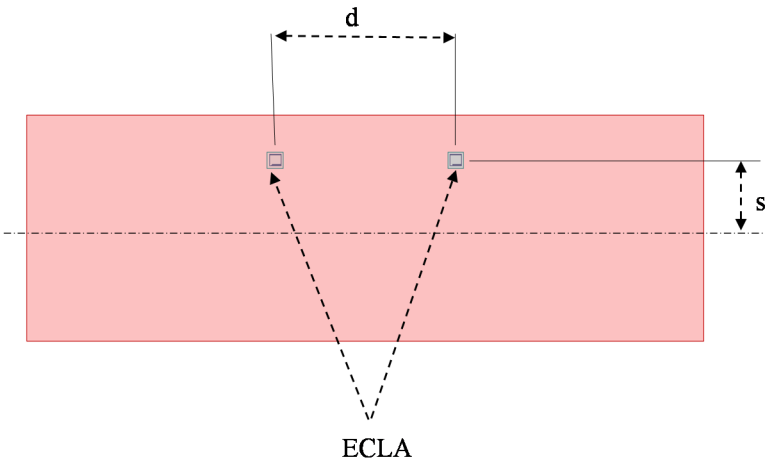

Figure 4.11: Two ECLAs inside one-layer muscle equivalent human body model at different ECLA locations.

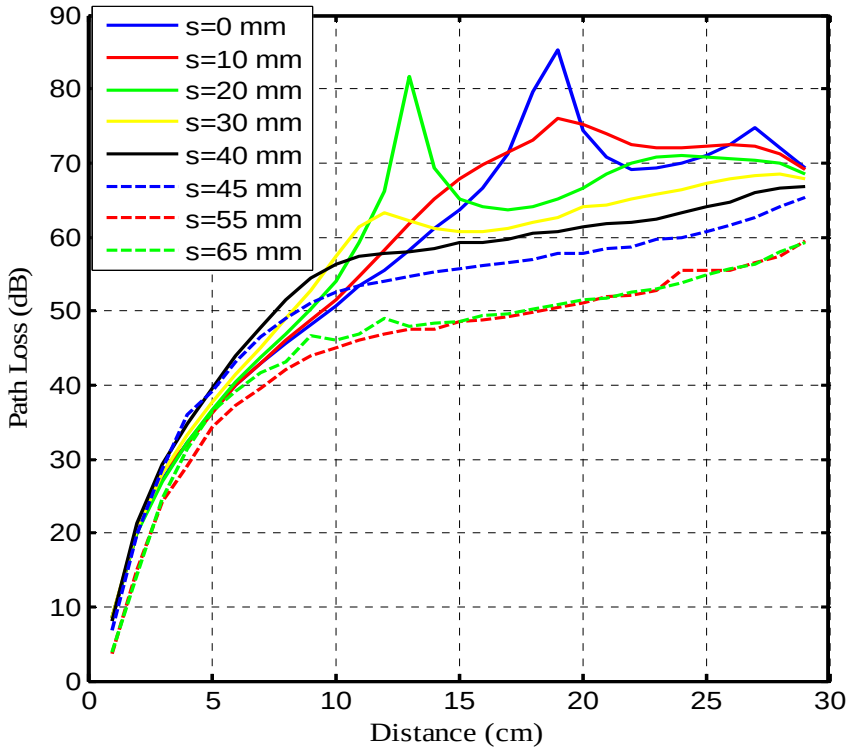

Figure 4.12: PL inside one-layer muscle equivalent human body model at different ECLA locations.

4.5 PL between Four ECLAs inside Human Body Model

PL using four ECLAs inside a muscle equivalent human body model with dimensions (800x400x400 mm^3) which can represent the upper part of the human body will be investigated using HFSS (Figure 4.13.). These ECLAs are located at the center of the model. The distance between ECLAs (d_1 and d_2) will change and the effect on PL will be shown. PL between four

ECLAs inside the human body model at different separations between ECLAs is shown in Table 4.2. From this table, PL between any two ECLAs is constant as the distance between them does not change independent of other ECLAs locations.

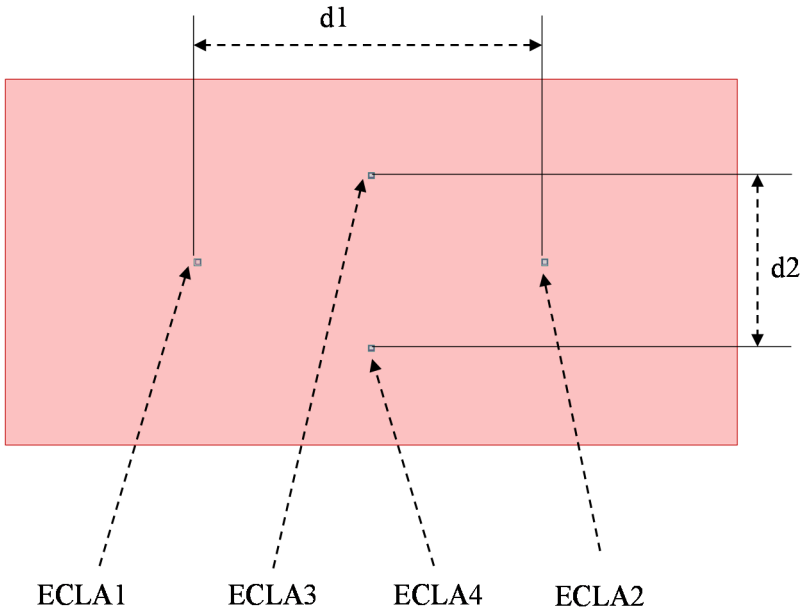

Figure 4.13: Four ECLAs inside one-layer muscle equivalent human body model at different ECLA locations.

Table 4.2: PL between four ECLAs inside muscle model at different distance between ECLAs.

Distance (mm)	PL_{12}	PL_{13}	PL_{14}	PL_{23}	PL_{24}	PL_{34}
780-380	94.7	91.3	91.4	91.1	91.6	98.7
780-190	94.2	111.6	113.2	114	112	82.7
780-95	94.4	127	127	126	127	53.8
780-50	94.4	130	130	120	127	37
780-25	94.2	129	128	128	128	24
390-380	145	109	110	108	109	99
195-380	84.2	80	89	89	90	96
100-380	55.4	84	84	84	84	96
50-380	37	83	83	83	83	97
25-380	24	83	83	83	83	96

4.6 PL inside Simple Human Body Model

To find approximate value for PL inside the human body, PL inside a simple one-layer human body model has the electrical properties of muscle equivalent model at MICS band as shown in Figure 4.14, will be discussed. Nine ECLAs are placed inside the model at different locations and each ECLA is located at the center of each parts. The scattering matrix (S) between all nine ECLAs is shown in (4.4), also the magnitude of electric field and real part of Poynting vector are shown in Figure 4.15. One can see from these figures that the spherical wave radiated from the transmitting antenna decays rapidly by distance. Far from the transmitting antenna, the communication channel is through the wave which excites the body and travels around the body and reenter at each point of the body. The maximum computed loss through this model is 135 dB for the case that all antennas are inside human body.

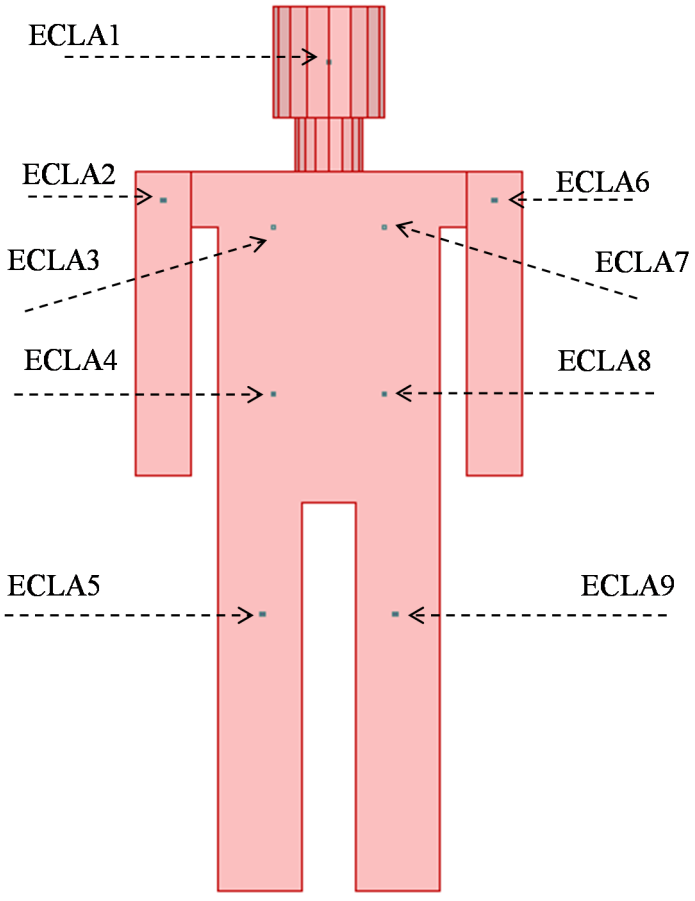

Figure 4.14: Nine ECLAs inside the human body model at different ECLA locations.

$$S(dB) = -\begin{bmatrix} 12 & 89 & 100 & 118 & 129 & 89 & 100 & 118 & 135 \\ 89 & 12 & 81 & 102 & 102 & 94 & 107 & 114 & 110 \\ 100 & 81 & 12 & 108 & 119 & 108 & 86 & 122 & 134 \\ 118 & 102 & 108 & 12 & 112 & 113 & 122 & 86 & 128 \\ 129 & 102 & 119 & 112 & 12 & 111 & 133 & 130 & 93 \\ 89 & 94 & 108 & 113 & 111 & 12 & 81 & 101 & 102 \\ 100 & 107 & 86 & 122 & 133 & 81 & 12 & 109 & 119 \\ 118 & 114 & 122 & 86 & 130 & 101 & 109 & 12 & 111 \\ 135 & 110 & 134 & 128 & 93 & 102 & 119 & 111 & 12 \end{bmatrix} \quad (4.4)$$

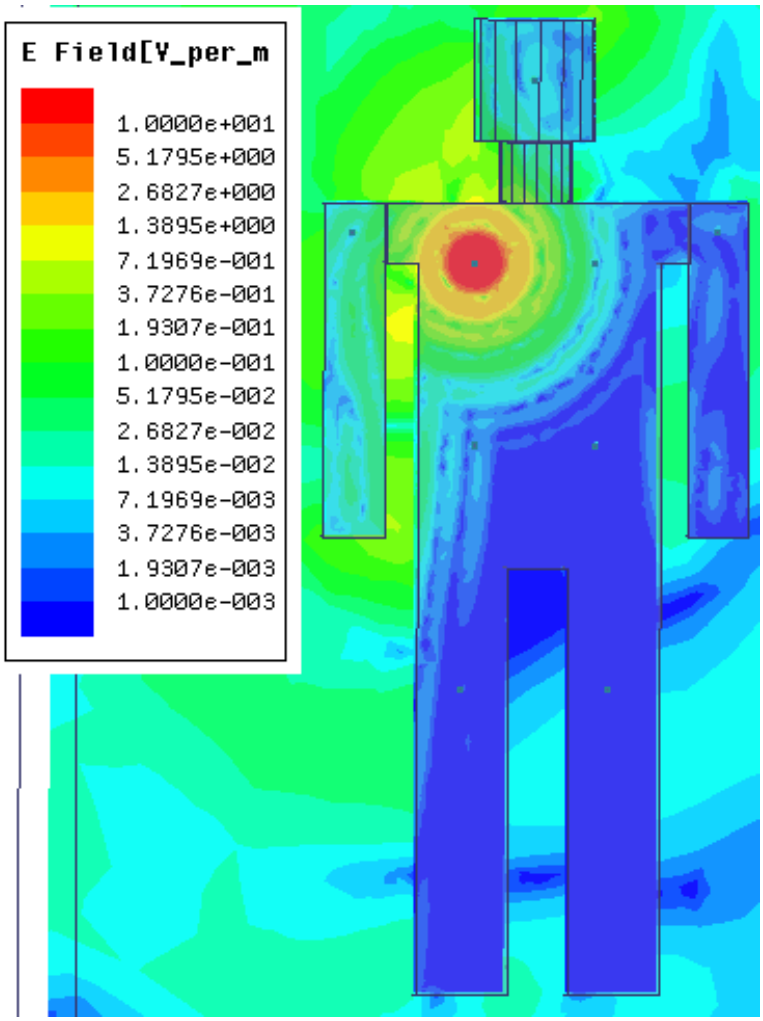

(a)

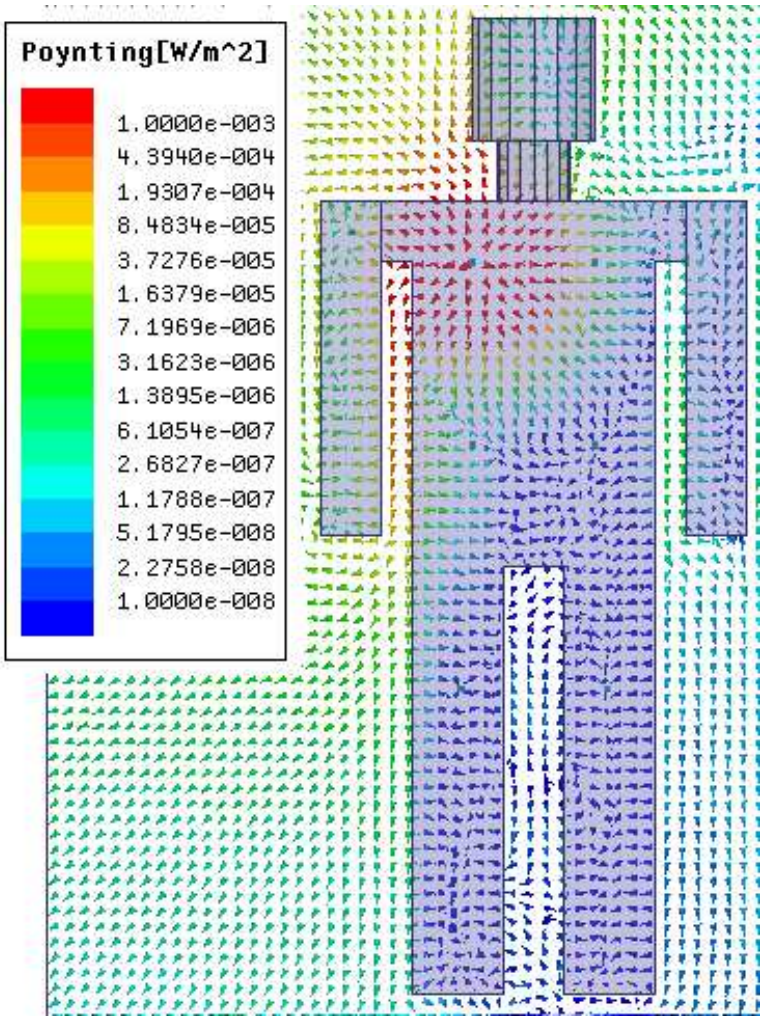

(b)

Figure 4.15: Magnitude of electric field and real part of Poynting vector inside muscle model at different ECLA locations.

4.7 PL inside the Human Body

The previous simple model in previous section is replaced with a more realistic model to compute the PL more accurately. Practical WBAN channel model will be investigated using XF7 simulation software, in which a model of the human body is created, consisting of 39 human tissues. The transmitting (Tx) antenna is an ECLA with dimensions (20x20 x5 mm^3) and it is located 2 mm away from the chest. All the Receiving (Rx1: Rx5) antennas are ECLAs with dimensions (5x5x3 mm^3) and are installed at different vertical locations inside the human body as shown in Figure 4.16. An ECLA with dimensions (10x10x3 mm^3) (Rx6) is placed inside the human body, aligned with the transmitter, at 12 cm distance. Transmitting and receiving ECLAs have a resonance

frequency in the MICS band. Table 4.3, shows PL between the transmitting and receiving antennas with different distances between ECLAs. From these results, maximum PL between the transmitting and receiving antenna at any location inside the human body is about 90 dB. Also, antenna size reduction from (10x10x3 mm^3) to (5x5x3 mm^3) increases PL by 5 dB.

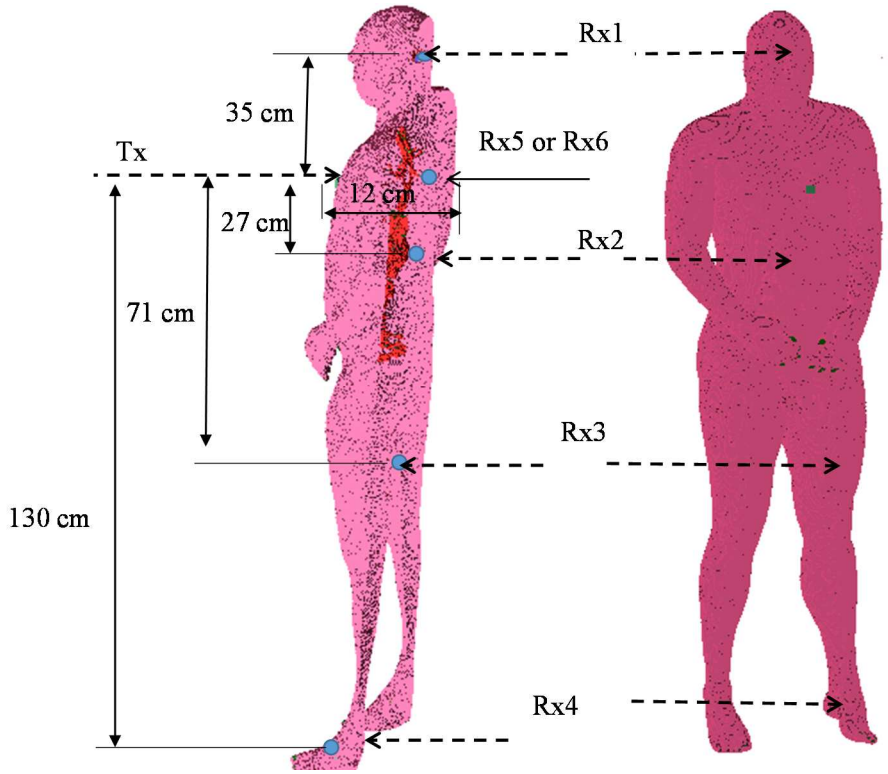

Figure 4.16: ECLAs inside exact human body model at different locations.

Table 4.3: PL between ECLAs inside exact human body model.

ECLAs	PL (dB)	Distance between ECLAs (cm)
(Tx,Rx1)	76	35
(Tx,Rx2)	81	27
(Tx,Rx3)	86.4	71
(Tx,Rx4)	89	130
(Tx,Rx5)	45	12
(Tx,Rx6)	27	6.5
(Tx,Rx7)	40	12
(Rx1,Rx5)	94	35

4.8 PL using Ferrite-Loaded ECLA

In this part, PL between two ferrite-loaded ECLAs inside one-layer model is calculated and compared with PL between non-ferrite-loaded ECLAs. ECLAs have dimensions (5x5x3 mm^3), (3x3x3 mm^3), (2x2x2 mm^3) and (1x1x1 mm^3) at MICS frequency bands and are located at the center of the model. The one-layer model has dimensions (200x50x50 mm^3) and has the electrical properties of skin tissues at MICS frequency band (Figure 4.19). The distance between ECLAs is changed and PL is calculated using HFSS. Figure 4.20, shows PL between ECLAs with different dimensions in the two cases of ferrite-loaded ECLA and non-ferrite-loaded ECAL. Based on this figure as the dimensions of ECLA decrease, ferrite-loaded ECLA has lower PL compared to non-ferrite-loaded ECLA. So for small antenna size ferrite-loaded ECLA has better propagation channel inside human body compared to non-ferrite-loaded ECLA.

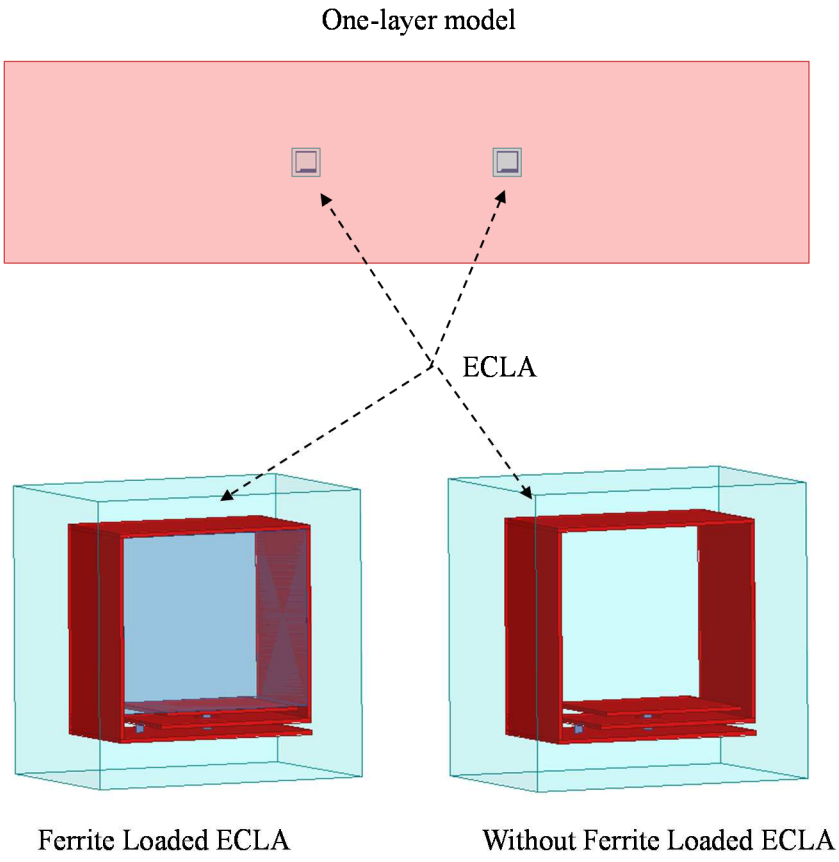

Figure 4.17: Two ECLAs with and without ferrite-loaded material inside one-layer human body model.

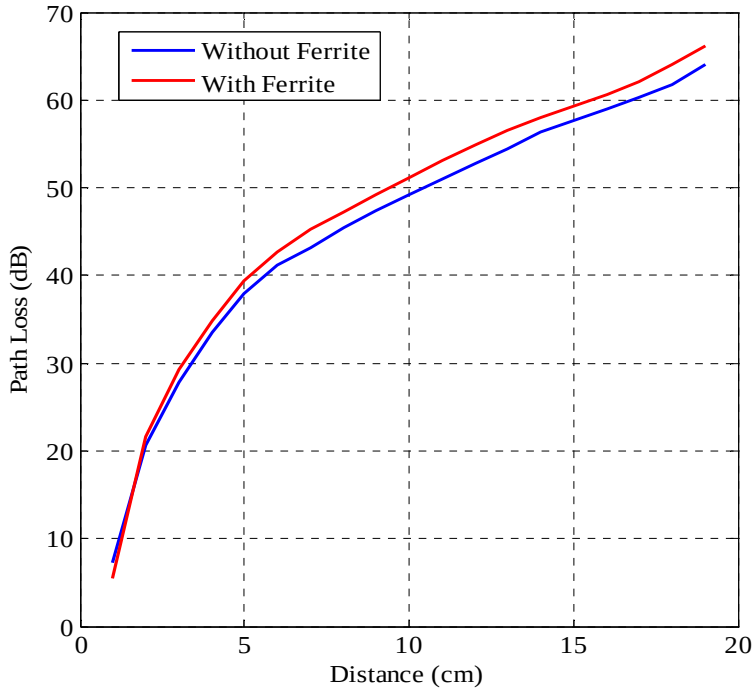
Without Ferrite
With Ferrite
Path Loss (dB)
Distance (cm)
0
10
20
30
40
50
60
70
0
5
10
15
20

(a)

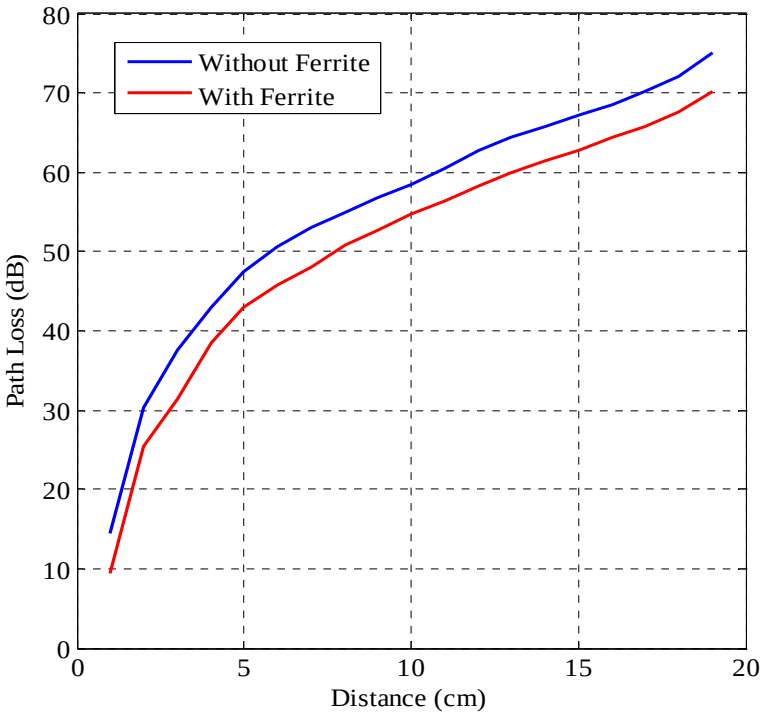
Without Ferrite
With Ferrite
Path Loss (dB)
Distance (cm)
0
10
20
30
40
50
60
70
80
0
5
10
15
20

(b)

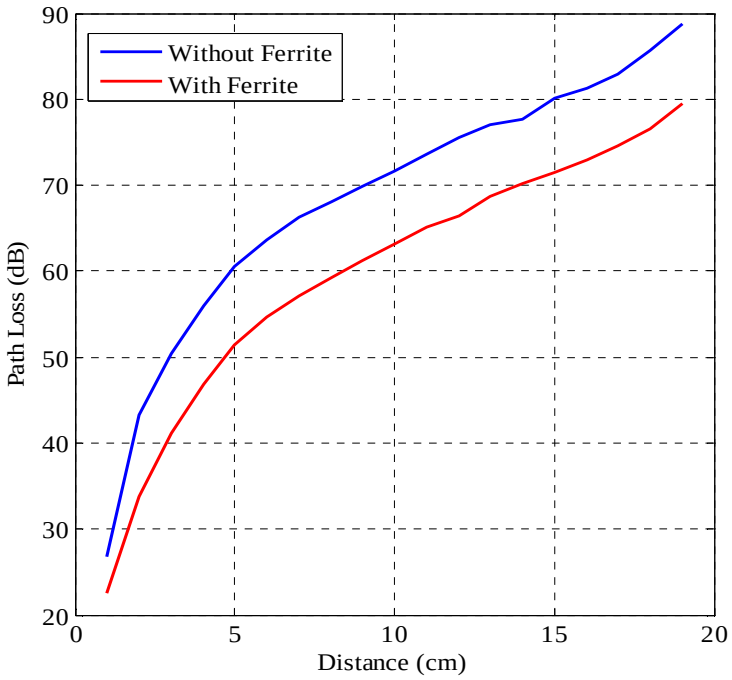

(c)

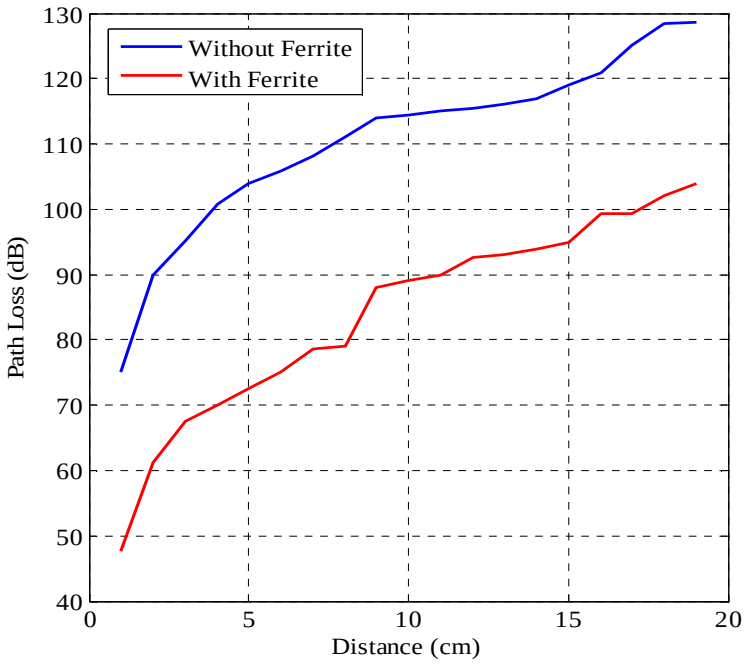

(d)

Figure 4.18: PL between Two ECLAs with and without ferrite-loaded material inside one-layer human body model. ECLA has dimensions (a) (5x5x3 mm^3), (b) (3x3x3 mm^3), (c) (2x2x2 mm^3) and (d) (1x1x1 mm^3)

4.9 PL Model

To simplify the design of WBAN, a model for PL inside the human body must be specified. PL inside the human body will be related to human body electrical properties, distance between antennas, antenna polarization, human body shape and dimensions, and different parameters of the environment. PL for WBAN can be described using three models: theoretical model, empirical model and statistical model. Theoretical model is intended for detail exploration of influence of the body structure on antenna pattern. Also this model requires a detail description of the propagation environment and is therefore probably not suitable for modeling macro environment. Empirical model is traceable to agreed set of propagation measurement and is intended to provide a convenient base for statistical modeling of WBAN networks. Compared to the theoretical model, the empirical model will use a greatly simplified description of the environment and although statistically accurate at the network level, it will not be precise at the link level. Statistical model is described in Chapter 1and can be calculated using equation (1.5).

4.10 Experimental Work

Two ECLAs with dimensions (20x20x5 mm^3) and (5x5x3 mm^3) are designed as transmitting and receiving antennas respectively. A box with dimensions (30x20x10 cm^3) filled with ground pork is designed as one-layer model. Receiving ECLA is located at distance 7 cm inside the model and transmitting ECLA is located 2 mm from the model surface. The horizontal distance between transmitting and receiving antennas changes from 2 cm to 17 cm (Figure 4.19). PL between the two ECLAs using both HFSS and experimental work is shown in Figure 4.20. From this figure the experimental and simulation results are approximately the same with small differences due to measurement error. Compared with Table 4.3 (at distance 12 cm ,simulation PL inside human body equal to 45 dB and measurement PL inside ground pork is 42 dB) these results are approximately the same. So the simulation work described in this chapter is validated by the experimental work.

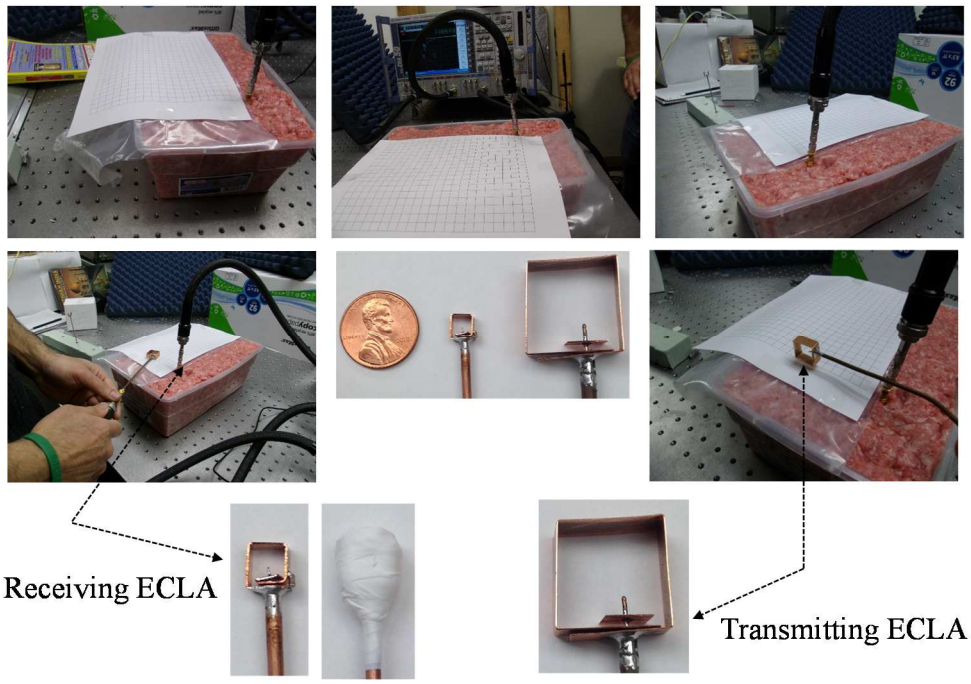

Figure 4.19: . Experimental work setup of two ECLAs with ground pork.

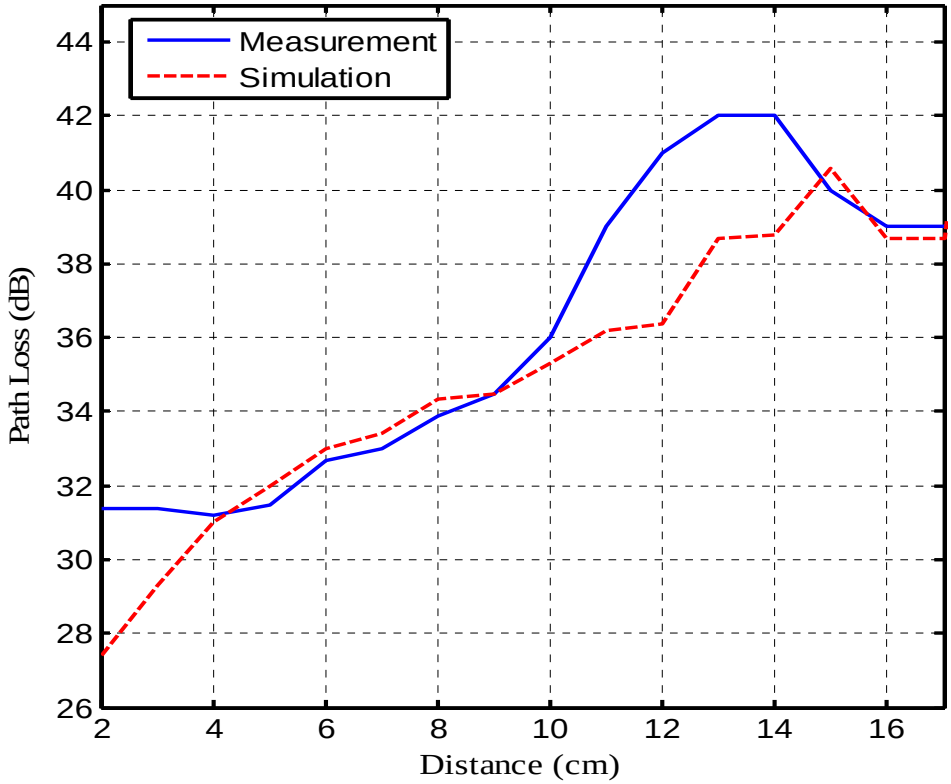

Figure 4.20: Experimental and simulation PL between two ECLA using ground pork.

4.11 Chapter Summary

Intra-body propagation channel inside the human body model was investigated using ECLA. Propagation channel was investigated in terms of PL which includes: antenna loss, near-field loss and path loss. The effect of different parameters as operating frequency bands, ECLA Polarization, ECLA location and human body parameters on PL were investigated. PL between ferrite-loaded ECLAs was provided to see the effectiveness of ferrite-loaded antenna. Also the simulation results were validated using an experimental work. It was found that, MICS band is the suitable band for propagation channel inside the human body model. Based on this study, the maximum PL inside the human body is about 90 dB at MICS band for an antenna size of (20x20x5 mm^3) as the transmitting antenna and (5x5x3 mm^3) as the receiving antenna. The ferrite-loaded ECLA has better propagation channel inside the human body model compared to non-ferrite-loaded ECLA at small ECLA size.

Chapter 5

Wireless Power Transfer for Implanted Devices

Wireless power transfer is studied using ECLA as a self-matched coupler for implanted applications. The implanted ECLA is investigated with two different sizes to show the effect of the antenna miniaturization on the power transfer efficiency. Furthermore, the SAR is computed to estimate the maximum delivered power to the implanted device. The prototyped antennas are used for experimental validation of the simulated data. It is shown that the power transfer efficiency of 63% is possible for implanted devices located 2 cm inside the human body chest.

5.1 Introduction

Although artificial organs and implanted sensors/actuators have been subjects of science fiction books and movies for a long time, they are coming to the reality in the modern healthcare technology [167]. Smart pills [168] and pacemakers [169] have already been used as mobile and static implanted devices while the implanted brain machine interface, BMI, [170] are becoming popular. However, powering up these devices is still a challenge since many of implanted devices cannot exclusively rely on the batteries as power sources. WPT is one of the important candidates to support implanted devices.

Action at a distance was one of the major concepts in the early electromagnetics theorem [171] which led to develop the concept of electromagnetic fields and later radiation. One of the essential points of action at a distance is power transfer in free space. Heinrich Hertz validated the possibility of transferring electromagnetic energy without using a metallic structure [172] in 1888. Soon after him, Nikola Tesla demonstrated a wireless power transfer technique [173] based on electric field in 1891. Since then, WPT has been the subject of research for many scientists and researchers until Marin Soljacic's team's demonstration in 2007 [174] which brought the subject of WPT to the

spotlight. This was the beginning of a new race on WPT for wireless charging application both in the industry and academia [23, 175].

The smart implanted medical devices have been the focus of many research programs over the last few decades [146, 164]. Most of the modern implanted devices are able to receive commands from the outside world or relay information from various sensors within the host body. This makes the implanted antenna an important component of the implanted devices in the future of healthcare technology. However, there are many challenges involved in the design of implanted antennas, including but not limited to: antenna miniaturization, antenna loss, compatibility with the human tissues, detuning due to the dynamic nature of human body as described in Chapters 1 and 3.

The classical WPT design introduced in [174] consists of a drive coil, transmitting or primary coupler, receiving or secondary coupler, and the load coil. This system in addition to the matching circuits of drive and load coils should be optimized for any specific application. The optimization goal is the wireless power transfer efficiency which can be translate to the ratio of the delivered power to the load over the available power to the drive coil. Although the size and shape of the coils are not the most important optimization parameters for wireless charger in the case of cellphones or consumer devices, implanted devices are very sensitive to the size and shape of the implant. One of the main issues with the classical design proposed in [174], which has been followed by many inventors, is its number of coils and three dimensional nature of the transmitting side and the receiving side. The proper design for an implanted device would be a flat structure to reduce the occupied volume with the implant.

ECLA was proposed as a self-matched coupler both as a radiating and coupling component. As a coupler, it has been shown that ECLA can reach proper quality factor for an efficient WPT system. At the same time, there is no required matching circuitry or drive coil which decrease the loss and the volume of the implant. Therefore, ECLA will be used in this effort for the main coupling device.

The design of implanted WPT and the simulation results are described in Section 5.2 and Section 5.3. Measurement setup in addition to the measured data is studied in section 5.4. The summary of the chapter is provided in Section 5.5.

5.2 Implanted Wireless Power Transfer

Wireless implanted devices in general have to satisfy the limits on the SAR dictate by the FCC and ERC as described in chapter 1. As described on Chapters 2 and 3, the loop antenna is the suitable design for implanted devices application. So in this chapter the WPT for implanted devices will be explained using our proposed ECLA.

Two different antenna sizes are considered in this chapter for two different applications. The small ECLA is (5x5x3 mm^3) and will be used in a small sensor node or a smart pill. The large ECLA is a circular loop of radius 10 mm and will be used for higher required power where there is not very strict limitation on the coupler size. Both ECLAs are surrounded with a biocompatible insulation layer, has thickness of 1mm, relative dielectric constant of 2.07 and zero conductivity. Another circular ECLA with radius of 17.25 mm is used as a driver (transmitting) antenna. The three ECLAs have a resonant frequency at MICS band dedicated by FCC and ERC for implanted applications. The resonant frequency of each ECLA is fixed at MICS frequency band using the distributed capacitor dimensions.

5.2.1 WPT inside One-Layer Model

The preliminary simulation is performed in a block of material with the electrical property of muscle tissue (relative dielectric constant "$\varepsilon_r = 58$ "and conductivity"$\sigma = 0.81$ ") and size of (200x200x200 mm^3) as shown in the Figure 5.1. Using HFSS, the scattering parameters (S_{11}) of the three ECLAs inside one-layer muscle model and free space are shown in Figure 5.2.

The parameter of interest is S_{12} which includes all the loss mechanism and represents the total power transfer loss. Scattering parameters (S_{12}) between two circular ECLAs and between circular and square ECLAs at distance 2 cm and 3 cm between implanted devices are shown on Figure 5.3 and Figure 5.4. It has been shown that the electric size of the resonators can affect the coupling; the larger the coupler, the higher the coupling efficiency [176, 177]. Figure 5.3 shows that S_{12} for the small implanted antenna varies from -10.5 dB to -16.5 dB as the implanted ECLA moves 10 mm deeper into the lossy material. Figure 5.4 shows that the larger ECLA performs much better and its S_{12} changes from -7.2 dB to -13 dB for the same situation. This experiment has been repeated for different distances d for both receiving antennas, and the result are presented in Figure 5.5. One can see the effect of antenna size and also distance on the WPT efficiency. The PL for

the small antenna is almost 5 dB higher than the large antenna for distances larger than 15 mm which can be assigned to the higher antenna loss in the small antenna. Although large distances impose high path loss to the implanted WPT system, based on this simulations, one can have a realistic WPT system 2 cm to 3 cm below the skin.

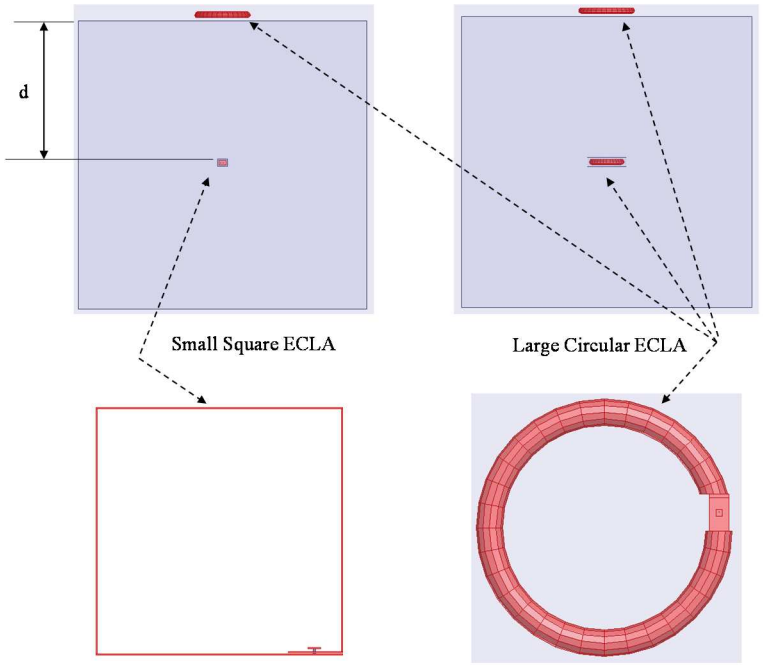

Figure 5.1: Small square and large circular ECLAs with one-layer muscle model.

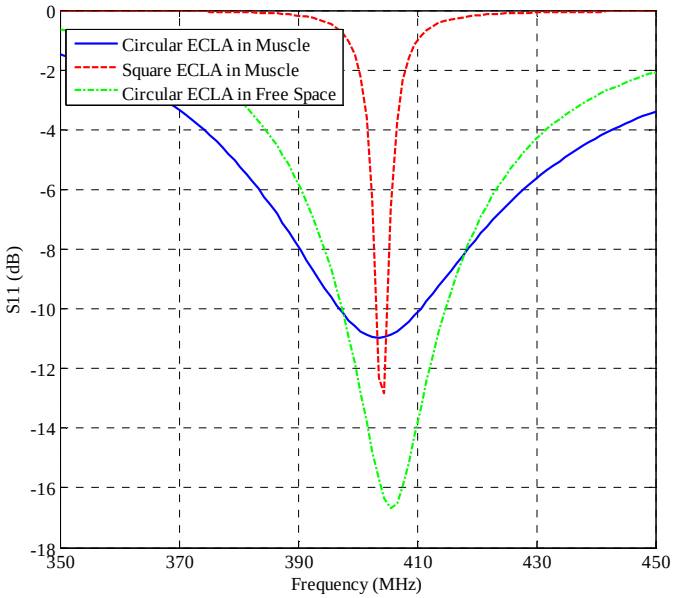

Figure 5.2: Scattering Parameters (S_{11}) of circular and small square ECLAs inside one-layer muscle tissue and free space.

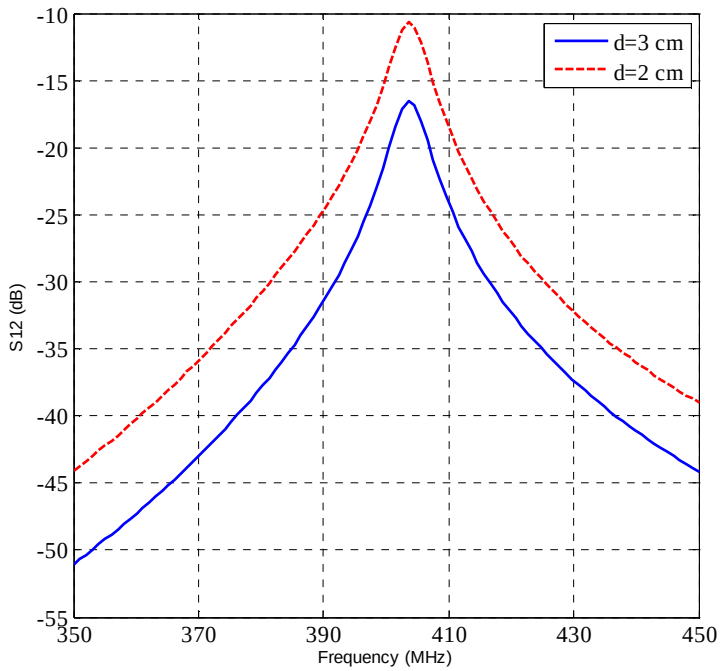

Figure 5.3: Scattering Parameters (S_{12}) between square and circular ECLAs inside one-layer muscle tissue at different distance 'd' between ECLAs.

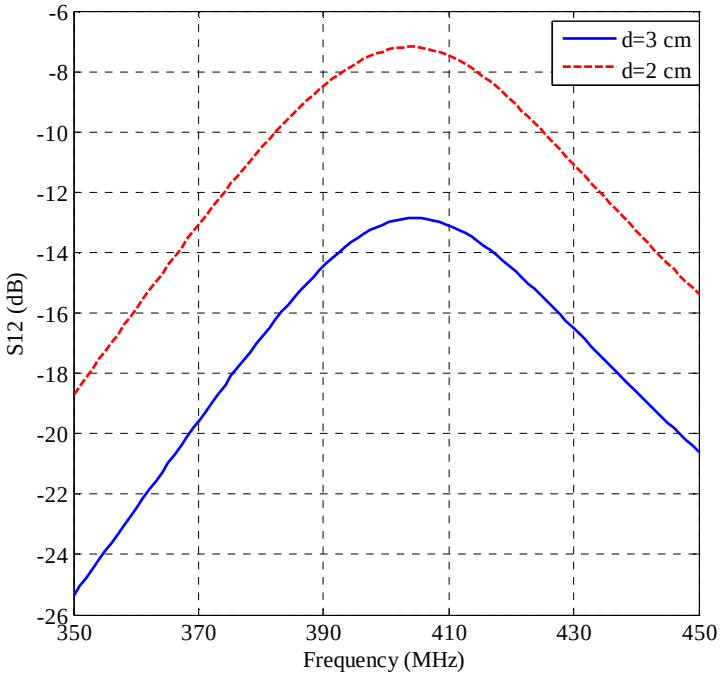

Figure 5.4: Scattering Parameters (S_{12}) between two circular ECLAs inside one-layer muscle tissue at different distance 'd' between ECLAs.

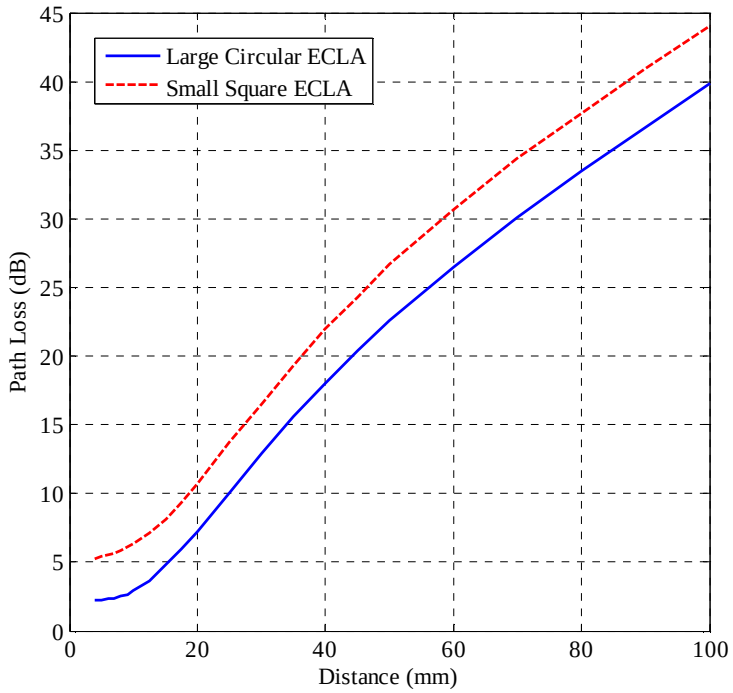

Figure 5.5: Path Loss between two circular ECLAs and between circular and square ECLAs verse distance "d" between ECLAs.

5.2.2 Effect of ECLA Polarization on WPT

ECLA inside human body models can have either parallel or perpendicular polarization, where implanted receiving ECLA parallel or perpendicular to the transmitting ECLA, respectively. ECLA with two cases of polarization are shown in Figure 5.6, and the PL between the two ECLAs in the two cases of polarization are shown in Figure 5.7. Based on these results, ECLA with perpendicular polarization has around 15 dB gain in PL compared to ECLA with parallel polarization.

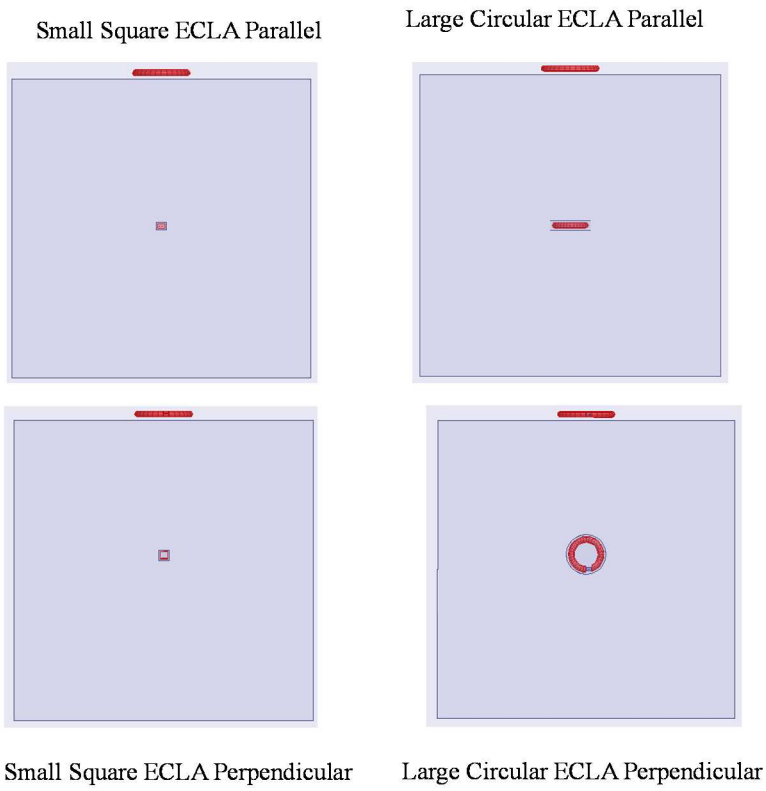

Figure 5.6: Small square and large circular ECLAs with one-layer muscle model in the two cases of polarization.

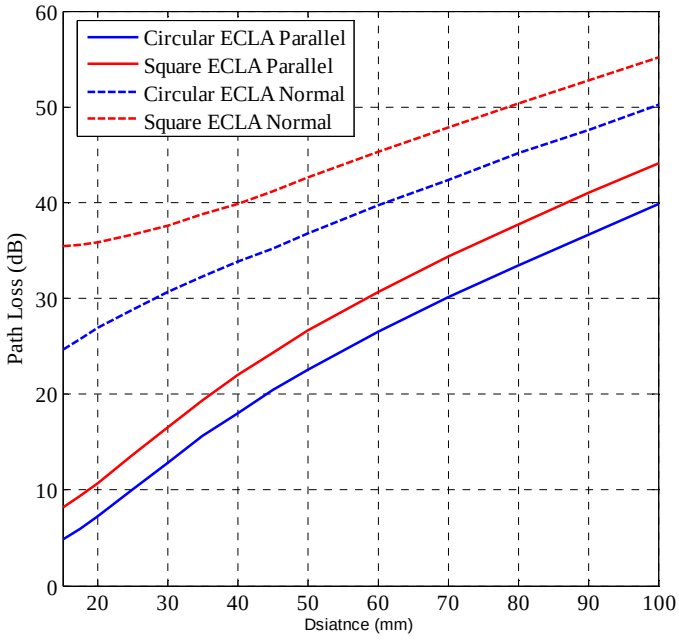

Figure 5.7: Scattering parameters between two circular ECLAs and between square and circular ECLA in the two cases of polarization.

5.2.3 Effect of Feeding Port Metal on WPT

To measure the ECLA performance inside human body models using vector network analyzer, a metal part must be connected to the feeding port of ECLA as shown in Figure 5.8. The PL between two circular ECLAs and between circular and square ECLAs with and without metal parts are shown in Figure 5.9. From these results, the adding of the metal parts increase the PL by around 1dB to 2 dB compared to ECLA without metal parts

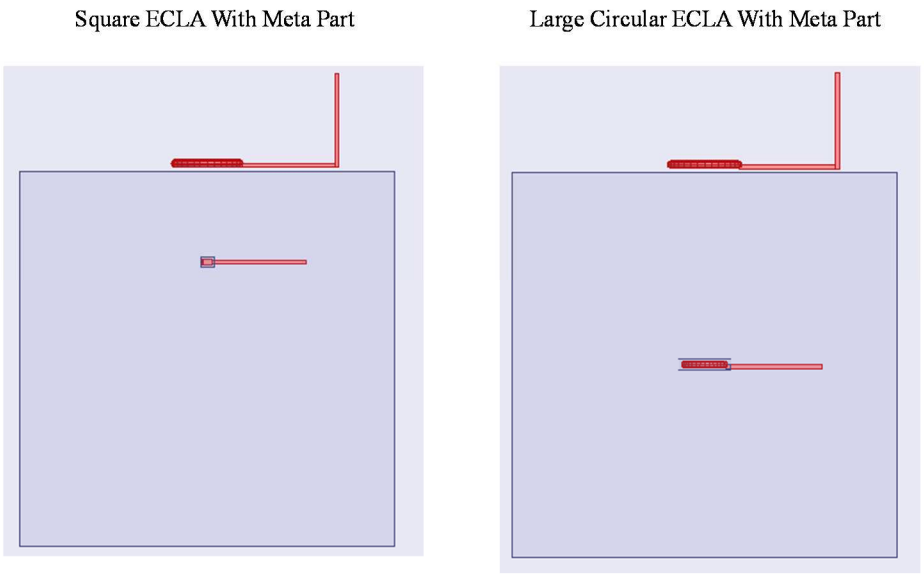

Figure 5.8: Small square and large circular ECLAs with one-layer muscle model with metal parts

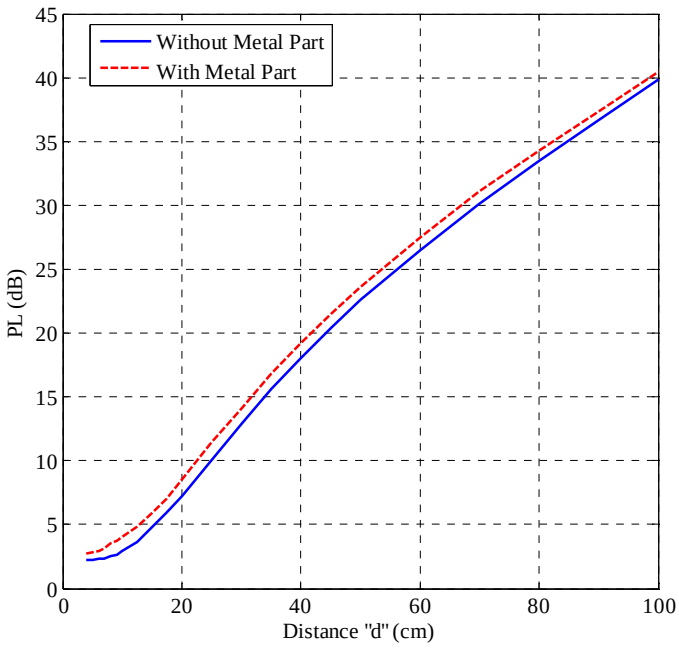

(a)

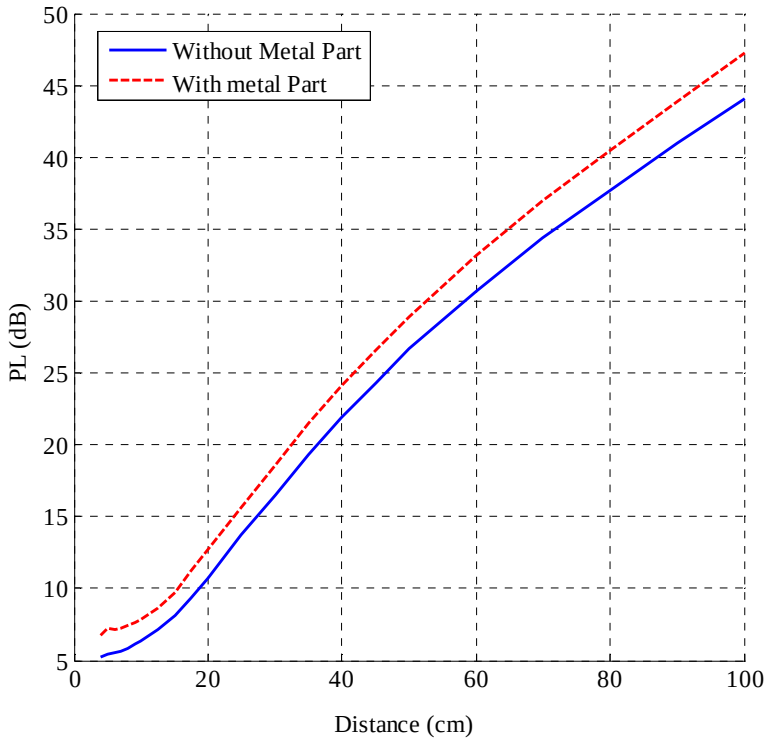

(b)

Figure 5.9: PL between two ECLAs with metal parts (a) two circular ECLA and (b) square and circular ECLA.

5.3 WPT inside Human Head and Body Models

Figure 5.10 and Figure 5.11 show the simulation setup using a more sophisticated human head and human body models using XF7. The larger antenna (circular ECLA with radius 10 mm) is located in the chest, 2 cm and 3 cm under the skin, next to the heart which can be used for charging a pacemaker battery (Figure 5.11). The small antenna (square ECLA with dimensions 5x5x3 mm^3) is located in the brain "2 cm and 3 cm under the skin" as a BMI device which might operate based on RFID technology (Figure 5.10). In both cases the transmitting antenna is a circular ECLA with radius 17.25 mm located 2 mm from the skin of the human body chest or human head in free space. All ECLAs have a resonant frequency at MICS frequency band as shown in Figure 5.12.

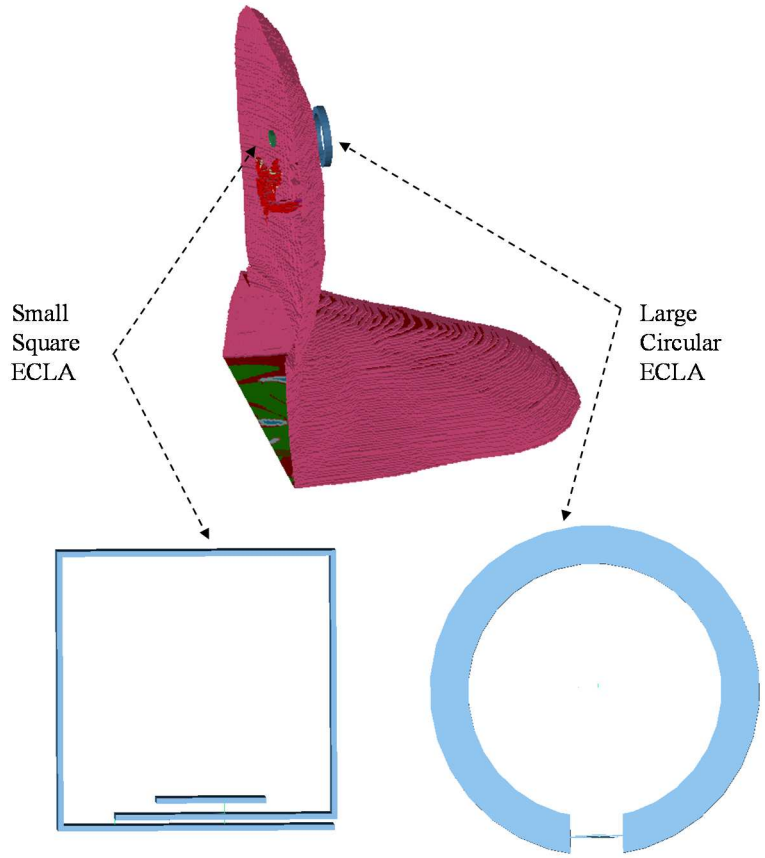

Figure 5.10: Small square and large circular ECLAs with human head.

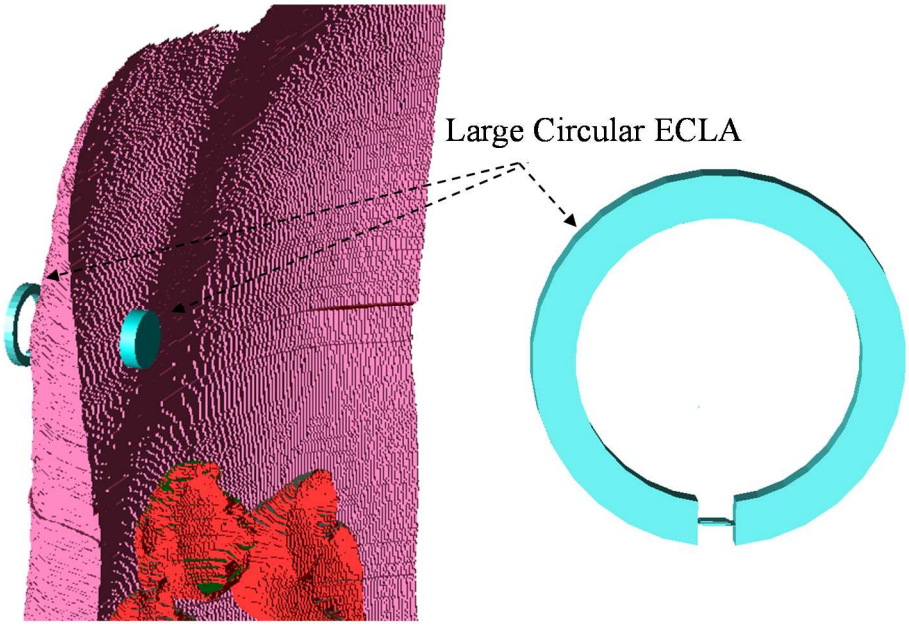

Figure 5.11: Large circular ECLAs with human body chest.

The scattering parameters (S_{12}) between circular and square ECLAs with human head model and between two circular ECLAs with human chest model are presented in the Figure 5.13 and Figure 5.14 respectively. Due to the problem complexity and simulation time the results are calculated at the required distances (2 cm and 3 cm) between ECLAs. The maximum WPT efficiency computed by XF7 for implanted devices located 2 cm and 3 cm under the skin in the chest is about 63% (-2 dB) and 26% (-5.8 dB) respectively. The results for the small square ECLA inside the head for distances 2 cm and 3 cm are 8.9% (-10.5 dB) and 4% (-14 dB), respectively.

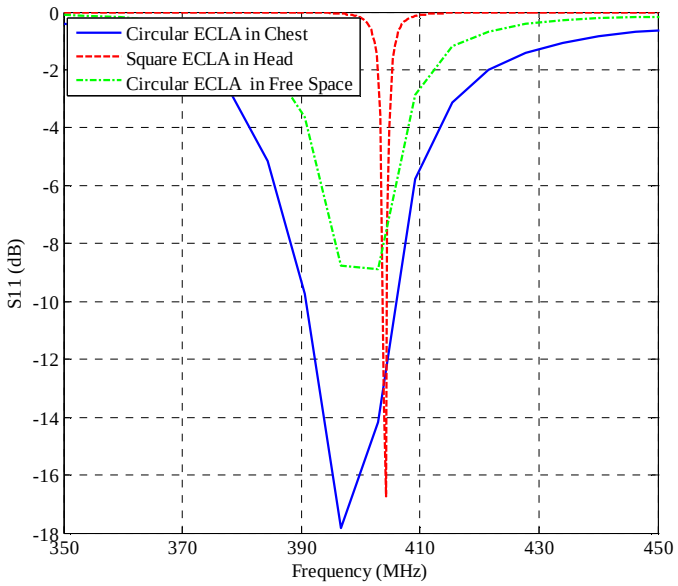

Figure 5.12: Scattering Parameters (S_{11}) of circular and small square ECLAs inside human chest, human head and free space.

Figure 5.15 shows the SAR values inside the human head and chest averaged over 1 g of tissue mass for 1 W input power from a circular ECLA located 2 mm from the surface of the human head or chest. From these results, the maximum 1 g averaged SAR for 1 W input power inside the human chest and head are 27.3 W/kg and 24 W/kg, respectively. The maximum 1 g averaged SAR inside one-layer muscle tissue using HFSS is about 27 W/kg. Due to the SAR limitation, the maximum power allowed for the antenna in the brain would be 60 mW, which delivers 37 mW and 15.6 mW to the antennas located at 2 cm and 3 cm under the skin in the human chest, respectively. These values for the square ECLAs in the head are 5.93 mW (7.73 dBm) and 2.66 mW (4.25 dBm), which sufficiently exceed the minimum required power for modern RFID tags (-18 dBm).

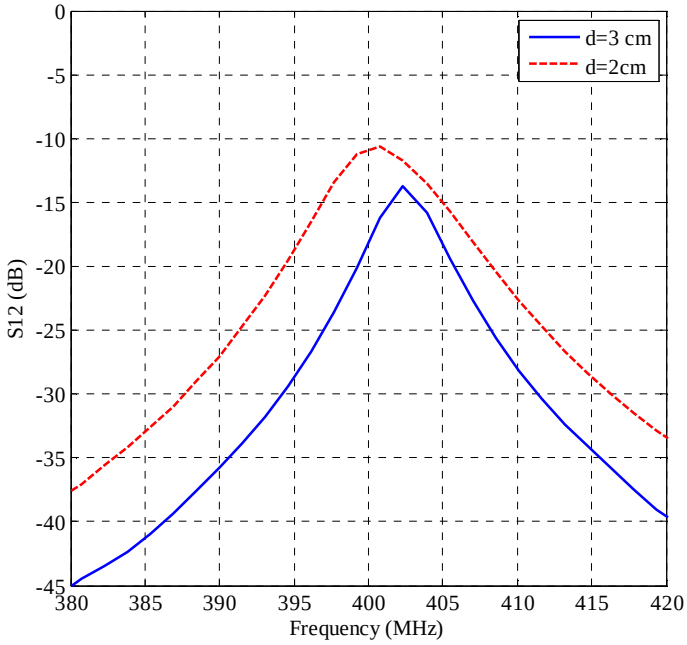

Figure 5.13: Scattering Parameters (S_{12}) between square and circular ECLAs with human head at different distance '*d*' between ECLAs.

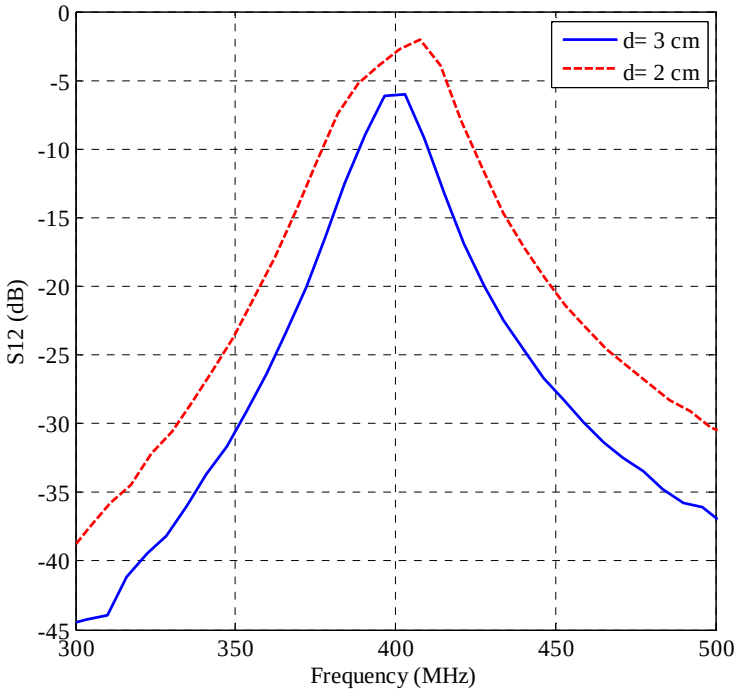

Figure 5.14: Scattering Parameters (S_{12}) between two circular ECLAs with human body chest at different distance '*d*' between ECLAs.

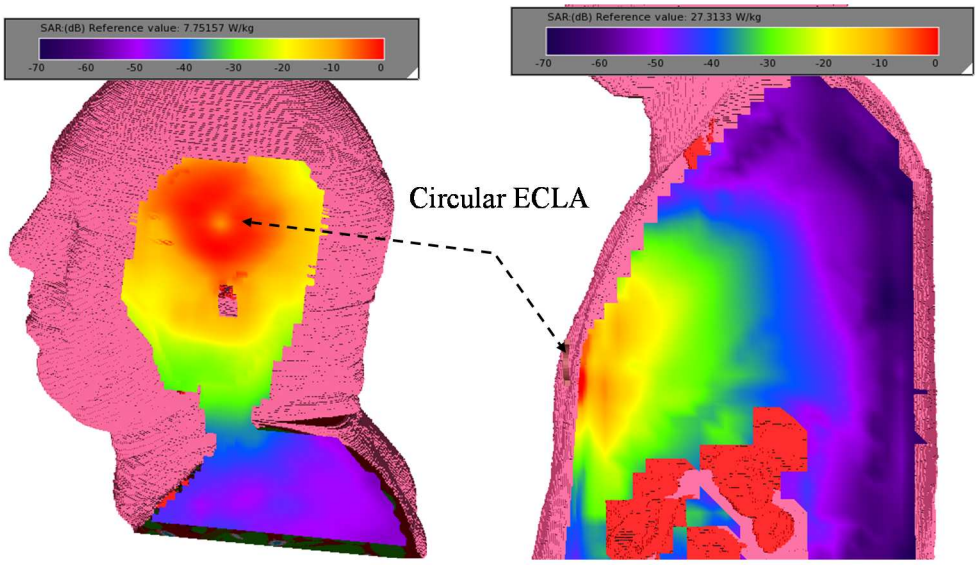

Figure 5.15: 1g averaged SAR inside human chest and human head due to circular ECLA.

5.4 Experimental Work

A solution made by 51.16% water, 46.78% sugar and 1.49% salt has electric properties close to muscle tissues at MICS frequency band (relative dielectric constant "$\varepsilon_r = 58$ "and conductivity"$\sigma = 0.83$ "). This solution has been used for the experimental results in this chapter. A box of size (35x25x25 cm^3) is filled with human body solution, the driver ECLA (circular ECLA with radius 17.25 mm) is placed 2 mm from the solution surface and the load ECLA (circular ECLA with radius 10 mm or square ECLA with dimensions 5x5x3 mm^3) is placed at the center of the solution and move toward the surface of the solution as shown in Figure 5.16. Using the vector network analyzer, the scattering parameters S_{11} of all ECLAs and S_{12} between the driver and load ECLAs with different separation distance 'd' are measured. Scattering parameters S_{11} of all ECLAs and S_{12} between the two circular ECLAs at distance 2 cm and 3 cm are shown in Figure 5.17 and Figure 5.18 respectively. The PL between the two circular ECLAs and between circular and square ECLAs verses distance "d" is shown in Figure 5.19.

Based on these results, the measured data inside this solution are much higher than the simulation results using HFSS. There are a few possibilities suggested here for the main cause of these discrepancies: The simulation results are computed for cases where the antennas are not connected to any feeding cable while the measured data include the effects of the feeding cables.

No balun was used to limit the currents on the outer surface of the coaxial cables. Also, the feeding cables are in direct connection with the lossy solution. This will increase the overall loss significantly. The other parameter which might be important is the accuracy of the solution in terms of electromagnetic properties. In practical cases, there will not be any coaxial cable connected to the implanted antenna.

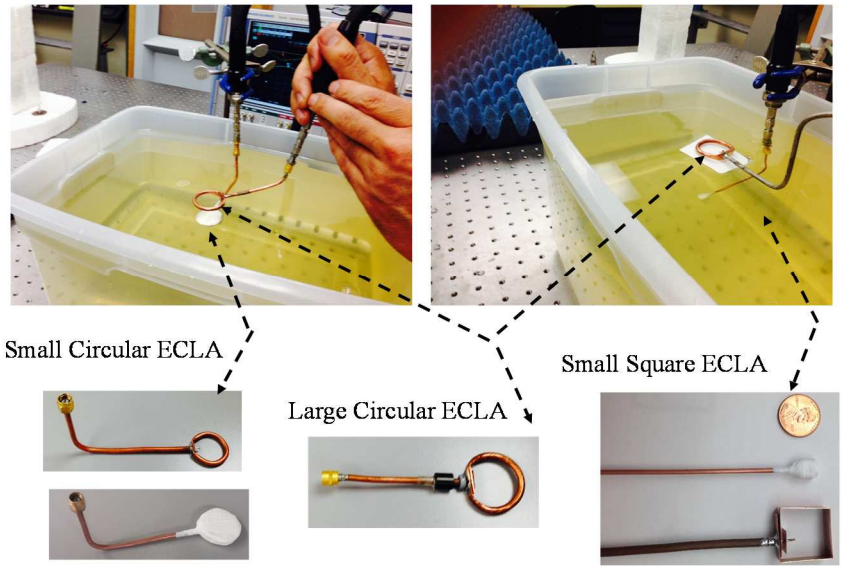

Figure 5.16: Experimental work setup for circular and square ECLAs with human body solution.

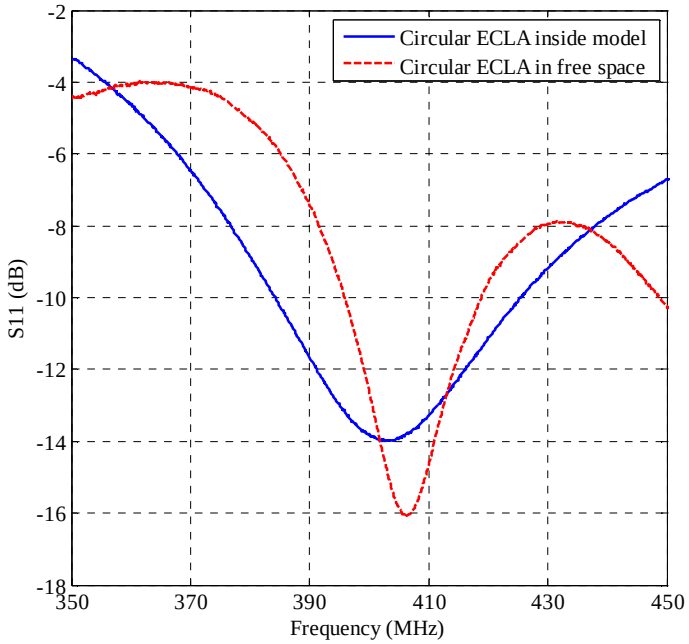

Figure 5.17: Scattering Parameters (S_{11}) of large circular and small circular ECLAs inside human body solution and free space.

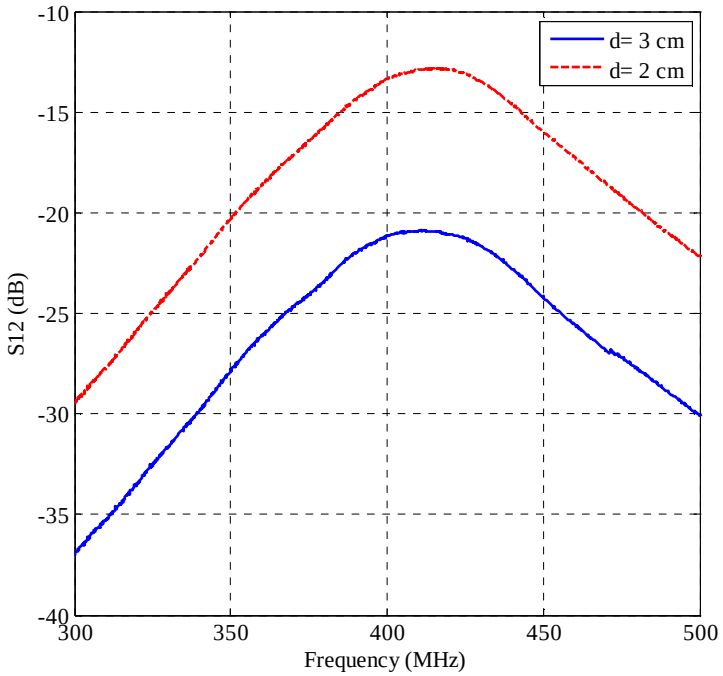

Figure 5.18: Scattering Parameters (S_{12}) between two circular ECLAs with human body solution at different distance "*d*" between ECLAs.

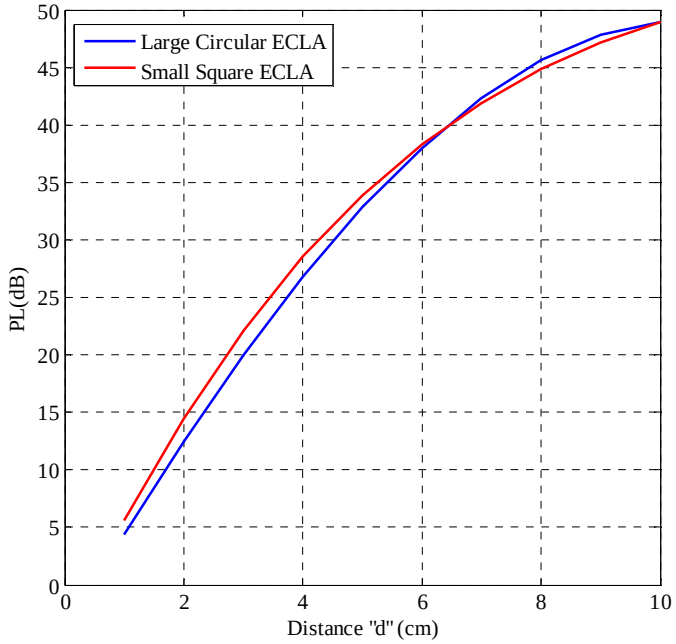

Figure 5.19: Path Loss between two circular ECLAs and between square and circular ECLAs with human body solution verses distance "*d*".

5.5 Chapter Summary

WPT is an important issue for the implanted device applications, where it is used to deliver the power to implanted devices instead of using batteries which have specific life time. WPT for implanted devices inside the human body was investigated using the proposed ECLA with different shapes and dimensions. The WPT was investigated using HFSS inside one-layer muscle model and inside the human body models using XF7. The simulation results were validated using experimental work. From these results an efficient WPT for implanted devices will be occurred when the implanted device located at 2 cm or 3 cm inside the human body. The maximum allowed power for implanted antenna is about 0.06 watts, and the maximum WPT efficiency for implanted devices located at 2 cm inside the human body is about -2 dB (63%). The power delivered to the implanted device is about 0.037 watts which it is large enough for charging its batteries.

Chapter 6

Conclusion & Future Work

This dissertation proposed a magnetic field antenna for implanted applications as in WBAN. The magnetic field antenna has a better performance inside a lossy medium (as human body) compared to the electric field antenna of the same size and the same input power. The performance of the antenna is measured in terms of power loss (SAR) and radiated power. The proposed ECLA as a self-resonator consists of distributed capacitance and inductance. ECLA can be tuned to any frequency using the distributed capacitor or using a lumped capacitor in parallel with the distributed capacitor. The input impedance of the antenna can be tuned to any frequency using the feeding head dimensions. ECLA is designed at the allowed frequency bands MICS, ISM and 3.5 GHz, which are dedicated by FCC and ERC for implanted applications. The channel model inside the human body for WBAN is studied using the proposed ECLA. Also, the WPT for implanted devices is investigated using the proposed ECLA.

6.1 Summary of the Dissertation

Extensive research has been conducted in the design of antennas for implanted devices applications. Most of the previous designs for implanted applications are electric field antennas which suffer from two main problems: high near-zone electric field leading to high SAR inside human body tissues and the detuning effect due to electrical properties of human body tissues. In this research an ECLA antenna is proposed as a magnetic field antenna to tackle all the above limitations for implanted devices applications. In the beginning, a brief description for the implanted antenna design challenges for WBAN applications as frequency bands, power loss, channel model, power source, energy consumption and etc. were investigated. All the previous research on antenna design and channel model was presented.

A fair comparison between the performance of magnetic field antenna and electric field antenna inside a lossy medium, such as a human body, was investigated. The comparison was investigated in terms of power loss and radiated power. It was found that the magnetic field antenna has a better performance inside a lossy medium compared to an electric field antenna of the same size and the same accepted power.

The proposed ECLA was investigated as a magnetic field antenna for implanted device applications as in WBAN. ECLA structure and the control of the resonant frequency were explained. The performance of ECLA inside different human body models at the allowed frequency bands was investigated using simulation software and validated using experimental work. The effect of ECLA dimensions and the insulation layer on ECLA performance were investigated. Also, the performance of ferrite-loaded ECLA was investigated inside the human body models. It was found that ECLA has better performance inside the human body models in terms of power loss, and it is less-sensitive to the detuning effect due to the electrical properties of human body tissues.

The channel models for WBAN inside and near the human body was investigated using the proposed ECLA antenna. Channel model was investigated in term of PL which contains all the loss mechanisms associated with the antenna. PL was investigated inside different human body models at the allowed frequency bands using simulation software and validated using some experimental work. Effects of antenna size, antenna polarization, model shape & dimensions, model electrical properties on PL were investigated. Also, PL between the ferrite-loaded ECLA inside the human body model was investigated and compared to non-ferrite-loaded ECLA. It was found that MICS band has the best propagation channel inside human body models compared to other frequency bands. ECLA polarization and ECLA size have a considerable effect on PL; on the other hand, the human body shape and dimensions have small effect on PL. Human body conductivity has a large effect on PL compared to human body relative dielectric constant. The maximum PL inside the human body models equals 90 dB in the worst case scenario.

Finally, the WPT as a powering technology for implanted devices instead of using batteries which have a specific life-time was investigated. WPT was investigated inside different human body models using simulation software and validated using some experimental work. It was found that an efficient WPT for implanted devices can be achieved for implanted devices located at a distance of 2 or 3 cm inside the human body. The maximum WPT efficiency of 63% can be

achieved inside the human body. Due to the SAR limitation the maximum allowed input power to antenna is about 0.06 watts which will deliver a 0.04 watts to the implanted devices.

6.2 Suggestions for Future Work

The patient's safety is an important factor in the design of the WBAN for implanted applications. The power lost inside the human body due to the WBAN components, which is measured using SAR, must be kept as small as possible. For future research, the following parameters must be considered in the WBAN design:

- Antenna types, materials and shapes.
- Operating frequency band.

A large amount of research has been conducted to design WBANs protocols in the PHY layer, MAC layer and network layer. The following points must be considered in the future research of the WBAN protocols design for implanted applications:

- Take the movement of the human body into consideration.
- Consider the mobility of the WBAN nodes.
- Low power features such as an adaptive duty cycle for lowering the idle listening and overhearing.
- The uses of the human physiology such as heart rate for time synchronization.
- Use a combination of thermal aware routing with an energy efficient mechanisms.
- Dynamic management of resource.
- Power management, sensor calibration and context aware network configuration.
- The computational load should be limited.

All WBAN devices require an energy source for data collection, processing and transmission, so the developing of suitable power supply is an important issue. Most of WBAN devices are powering up using batteries which have a specific life-time and may not be replaced as in implanted applications. It is important to develop a suitable technique for recharging the batteries. The most suitable technique for recharging batteries is the WPT. Due to the limited energy provided by batteries, the following points must be considered in the future research:

- Study the energy scavenging techniques in details for implanted applications.

- Energy scavenging from body sources such as body heat.
- Develop a better scheduling algorithm and power management.

For the design of a power efficient WBAN the following parameters must be considered:

- Average bandwidth.
- Maximum required bandwidth.
- Active power.
- Standby power.
- Startup time.
- Communication setup.

The material used in the design of the WBAN sensor and actuator for implanted application are very important, so the following points must be considered in the future research:

- Develop a biocompatible material for sensor and actuator.
- The size, shape and types of the materials are very important for implanted applications.

The communication of health related information between sensors in WBAN and over the internet to servers is strictly private and confidential, so security, authentication, privacy, QoS, and reliability are very important for implanted applications which must be considered for future research.

In most cases, WBAN are designed by engineers and set up in the hospital by medical staff, so the WBAN must be capable for configuring and maintaining itself automatically which must be considered as an important point for future research.

Much research has been conducted to model signal loss through the human body. Another interesting research point is to use the human body model as a medium to transmit the electrical signal from one area of the body to another area. Also, a complete PL model inside the human body in terms of different parameters is an important issue in the future research.

REFERENCES

[1] S. Patel, K. Lorincz, R. Hughes, N. Huggins, J. Growdon, D. Standaert, *et al.*, "Monitoring Motor Fluctuations in Patients With Parkinson's Disease Using Wearable Sensors," *Information Technology in Biomedicine, IEEE Transactions on,* vol. 13, pp. 864-873, 2009.

[2] A. Wheeler, "Commercial Applications of Wireless Sensor Networks Using ZigBee," *Communications Magazine, IEEE,* vol. 45, pp. 70-77, 2007.

[3] E. Monton, J. F. Hernandez, J. M. Blasco, T. Herve, J. Micallef, I. Grech, *et al.*, "Body area network for wireless patient monitoring," *Communications, IET,* vol. 2, pp. 215-222, 2008.

[4] T. Xiao-Fei, Z. Yuan-Ting, C. C. Y. Poon, and P. Bonato, "Wearable Medical Systems for p-Health," *Biomedical Engineering, IEEE Reviews in,* vol. 1, pp. 62-74, 2008.

[5] K. Wac, "Healthcare to go - [comms healthcare]," *Engineering & Technology,* vol. 4, pp. 62-65, 2009.

[6] M. Patel and W. Jianfeng, "Applications, challenges, and prospective in emerging body area networking technologies," *Wireless Communications, IEEE,* vol. 17, pp. 80-88, 2010.

[7] N. Agoulmine, M. J. Deen, L. Jeong-Soo, and M. Meyyappan, "U-Health Smart Home," *Nanotechnology Magazine, IEEE,* vol. 5, pp. 6-11, 2011.

[8] K. Kihyun, Y. Sumin, L. Sungho, N. Sangwook, Y. Young Joong, and C. Changyul, "A Design of a High-Speed and High-Efficiency Capsule Endoscopy System," *Biomedical Engineering, IEEE Transactions on,* vol. 59, pp. 1005-1011, 2012.

[9] M. Kim and J. I. Takada, "Characterization of Wireless On-Body Channel Under Specific Action Scenarios at Sub-GHz Bands," *Antennas and Propagation, IEEE Transactions on,* vol. 60, pp. 5364-5372, 2012.

[10] U. Mitra, B. A. Emken, L. Sangwon, L. Ming, V. Rozgic, G. Thatte, *et al.*, "KNOWME: a case study in wireless body area sensor network design," *Communications Magazine, IEEE,* vol. 50, pp. 116-125, 2012.

[11] Z. Zhaoyang, W. Honggang, A. V. Vasilakos, and F. Hua, "ECG-Cryptography and Authentication in Body Area Networks," *Information Technology in Biomedicine, IEEE Transactions on,* vol. 16, pp. 1070-1078, 2012.

[12] Z. Zhilin, J. Tzyy-Ping, S. Makeig, and B. D. Rao, "Compressed Sensing of EEG for Wireless Telemonitoring With Low Energy Consumption and Inexpensive Hardware," *Biomedical Engineering, IEEE Transactions on,* vol. 60, pp. 221-224, 2013.

[13] G. R. Tsouri and O. Maimon, "Respiration rate estimation from channel state information in wireless body area networks," *Electronics Letters,* vol. 50, pp. 732-733, 2014.

[14] E. Jovanov, A. O'Donnell Lords, D. Raskovic, P. G. Cox, R. Adhami, and F. Andrasik, "Stress monitoring using a distributed wireless intelligent sensor system," *Engineering in Medicine and Biology Magazine, IEEE,* vol. 22, pp. 49-55, 2003.

[15] A. Boulis, D. Smith, D. Miniutti, L. Libman, and Y. Tselishchev, "Challenges in body area networks for healthcare: the MAC," *Communications Magazine, IEEE,* vol. 50, pp. 100-106, 2012.

[16] B. Johny and A. Anpalagan, "Body Area Sensor Networks: Requirements, Operations, and Challenges," *Potentials, IEEE,* vol. 33, pp. 21-25, 2014.

[17] N. Vidal, S. Curto, J. M. Lopez-Villegas, J. Sieiro, and F. M. Ramos, "Detuning effects on implantable antenna at various human positions," in *Antennas and Propagation (EUCAP), 2012 6th European Conference on*, 2012, pp. 1231-1234.

[18] F. Merli, L. Bolomey, E. Meurville, and A. K. Skrivervik, "Implanted antenna for biomedical applications," in *Antennas and Propagation Society International Symposium, 2008. AP-S 2008. IEEE*, 2008, pp. 1-4.

[19] A. Kiourti and K. S. Nikita, "A Review of Implantable Patch Antennas for Biomedical Telemetry: Challenges and Solutions [Wireless Corner]," *Antennas and Propagation Magazine, IEEE,* vol. 54, pp. 210-228, 2012.

[20] M. Manteghi, "Electrically coupled loop antenna as a dual for the planar inverted-f antenna," *Microwave and Optical Technology Letters,* vol. 55, pp. 1409-1412, 2013.

[21] A. Ibraheem and M. Manteghi, "Performance of an Implanted Electrically Coupled Loop Antenna inside Human Body," *Progress In Electromagnetics Research,* vol. 145, p. 8, 2014.

[22] M. Da and Z. Wen-Xun, "Analytic Propagation Model for Wireless Body-Area Networks," *Antennas and Propagation, IEEE Transactions on,* vol. 59, pp. 4749-4756, 2011.

[23] K. Jinwook, S. Hyeon-Chang, K. Do-Hyeon, and P. Young-Jin, "Optimal design of a wireless power transfer system with multiple self-resonators for an LED TV," *Consumer Electronics, IEEE Transactions on,* vol. 58, pp. 775-780, 2012.

[24] C. Huasong, V. Leung, C. Chow, and H. Chan, "Enabling technologies for wireless body area networks: A survey and outlook," *Communications Magazine, IEEE,* vol. 47, pp. 84-93, 2009.

[25] A. Lea, H. Ping, J. Ollikainen, and R. G. Vaughan, "Propagation Between On-Body Antennas," *Antennas and Propagation, IEEE Transactions on,* vol. 57, pp. 3619-3627, 2009.

[26] Q. H. Abbasi, A. Sani, A. Alomainy, and H. Yang, "On-Body Radio Channel Characterization and System-Level Modeling for Multiband OFDM Ultra-Wideband Body-Centric Wireless Network," *Microwave Theory and Techniques, IEEE Transactions on,* vol. 58, pp. 3485-3492, 2010.

[27] V. De Santis and M. Feliziani, "Intra-body channel characterization of medical implant devices," in *EMC Europe 2011 York,* 2011, pp. 816-819.

[28] D. B. Smith, D. Miniutti, T. A. Lamahewa, and L. W. Hanlen, "Propagation Models for Body-Area Networks: A Survey and New Outlook," *Antennas and Propagation Magazine, IEEE,* vol. 55, pp. 97-117, 2013.

[29] A. Alomainy, Y. Hao, Y. Yuan, and Y. Liu, "Modelling and Characterisation of Radio Propagation from Wireless Implants at Different Frequencies," in *Wireless Technology, 2006. The 9th European Conference on*, 2006, pp. 119-122.

[30] J. Ryckaert, P. De Doncker, R. Meys, A. de Le Hoye, and S. Donnay, "Channel model for wireless communication around human body," *Electronics Letters*, vol. 40, pp. 543-544, 2004.

[31] P. S. Hall, H. Yang, Y. I. Nechayev, A. Alomainy, C. C. Constantinou, C. Parini, *et al.*, "Antennas and propagation for on-body communication systems," *Antennas and Propagation Magazine, IEEE*, vol. 49, pp. 41-58, 2007.

[32] E. Reusens, W. Joseph, B. Latre, B. Braem, G. Vermeeren, E. Tanghe, *et al.*, "Characterization of On-Body Communication Channel and Energy Efficient Topology Design for Wireless Body Area Networks," *Information Technology in Biomedicine, IEEE Transactions on*, vol. 13, pp. 933-945, 2009.

[33] A. Khaleghi and I. Balasingham, "Non-line-of-sight on-body ultra wideband (1ߝ6 GHz) channel characterisation using different antenna polarisations," *Microwaves, Antennas & Propagation, IET*, vol. 3, pp. 1019-1027, 2009.

[34] Z. Lucev, I. Krois, and M. Cifrek, "A Capacitive Intrabody Communication Channel from 100 kHz to 100 MHz," *Instrumentation and Measurement, IEEE Transactions on*, vol. 61, pp. 3280-3289, 2012.

[35] M. S. Wegmueller, A. Kuhn, J. Froehlich, M. Oberle, N. Felber, N. Kuster, *et al.*, "An Attempt to Model the Human Body as a Communication Channel," *Biomedical Engineering, IEEE Transactions on*, vol. 54, pp. 1851-1857, 2007.

[36] O. Omeni, A. Wong, A. J. Burdett, and C. Toumazou, "Energy Efficient Medium Access Protocol for Wireless Medical Body Area Sensor Networks," *Biomedical Circuits and Systems, IEEE Transactions on*, vol. 2, pp. 251-259, 2008.

[37] S. J. Marinkovic, E. M. Popovici, C. Spagnol, S. Faul, and W. P. Marnane, "Energy-Efficient Low Duty Cycle MAC Protocol for Wireless Body Area Networks," *Information Technology in Biomedicine, IEEE Transactions on*, vol. 13, pp. 915-925, 2009.

[38] M. M. Alam, O. Berder, D. Menard, and O. Sentieys, "TAD-MAC: Traffic-Aware Dynamic MAC Protocol for Wireless Body Area Sensor Networks," *Emerging and Selected Topics in Circuits and Systems, IEEE Journal on*, vol. 2, pp. 109-119, 2012.

[39] B. Otal, L. Alonso, and C. Verikoukis, "Highly reliable energy-saving mac for wireless body sensor networks in healthcare systems," *Selected Areas in Communications, IEEE Journal on*, vol. 27, pp. 553-565, 2009.

[40] M. Ur Rehman, Y. Gao, Z. Wang, J. Zhang, Y. Alfadhl, X. Chen, *et al.*, "Investigation of on-body Bluetooth transmission," *Microwaves, Antennas & Propagation, IET*, vol. 4, pp. 871-880, 2010.

[41] B. Shrestha, E. Hossain, and S. Camorlinga, "IEEE 802.15.4 MAC With GTS Transmission for Heterogeneous Devices With Application to Wheelchair Body-Area

Sensor Networks," *Information Technology in Biomedicine, IEEE Transactions on,* vol. 15, pp. 767-777, 2011.

[42] M. N. Deylami and E. Jovanov, "A Distributed Scheme to Manage The Dynamic Coexistence of IEEE 802.15.4-Based Health-Monitoring WBANs," *Biomedical and Health Informatics, IEEE Journal of,* vol. 18, pp. 327-334, 2014.

[43] T. Hsueh-Wen, S. Shiann-Tsong, and S. Yun-Yen, "Rotational Listening Strategy for IEEE 802.15.4 Wireless Body Networks," *Sensors Journal, IEEE,* vol. 11, pp. 1841-1855, 2011.

[44] N. F. Timmons and W. G. Scanlon, "Improving the ultra-low-power performance of IEEE 802.15.6 by adaptive synchronisation," *Wireless Sensor Systems, IET,* vol. 1, pp. 161-170, 2011.

[45] R. Chavez-Santiago, K. Sayrafian-Pour, A. Khaleghi, K. Takizawa, W. Jianqing, I. Balasingham, *et al.*, "Propagation models for IEEE 802.15.6 standardization of implant communication in body area networks," *Communications Magazine, IEEE,* vol. 51, pp. 80-87, 2013.

[46] Z. Lingwei, J. Hanjun, W. Jianjun, D. Jingjing, L. Fule, L. Weitao, *et al.*, "A Reconfigurable Sliding-IF Transceiver for 400 MHz/2.4 GHz IEEE 802.15.6/ZigBee WBAN Hubs With Only 21% Tuning Range VCO," *Solid-State Circuits, IEEE Journal of,* vol. 48, pp. 2705-2716, 2013.

[47] A. C. W. Wong, M. Dawkins, G. Devita, N. Kasparidis, A. Katsiamis, O. King, *et al.*, "A 1 V 5 mA Multimode IEEE 802.15.6/Bluetooth Low-Energy WBAN Transceiver for Biotelemetry Applications," *Solid-State Circuits, IEEE Journal of,* vol. 48, pp. 186-198, 2013.

[48] C. Yuh-Shyan, H. Chih-Shun, and L. Hau-Kai, "An Enhanced Group Mobility Protocol for 6LoWPAN-Based Wireless Body Area Networks," *Sensors Journal, IEEE,* vol. 14, pp. 797-807, 2014.

[49] I. Stojmenovic, A. Nayak, and J. Kuruvila, "Design guidelines for routing protocols in ad hoc and sensor networks with a realistic physical layer," *Communications Magazine, IEEE,* vol. 43, pp. 101-106, 2005.

[50] M. C. Vuran and I. F. Akyildiz, "XLP: A Cross-Layer Protocol for Efficient Communication in Wireless Sensor Networks," *Mobile Computing, IEEE Transactions on,* vol. 9, pp. 1578-1591, 2010.

[51] A. Segall, "Distributed network protocols," *Information Theory, IEEE Transactions on,* vol. 29, pp. 23-35, 1983.

[52] C. Yao-Chung, L. Zhi-Sheng, and C. Jiann-Liang, "Cluster based self-organization management protocols for wireless sensor networks," *Consumer Electronics, IEEE Transactions on,* vol. 52, pp. 75-80, 2006.

[53] R. Baumann, S. Heimlicher, and B. Plattner, "Routing in Large-Scale Wireless Mesh Networks Using Temperature Fields," *Network, IEEE,* vol. 22, pp. 25-31, 2008.

[54] H. Ghasemzadeh, V. Loseu, S. Ostadabbas, and R. Jafari, "Burst communication by means of buffer allocation in body sensor networks: Exploiting signal processing to reduce the number of transmissions," *Selected Areas in Communications, IEEE Journal on,* vol. 28, pp. 1073-1082, 2010.

[55] W. Qiong, K. Masami, and W. Jianqing, "Channel modeling and BER performance for wearable and implant UWB body area links on chest," in *Ultra-Wideband, 2009. ICUWB 2009. IEEE International Conference on*, 2009, pp. 316-320.

[56] J. Abouei, J. D. Brown, K. N. Plataniotis, and S. Pasupathy, "Energy Efficiency and Reliability in Wireless Biomedical Implant Systems," *Information Technology in Biomedicine, IEEE Transactions on,* vol. 15, pp. 456-466, 2011.

[57] E. Rebeiz, G. Caire, and A. F. Molisch, "Energy-Delay Tradeoff and Dynamic Sleep Switching for Bluetooth-Like Body-Area Sensor Networks," *Communications, IEEE Transactions on,* vol. 60, pp. 2733-2746, 2012.

[58] D. S. Zois, M. Levorato, and U. Mitra, "Energy-Efficient, Heterogeneous Sensor Selection for Physical Activity Detection in Wireless Body Area Networks," *Signal Processing, IEEE Transactions on,* vol. 61, pp. 1581-1594, 2013.

[59] T. Robles, A. Kadelka, H. Velayos, A. Lappetelainen, A. Kassler, L. Hui, *et al.*, "QoS support for an all IP system beyond 3G," *Communications Magazine, IEEE,* vol. 39, pp. 64-72, 2001.

[60] C. Xiangqian, M. Kia, Y. Kang, and N. Pissinou, "Sensor network security: a survey," *Communications Surveys & Tutorials, IEEE,* vol. 11, pp. 52-73, 2009.

[61] M. Li, L. Wenjing, and R. Kui, "Data security and privacy in wireless body area networks," *Wireless Communications, IEEE,* vol. 17, pp. 51-58, 2010.

[62] J. Gozalvez, "Spectrum for Medical Area Body Networks [Mobile Radio]," *Vehicular Technology Magazine, IEEE,* vol. 7, pp. 11-17, 2012.

[63] M. Contaldo, B. Banerjee, D. Ruffieux, J. Chabloz, E. Le Roux, and C. C. Enz, "A 2.4-GHz BAW-Based Transceiver for Wireless Body Area Networks," *Biomedical Circuits and Systems, IEEE Transactions on,* vol. 4, pp. 391-399, 2010.

[64] X. Liu, Z. Yuanjin, Z. Bin, W. Yisheng, and P. Myint Wai, "An Ultra Low Power Baseband Transceiver IC for Wireless Body Area Network in 0.18-<formula formulatype="inline"> <img src="/images/tex/241.gif" alt="\mu"> </formula>m CMOS Technology," *Very Large Scale Integration (VLSI) Systems, IEEE Transactions on,* vol. 19, pp. 1418-1428, 2011.

[65] M. Vidojkovic, X. Huang, P. Harpe, S. Rampu, C. Zhou, L. Huang, *et al.*, "A 2.4 GHz ULP OOK Single-Chip Transceiver for Healthcare Applications," *Biomedical Circuits and Systems, IEEE Transactions on,* vol. 5, pp. 523-534, 2011.

[66] A. Heragu, D. Ruffieux, and C. C. Enz, "A 2.4-GHz MEMS-Based PLL-Free Multi-Channel Receiver With Channel Filtering at RF," *Solid-State Circuits, IEEE Journal of,* vol. 48, pp. 1689-1700, 2013.

[67] J. Ryckaert, C. Desset, A. Fort, M. Badaroglu, V. De Heyn, P. Wambacq, *et al.*, "Ultra-wide-band transmitter for low-power wireless body area networks: design and evaluation," *Circuits and Systems I: Regular Papers, IEEE Transactions on,* vol. 52, pp. 2515-2525, 2005.

[68] A. Alomainy, Y. Hao, X. Hu, C. G. Parini, and P. S. Hall, "UWB on-body radio propagation and system modelling for wireless body-centric networks," *Communications, IEE Proceedings-,* vol. 153, pp. 107-114, 2006.

[69] Z. Yan, H. Yang, A. Alomainy, and C. Parini, "UWB on-body radio channel modeling using ray theory and subband FDTD method," *Microwave Theory and Techniques, IEEE Transactions on,* vol. 54, pp. 1827-1835, 2006.

[70] T. Zasowski, G. Meyer, F. Althaus, and A. Wittneben, "UWB signal propagation at the human head," *Microwave Theory and Techniques, IEEE Transactions on,* vol. 54, pp. 1836-1845, 2006.

[71] A. A. Goulianos, T. W. C. Brown, B. G. Evans, and S. Stavrou, "Wideband Power Modeling and Time Dispersion Analysis for UWB Indoor Off-Body Communications," *Antennas and Propagation, IEEE Transactions on,* vol. 57, pp. 2162-2171, 2009.

[72] M. R. Yuce, K. Ho Chee, and C. Moo Sung, "Wideband Communication for Implantable and Wearable Systems," *Microwave Theory and Techniques, IEEE Transactions on,* vol. 57, pp. 2597-2604, 2009.

[73] K. Eun Cheol, P. Seho, C. Jae Sang, and K. Jin Young, "Improved performance of UWB system for wireless body area networks," *Consumer Electronics, IEEE Transactions on,* vol. 56, pp. 1373-1379, 2010.

[74] A. Ghildiyal, B. Godara, K. Amara, R. Dalmolin, and A. Amara, "UWB for low power, short range, in-body medical implants," in *Wireless Information Technology and Systems (ICWITS), 2010 IEEE International Conference on*, 2010, pp. 1-4.

[75] S. Van Roy, C. Oestges, F. Horlin, and P. De Doncker, "A Comprehensive Channel Model for UWB Multisensor Multiantenna Body Area Networks," *Antennas and Propagation, IEEE Transactions on,* vol. 58, pp. 163-170, 2010.

[76] D. Anzai, K. Katsu, R. Chavez-Santiago, W. Qiong, D. Plettemeier, W. Jianqing, *et al.*, "Experimental Evaluation of Implant UWB-IR Transmission With Living Animal for Body Area Networks," *Microwave Theory and Techniques, IEEE Transactions on,* vol. 62, pp. 183-192, 2014.

[77] C. Namjun, R. Taehwan, B. Joonsung, and Y. Hoi-Jun, "A Planar MICS Band Antenna Combined With a Body Channel Communication Electrode for Body Sensor Network," *Microwave Theory and Techniques, IEEE Transactions on,* vol. 57, pp. 2515-2522, 2009.

[78] K. M. Jones, J. A. Mechling, J. W. Strohbehn, and B. S. Trembly, "Theoretical and experimental SAR distributions for interstitial dipole antenna arrays used in hyperthermia," *Microwave Theory and Techniques, IEEE Transactions on,* vol. 37, pp. 1200-1209, 1989.

[79] D. Kurup, W. Joseph, G. Vermeeren, and L. Martens, "Specific absorption rate and path loss in specific body location in heterogeneous human model," *Microwaves, Antennas & Propagation, IET*, vol. 7, pp. 35-43, 2013.

[80] R. Kohno, K. Hamaguchi, L. Huan-Bang, and K. Takizawa, "R&D and standardization of body area network (BAN) for medical healthcare," in *Ultra-Wideband, 2008. ICUWB 2008. IEEE International Conference on*, 2008, pp. 5-8.

[81] K. M. S. Thotahewa, J. M. Redoute, and M. R. Yuce, "SAR, SA, and Temperature Variation in the Human Head Caused by IR-UWB Implants Operating at 4 GHz," *Microwave Theory and Techniques, IEEE Transactions on*, vol. 61, pp. 2161-2169, 2013.

[82] L. Roelens, S. Van den Bulcke, W. Joseph, G. Vermeeren, and L. Martens, "Path loss model for wireless narrowband communication above flat phantom," *Electronics Letters*, vol. 42, pp. 10-11, 2006.

[83] V. G. Chaganti, D. B. Smith, and L. W. Hanlen, "Second-Order Statistics for Many-Link Body Area Networks," *Antennas and Wireless Propagation Letters, IEEE*, vol. 9, pp. 322-325, 2010.

[84] T. Alves, B. Poussot, and J. M. Laheurte, "Analytical Propagation Modeling of BAN Channels Based on the Creeping-Wave Theory," *Antennas and Propagation, IEEE Transactions on*, vol. 59, pp. 1269-1274, 2011.

[85] K. T. Herring, J. W. Holloway, D. H. Staelin, and D. W. Bliss, "Path-Loss Characteristics of Urban Wireless Channels," *Antennas and Propagation, IEEE Transactions on*, vol. 58, pp. 171-177, 2010.

[86] D. Kurup, W. Joseph, G. Vermeeren, and L. Martens, "Path loss model for in-body communication in homogeneous human muscle tissue," *Electronics Letters*, vol. 45, pp. 453-454, 2009.

[87] K. Sayrafian-Pour, Y. Wen-Bin, J. Hagedorn, J. Terrill, and K. Y. Yazdandoost, "A statistical path loss model for medical implant communication channels," in *Personal, Indoor and Mobile Radio Communications, 2009 IEEE 20th International Symposium on*, 2009, pp. 2995-2999.

[88] D. Kurup, W. Joseph, G. Vermeeren, and L. Martens, "In-body Path Loss Model for Homogeneous Human Tissues," *Electromagnetic Compatibility, IEEE Transactions on*, vol. 54, pp. 556-564, 2012.

[89] K. Jaehoon and Y. Rahmat-Samii, "Implanted antennas inside a human body: simulations, designs, and characterizations," *Microwave Theory and Techniques, IEEE Transactions on*, vol. 52, pp. 1934-1943, 2004.

[90] F. Merli, L. Bolomey, J. Zurcher, G. Corradini, E. Meurville, and A. K. Skriverviky, "Design, Realization and Measurements of a Miniature Antenna for Implantable Wireless Communication Systems," *Antennas and Propagation, IEEE Transactions on*, vol. 59, pp. 3544-3555, 2011.

[91] N. Miura, Y. Kohama, Y. Sugimori, H. Ishikuro, T. Sakurai, and T. Kuroda, "A High-Speed Inductive-Coupling Link With Burst Transmission," *Solid-State Circuits, IEEE Journal of,* vol. 44, pp. 947-955, 2009.

[92] P. Soontornpipit, C. M. Furse, and C. You Chung, "Design of implantable microstrip antenna for communication with medical implants," *Microwave Theory and Techniques, IEEE Transactions on,* vol. 52, pp. 1944-1951, 2004.

[93] C. M. Lee, T. C. Yo, C. H. Luo, C. H. Tu, and Y. Z. Juang, "Compact broadband stacked implantable antenna for biotelemetry with medical devices," *Electronics Letters,* vol. 43, pp. 660-662, 2007.

[94] T. Karacolak, A. Z. Hood, and E. Topsakal, "Design of a Dual-Band Implantable Antenna and Development of Skin Mimicking Gels for Continuous Glucose Monitoring," *Microwave Theory and Techniques, IEEE Transactions on,* vol. 56, pp. 1001-1008, 2008.

[95] C. M. Lee, T. C. Yo, F. J. Huang, and C. H. Luo, "Dual-resonant π-shape with double L-strips PIFA for implantable biotelemetry," *Electronics Letters,* vol. 44, pp. 837-838, 2008.

[96] A. Alomainy and H. Yang, "Modeling and Characterization of Biotelemetric Radio Channel From Ingested Implants Considering Organ Contents," *Antennas and Propagation, IEEE Transactions on,* vol. 57, pp. 999-1005, 2009.

[97] X. Wei, K. Saito, M. Takahashi, and K. Ito, "Performances of an Implanted Cavity Slot Antenna Embedded in the Human Arm," *Antennas and Propagation, IEEE Transactions on,* vol. 57, pp. 894-899, 2009.

[98] K. Y. Yazdandoost, "A 2.4 GHz antenna for medical implanted communications," in *Microwave Conference, 2009. APMC 2009. Asia Pacific,* 2009, pp. 1775-1778.

[99] H. Fu-Jhuan, L. Chien-Ming, C. Chia-Lin, C. Liang-Kai, Y. Tzong-Chee, and L. Ching-Hsing, "Rectenna Application of Miniaturized Implantable Antenna Design for Triple-Band Biotelemetry Communication," *Antennas and Propagation, IEEE Transactions on,* vol. 59, pp. 2646-2653, 2011.

[100] Basari, D. Zakaria, F. Y. Zulkifli, and E. T. Rahardjo, "Implanted helical dipole antenna for UHF band applications," in *Antennas and Propagation (ISAP), 2012 International Symposium on,* 2012, pp. 1256-1259.

[101] A. Kiourti and K. S. Nikita, "Miniature Scalp-Implantable Antennas for Telemetry in the MICS and ISM Bands: Design, Safety Considerations and Link Budget Analysis," *Antennas and Propagation, IEEE Transactions on,* vol. 60, pp. 3568-3575, 2012.

[102] K. Y. Yazdandoost, "UWB antenna for body implanted applications," in *Microwave Conference (EuMC), 2012 42nd European,* 2012, pp. 932-935.

[103] Basari, D. C. Sirait, F. Y. Zulkifli, and E. T. Rahardjo, "A helical folded dipole antenna for medical implant communication applications," in *Microwave Workshop Series on RF and Wireless Technologies for Biomedical and Healthcare Applications (IMWS-BIO), 2013 IEEE MTT-S International,* 2013, pp. 1-3.

[104] L. Ho-Yu, M. Takahashi, K. Saito, and K. Ito, "Performance of Implantable Folded Dipole Antenna for In-Body Wireless Communication," *Antennas and Propagation, IEEE Transactions on,* vol. 61, pp. 1363-1370, 2013.

[105] Y. Morimoto, D. Anzai, and J. Wang, "Design of ultra wide-band low-band implant antennas for capsule endoscope application," in *Medical Information and Communication Technology (ISMICT), 2013 7th International Symposium on*, 2013, pp. 61-65.

[106] T. Tuovinen, M. Berg, K. Y. Yazdandoost, and J. Iinatti, "Ultra wideband loop antenna on contact with human body tissues," *Microwaves, Antennas & Propagation, IET,* vol. 7, pp. 588-596, 2013.

[107] A. Alomainy, Y. Hao, C. G. Parini, and P. S. Hall, "Comparison between two different antennas for UWB on-body propagation measurements," *Antennas and Wireless Propagation Letters, IEEE,* vol. 4, pp. 31-34, 2005.

[108] M. Klemm, I. Z. Kovcs, G. F. Pedersen, and G. Troster, "Novel small-size directional antenna for UWB WBAN/WPAN applications," *Antennas and Propagation, IEEE Transactions on,* vol. 53, pp. 3884-3896, 2005.

[109] M. Klemm and G. Troester, "Textile UWB Antennas for Wireless Body Area Networks," *Antennas and Propagation, IEEE Transactions on,* vol. 54, pp. 3192-3197, 2006.

[110] R. K. Raj, M. Joseph, C. K. Aanandan, K. Vasudevan, and P. Mohanan, "A New Compact Microstrip-Fed Dual-Band Coplanar Antenna for WLAN Applications," *Antennas and Propagation, IEEE Transactions on,* vol. 54, pp. 3755-3762, 2006.

[111] A. Tronquo, H. Rogier, C. Hertleer, and L. Van Langenhove, "Robust planar textile antenna for wireless body LANs operating in 2.45 GHz ISM band," *Electronics Letters,* vol. 42, pp. 142-143, 2006.

[112] J. R. Verbiest and G. A. E. Vandenbosch, "A Novel Small-Size Printed Tapered Monopole Antenna for UWB WBAN," *Antennas and Wireless Propagation Letters, IEEE,* vol. 5, pp. 377-379, 2006.

[113] W. Kin-Lu, C. Chih-Hua, and L. Yuan-Chih, "Printed PIFA EM Compatible With Nearby Conducting Elements," *Antennas and Propagation, IEEE Transactions on,* vol. 55, pp. 2919-2922, 2007.

[114] G. A. Conway and W. G. Scanlon, "Antennas for Over-Body-Surface Communication at 2.45 GHz," *Antennas and Propagation, IEEE Transactions on,* vol. 57, pp. 844-855, 2009.

[115] T. F. Kennedy, P. W. Fink, A. W. Chu, N. J. Champagne, G. Y. Lin, and M. A. Khayat, "Body-Worn E-Textile Antennas: The Good, the Low-Mass, and the Conformal," *Antennas and Propagation, IEEE Transactions on,* vol. 57, pp. 910-918, 2009.

[116] B. Sanz-Izquierdo, J. C. Batchelor, and M. I. Sobhy, "Button antenna on textiles for wireless local area network on body applications," *Microwaves, Antennas & Propagation, IET,* vol. 4, pp. 1980-1987, 2010.

[117] T. Alves, B. Poussot, and J. M. Laheurte, "PIFA–Top-Loaded-Monopole Antenna With Diversity Features for WBAN Applications," *Antennas and Wireless Propagation Letters, IEEE,* vol. 10, pp. 693-696, 2011.

[118] N. Chahat, M. Zhadobov, R. Sauleau, and K. Ito, "A Compact UWB Antenna for On-Body Applications," *Antennas and Propagation, IEEE Transactions on,* vol. 59, pp. 1123-1131, 2011.

[119] E. K. Kaivanto, M. Berg, E. Salonen, and P. de Maagt, "Wearable Circularly Polarized Antenna for Personal Satellite Communication and Navigation," *Antennas and Propagation, IEEE Transactions on,* vol. 59, pp. 4490-4496, 2011.

[120] J. Lee, S. I. Kwak, and S. Lim, "Wrist-wearable zeroth-order resonant antenna for wireless body area network applications," *Electronics Letters,* vol. 47, pp. 431-433, 2011.

[121] K. Cheng-Hung, W. Sung-Jung, and T. Jenn-Hwan, "A Novel Folded UWB Antenna for Wireless Body Area Network," *Antennas and Propagation, IEEE Transactions on,* vol. 60, pp. 1139-1142, 2012.

[122] D. Chun-Ping, L. Xiong-Ying, Z. Zhen-Kun, and M. M. Tentzeris, "A Miniascape-Like Triple-Band Monopole Antenna for WBAN Applications," *Antennas and Wireless Propagation Letters, IEEE,* vol. 11, pp. 1330-1333, 2012.

[123] P. Shien-Piao, S. Jia-Yi, and T. Po-Jen, "Circularly Polarized Square Slot Antenna With a Largely Enhanced Axial-Ratio Bandwidth," *Antennas and Wireless Propagation Letters, IEEE,* vol. 11, pp. 969-972, 2012.

[124] P. J. Soh, G. A. E. Vandenbosch, O. Soo Liam, and N. H. M. Rais, "Design of a Broadband All-Textile Slotted PIFA," *Antennas and Propagation, IEEE Transactions on,* vol. 60, pp. 379-384, 2012.

[125] M. Koohestani, J. F. Zurcher, A. A. Moreira, and A. K. Skrivervik, "A Novel, Low-Profile, Vertically-Polarized UWB Antenna for WBAN," *Antennas and Propagation, IEEE Transactions on,* vol. 62, pp. 1888-1894, 2014.

[126] P. B. Samal, P. J. Soh, and G. A. E. Vandenbosch, "UWB All-Textile Antenna With Full Ground Plane for Off-Body WBAN Communications," *Antennas and Propagation, IEEE Transactions on,* vol. 62, pp. 102-108, 2014.

[127] W. G. Scanlon, B. Burns, and N. E. Evans, "Radiowave propagation from a tissue-implanted source at 418 MHz and 916.5 MHz," *Biomedical Engineering, IEEE Transactions on,* vol. 47, pp. 527-534, 2000.

[128] S. K. S. Gupta, S. Lalwani, Y. Prakash, E. Elsharawy, and L. Schwiebert, "Towards a propagation model for wireless biomedical applications," in *Communications, 2003. ICC '03. IEEE International Conference on,* 2003, pp. 1993-1997 vol.3.

[129] A. Fort, C. Desset, P. De Doncker, P. Wambacq, and L. Van Biesen, "An ultra-wideband body area propagation channel Model-from statistics to implementation," *Microwave Theory and Techniques, IEEE Transactions on,* vol. 54, pp. 1820-1826, 2006.

[130] A. Fort, J. Ryckaert, C. Desset, P. De Doncker, P. Wambacq, and L. Van Biesen, "Ultra-wideband channel model for communication around the human body," *Selected Areas in Communications, IEEE Journal on,* vol. 24, pp. 927-933, 2006.

[131] A. Alomainy, H. Yang, A. Owadally, C. G. Parini, Y. Nechayev, C. C. Constantinou, *et al.*, "Statistical Analysis and Performance Evaluation for On-Body Radio Propagation With Microstrip Patch Antennas," *Antennas and Propagation, IEEE Transactions on,* vol. 55, pp. 245-248, 2007.

[132] K. Y. Yazdandoost and R. Kohno, "Wireless Communications for Body Implanted Medical Device," in *Microwave Conference, 2007. APMC 2007. Asia-Pacific,* 2007, pp. 1-4.

[133] S. L. Cotton and W. G. Scanlon, "Channel Characterization for Single- and Multiple-Antenna Wearable Systems Used for Indoor Body-to-Body Communications," *Antennas and Propagation, IEEE Transactions on,* vol. 57, pp. 980-990, 2009.

[134] A. Fort, F. Keshmiri, G. R. Crusats, C. Craeye, and C. Oestges, "A Body Area Propagation Model Derived From Fundamental Principles: Analytical Analysis and Comparison With Measurements," *Antennas and Propagation, IEEE Transactions on,* vol. 58, pp. 503-514, 2010.

[135] M. A. Mellah, A. Sibille, C. Roblin, M. Nedil, and T. A. Denidni, "Statistical Modeling of the “Antenna–Head” Interaction," *Antennas and Wireless Propagation Letters, IEEE,* vol. 10, pp. 454-457, 2011.

[136] H. Sang-Hun and P. Sang Kyu, "Performance analysis of wireless body area network in indoor off-body communication," *Consumer Electronics, IEEE Transactions on,* vol. 57, pp. 335-338, 2011.

[137] A. Khaleghi, R. Chavez-Santiago, and I. Balasingham, "An improved ultra wideband channel model including the frequency-dependent attenuation for in-body communications," in *Engineering in Medicine and Biology Society (EMBC), 2012 Annual International Conference of the IEEE,* 2012, pp. 1631-1634.

[138] M. Balouchestani, K. Raahemifar, and S. Krishnan, "New channel model for wireless body area network with compressed sensing theory," *Wireless Sensor Systems, IET,* vol. 3, pp. 85-92, 2013.

[139] R. Chandra and A. J. Johansson, "An Analytical Link-Loss Model for On-Body Propagation Around the Body Based on Elliptical Approximation of the Torso With Arms' Influence Included," *Antennas and Wireless Propagation Letters, IEEE,* vol. 12, pp. 528-531, 2013.

[140] M. Hirvonen, C. Bohme, D. Severac, and M. Maman, "On-Body Propagation Performance With Textile Antennas at 867 MHz," *Antennas and Propagation, IEEE Transactions on,* vol. 61, pp. 2195-2199, 2013.

[141] S. Van Roy, F. Quitin, L. Lingfeng, C. Oestges, F. Horlin, J. Dricot, *et al.*, "Dynamic Channel Modeling for Multi-Sensor Body Area Networks," *Antennas and Propagation, IEEE Transactions on,* vol. 61, pp. 2200-2208, 2013.

[142] M. Grimm and D. Manteuffel, "Norton Surface Waves in the Scope of Body Area Networks," *Antennas and Propagation, IEEE Transactions on,* vol. 62, pp. 2616-2623, 2014.

[143] M. Manteghi and A. Ibraheem, "On the Study of the Near-fields of Electric and Magnetic Small Antennas in Lossy Media," *Antennas and Propagation, IEEE Transactions on,* vol. PP, pp. 1-1, 2014.

[144] D. Large, L. Ball, and A. Farstad, "Radio Transmission to and from Underground Coal Mines--Theory and Measurement," *Communications, IEEE Transactions on,* vol. 21, pp. 194-202, 1973.

[145] H. A. Wheeler, "Fundamental limitaions of a small VLF antenna for submarines," *Antennas and Propagation, IRE Transactions on,* vol. 6, pp. 123-125, 1958.

[146] T. G. Zimmerman, "Personal Area Networks: Near-field intrabody communication," *IBM Systems Journal,* vol. 35, pp. 609-617, 1996.

[147] H. A. Wheeler, "Fundamental Limitations of Small Antennas," *Proceedings of the IRE,* vol. 35, pp. 1479-1484, 1947.

[148] X. Xiaojing and W. Yuanxun Ethan, "Chu's Limit and Switched Electrically Small Antennas," in *Antenna Technology: Small and Smart Antennas Metamaterials and Applications, 2007. IWAT '07. International Workshop on*, 2007, pp. 463-466.

[149] J. S. McLean, "A re-examination of the fundamental limits on the radiation Q of electrically small antennas," *Antennas and Propagation, IEEE Transactions on,* vol. 44, p. 672, 1996.

[150] R. E. Collin and S. Rothschild, "Evaluation of antenna Q," *Antennas and Propagation, IEEE Transactions on,* vol. 12, pp. 23-27, 1964.

[151] W. A. Davis, T. Yang, E. D. Caswell, and W. L. Stutzman, "Fundamental limits on antenna size: a new limit," *Microwaves, Antennas & Propagation, IET,* vol. 5, pp. 1297-1302, 2011.

[152] A. Karlsson, "Physical limitations of antennas in a lossy medium," *Antennas and Propagation, IEEE Transactions on,* vol. 52, pp. 2027-2033, 2004.

[153] J. R. Wait, "The Magnetic Dipole Antenna Immersed in a Conducting Medium," *Proceedings of the IRE,* vol. 40, pp. 1244-1245, 1952.

[154] H. A. Wheeler, "Small antennas," *Antennas and Propagation, IEEE Transactions on,* vol. 23, pp. 462-469, 1975.

[155] H. G. S. a. A. H. Unden, "Simple Formulas for Near-Field Transmission," *the 2013 Antennas Applications Symposium, Allerton Park,* vol. IL, 2013.

[156] O. Jungsuek and K. Sarabandi, "Low Profile, Miniaturized, Inductively Coupled Capacitively Loaded Monopole Antenna," *Antennas and Propagation, IEEE Transactions on,* vol. 60, pp. 1206-1213, 2012.

[157] A. Arbabi and S. Safavi-Naeini, "Maximum Gain of a Lossy Antenna," *Antennas and Propagation, IEEE Transactions on,* vol. 60, pp. 2-7, 2012.

[158] "In the matter of guidelines for evaluating the environmental effects of radiofrequency radiation," *U. S. F. C. Commission,* 1996.

[159] "Human Exposure to Electromagnetic Fields, High Frequency (10 kHz to 300 GHz)," *E. R. Committee,* 1995.

[160] http://transition.fcc.gov/oet/rfsafety/dielectric.html.

[161] A. Ibraheem and M. Manteghi, "Performance of Electrically Coupled Loop Antenna inside human body at different frequency bands," in *Antennas and Propagation Society International Symposium (APSURSI), 2014 IEEE*, 2014, pp. 975-976.

[162] T. Basmer, N. Todtenberg, F. Popiela, S. Ortmann, and M. Birkholz, "Antennas for medical implant applications operating in the MICS band," in *Microwave Workshop Series on RF and Wireless Technologies for Biomedical and Healthcare Applications (IMWS-BIO), 2013 IEEE MTT-S International*, 2013, pp. 1-3.

[163] F. Merli, B. Fuchs, J. R. Mosig, and A. K. Skriverviky, "The Effect of Insulating Layers on the Performance of Implanted Antennas," *Antennas and Propagation, IEEE Transactions on,* vol. 59, pp. 21-31, 2011.

[164] P. S. Hall and Y. Hao, "Antennas and propagation for body centric communications," in *Antennas and Propagation, 2006. EuCAP 2006. First European Conference on*, 2006, pp. 1-7.

[165] A. Ibraheem and M. Manteghi, "Path Loss inside human body using Electrically Coupled Loop Antenna at different frequency bands," in *Antennas and Propagation Society International Symposium (APSURSI), 2014 IEEE*, 2014, pp. 977-978.

[166] A. Khaleghi and I. Balasingham, "On the Ultra Wideband Propagation Channel Characterizations of the Biomedical Implants," in *Vehicular Technology Conference, 2009. VTC Spring 2009. IEEE 69th*, 2009, pp. 1-4.

[167] J. o. A. O. t. y. i. review, *Journal of Artificial Organs,* vol. 13, p. 9, 2010.

[168] O. C. C. McCaffrey, C. O'Mathuna, and K. Twomey, "Swallowable-Capsule Technology," *Pervasive Computing, IEEE,* vol. 7, p. 7, 2008.

[169] R. S. S. S. Barold, and A. F. Sinnaeve, "Cardiacpacemakers and resynchronization step-by-step: an illustrated guide," *2nd ed. Chichester, UK: Wiley-Blackwell,* 2010.

[170] M. A. L. a. M. A. L. Nicolelis, "Brain–machine interfaces: past, present and future,," *Trends in Neurosciences,* vol. 29, p. 10, 2006.

[171] J. C. Maxwel, "A treatise on electricity and magnetism," *Oxford,: Clarendon press,* 1873.

[172] H. H. a. D. E. Jones, "Electric waves : being researches on the propagation of electric action with finite velocity through space.," *London ; New York: Macmillan and Co.,* 1900.

[173] H. W. Secor, "Tesla apparatus and experiments—How to build both large and small Tesla and Oudin coils and how to carry on spectacular experiments with them," *Practical Electrics,* 1921.

[174] J. D. J. A. Karalis, and M. Soljacic, "Efficient wireless non-radiative mid-range energy transfer,," *Annals of Physics,* vol. 323, p. 15, Jan 2008.

[175] J. C. Lin, "Wireless Power Transfer for Mobile Applications, and Health Effects [Telecommunications Health and Safety]," *Antennas and Propagation Magazine, IEEE,* vol. 55, pp. 250-253, 2013.

[176] M. Manteghi, "A new resonator for high efficiency wireless power transfer," in *Antennas and Propagation Society International Symposium (APSURSI), 2013 IEEE,* 2013, pp. 838-839.

[177] D. W. Williams and M. Manteghi, "High Power Near Field Magnetic Coupling Using a Dynamically Phased Antenna Array," presented at the URSI-USNC National Radio Science Meeting, Boulder, CO, 2011.